Two classes of amine/glutamate multi-transmitter neurons innervate Drosophila internal male reproductive organs

Martha Chaverra[1], John Paul Toney[1], Lizetta D. Dardenne-Ankringa[1], Jace Tolleson Knee[1], Ann R. Morris[1], Joseph B. Wadhams[1], Sarah J. Certel[2], and R. Steven Stowers[1,3]

[1]Montana State University, Department of Microbiology and Cell Biology, Bozeman, MT 59717

[2]The University of Montana, Division of Biological Sciences, Missoula, MT 59812

[3]corresponding author

Abstract

The essential outcome of a successful mating is the transfer of genetic material from males to females in sexually reproducing animals from insects to mammals. In males, this culminates in ejaculation, a precisely timed sequence of organ contractions driven by the concerted activity of interneurons, sensory neurons, and motor neurons. Although central command circuits that trigger copulation have been mapped, the motor architecture and the chemical logic that couple specific neuronal subclasses to organ specific contractility, seminal fluid secretion, and sperm emission remain largely uncharted. This gap in knowledge limits our ability to explain how neural circuits adapt to varying contexts and how their failure contributes to infertility. Here we present an in-depth anatomical and functional analysis of the motor neurons that innervate the internal male reproductive tract of Drosophila melanogaster. We identify two classes of multi-transmitter motor neurons based on neurotransmitter usage, namely octopamine and glutamate neurons (OGNs) and serotonin and glutamate neurons (SGNs), each with a biased pattern of innervation: SGNs predominate in the accessory glands, OGNs in the ejaculatory duct, with equal contributions of each to the seminal vesicles. Both classes co-express vesicular transporters for glutamate (vGlut) and amines (vMAT), confirming their dual chemical identity. Their target organs differentially express receptors for glutamate, octopamine, and serotonin, suggesting combinatorial neuromodulation of contractility. Functional manipulations show that SGNs are essential for male fertility but OGNs are dispensable. Glutamatergic transmission from both classes is also dispensable for fertility. These findings provide the first high-resolution map linking multi-transmitter motor neurons to specific reproductive organs, reveal an unexpected division of labor between serotonergic and octopaminergic signaling pathways, and establish a framework for dissecting conserved neural principles that govern ejaculation and male fertility.

Introduction

Reproduction is a biological imperative of all species. For most sexually reproducing animal species, this involves locating a mate, courtship, and most essentially, the transfer of genetic material via copulation. The endpoint of copulation, ejaculation, consists of two coordinated phases, emission and expulsion (Alwaal et al. 2015; Soni et al. 2022). During the emission phase, sperm and seminal fluid are relocated from their site of origin to a central canal for transfer to the female during the subsequent expulsion phase. The series of events that culminate in ejaculation are regulated by a spinal ejaculation generator located in the lumbar L3-L4 region of the spinal cord of mammals that executes a motor program coordinating a series of muscle contractions and relaxations of the internal and external male genitalia (Truitt and Coolen 2002; Carro-Juarez et al. 2003; Chehensse et al. 2017).

While male external genitalia exhibit remarkable evolutionary variation (Eberhard 1985), internal male reproductive organs exhibit remarkable evolutionary conservation over the last 600 million years since the last common ancestor of insects and mammals (Guerrero et al. 2004; Gomes et al. 2012; Beguelini et al. 2013; Tomas et al. 2019; Fromme et al. 2021; Oliveira et al. 2021; Yartsev and Evseeva 2021; Maciel et al. 2024). These evolutionarily conserved structures of the male reproductive system

include paired testes, seminal vesicles (SVs), and semen producing organs (prostate glands in humans, accessory glands (AGs) in insects), as well as a singular duct (urethra in humans, ejaculatory duct (ED) in insects) through which sperm and seminal fluid flow during mating.

Drosophila melanogaster has been instrumental in revealing fundamental principles of male reproductive behavior and physiology that extend beyond insects, including how neural circuits control mating drive, courtship, and the mechanics and duration of copulation (Acebes et al. 2004; Billeter et al. 2006a; Villella and Hall 2008; Tayler et al. 2012; Crickmore and Vosshall 2013; Pavlou et al. 2016; Jois et al. 2018; Baker et al. 2024). Among the findings of these studies is the existence of neural circuitry in the ventral nerve cord that regulates ejaculation similar to the spinal ejaculation generator circuitry of mammals, suggesting an ancient evolutionary origin. How the motor neurons directly innervating the internal male reproductive organs control the events leading to ejaculation is less well understood. It is also known in Drosophila and other species, including humans, that male ejaculate quality is plastic and can be adapted to environmental conditions, especially the level of male-male competition (Gage and Baker 1991; Wedell and Cook 1999; Pizzari et al. 2003; Pound and Gage 2004; Bretman et al. 2009; Garbaczewska et al. 2013; Hopkins et al. 2019; DeLecce et al. 2025), but the neural mechanisms underlying these adaptations remain to be identified.

Previous studies have determined there are at least three types of motor neurons innervating the Drosophila internal male reproductive system distinguished by neurotransmitter usage including serotonergic (Lee and Hall 2001), octopaminergic (Pauls et al. 2018), and glutamatergic (Pavlou et al. 2016) motor neurons, although there may be at least some overlap in neurotransmitter usage as serotonin/glutamate multi-transmitter motor neurons have been reported in the seminal vesicle (Castellanos et al. 2013). How these neurons coordinate the motor program to elicit ejaculation is an open question, as is their anatomical organization relative to each other. Clarifying the targets and anatomy of these motor neuron classes will uncover critical principles for how neuronal coordination of internal male reproductive organ function contributes to male fertility. To address these questions, we performed a comprehensive analysis of the neurons innervating each internal organ, defined their neurotransmitter complements and receptor profiles, and tested their necessity for successful sperm transfer and fecundity.

Results

Drosophila male reproductive system anatomy

The Drosophila male reproductive system consists of paired testes, SVs, and AGs, as well as a singular ED and ejaculatory bulb (Figure 1) (Demerec 1950). The testes are surrounded by smooth muscle with no neuronal innervation, while the SVs, AGs, and ED are ensheathed by neuronally innervated skeletal muscles (Lee and Hall 2001; Billeter *et al.* 2006b; Susic-Jung *et al.* 2012). The ejaculatory bulb also possesses neuronally innervated skeletal muscle for pumping sperm out of the ED to the female. The SVs fuse just prior to termination in the ED where they form a narrow sphincter that opens during mating to allow sperm to flow. The AGs, insect equivalent of mammalian

prostate glands, produce the bulk of seminal fluid (WOLFNER 1997; MAJANE et al. 2022) and remain separate before terminating in the ED (BAIRATI 1968). Underlying the muscles of the internal male reproductive system organs are a layer of secretory epithelial cells (BAIRATI 1968) that are the cellular source of the seminal fluid components (SEPIL et al. 2019; WIGBY et al. 2020).

Neurotransmitter identity of neurons innervating internal male reproductive organs

To confirm previous reports of innervation of the Drosophila male reproductive system by octopaminergic, serotonergic, and glutamatergic neurons, GAL4 drivers for the octopamine (OA) neurotransmitter synthesis enzyme tyrosine decarboxylase 2 (Tdc2), the serotonin (5-Hydroxytryptamine, 5-HT) neurotransmitter synthesis enzyme tryptophan hydroxylase (TRH) and the vesicular glutamate transporter (vGlut) were used to drive expression of a *UAS-CD8-mCherry* plasma membrane reporter. As expected, all three drivers exhibited expression in neurons of the male reproductive system, but with distinguishable differences in expression patterns. *Tdc2-GAL4* exhibited dense innervation of the SV and ED with sparse innervation of the AG (Figure 2, A). *TRH-GAL4* exhibited dense innervation of the SV and AGs, with modest innervation of the ED (Figure 2, B), and *vGlut-GAL4* exhibited dense innervation of all three organs (Figure 2, C).

OA/glutamate neurons are distinct from 5-HT/glutamate neurons

To determine if the observed neuronal expression of the GAL4 drivers for Tdc2, TRH, and vGlut are coincident or exclusive, two separate approaches were implemented. In the first approach, split-GAL4 drivers specific for each neurotransmitter were tested in pairwise combinations. Both *Tdc2-AD* paired with *vGlut-GAL4-DBD* (Figure 2, D) and *vGlut-AD* paired with *Tdc2-GAL4-DBD* (Figure 2, E) exhibited expression patterns very similar to *Tdc2-GAL4* with dense innervation of the SV and ED, and sparse innervation of the AGs. These results suggest that all the Tdc2 neurons innervating the male reproductive system are OA/glutamate dual neurotransmitter neurons (OGNs). Similarly, both *TRH-AD* paired with *vGlut-GAL4-DBD* (Figure 2, F) and *vGlut-AD* paired with *TRH-GAL4-DBD* (Figure 2, G) exhibited expression patterns very similar to *TRH-GAL4* with dense innervation of the SVs and AGs with modest innervation of the ED. These results suggest that all the serotonergic neurons innervating the male reproductive system are 5-HT/glutamate dual neurotransmitter neurons (SGNs). To determine if there is overlap between the OGNs and SGNs, *Tdc2-AD* was paired with *TRH-GAL4-DBD* with the result that no neuronal expression was observed (Figure 2, H). This result suggests the OGNs and SGNs are exclusive and non-overlapping.

A second approach to assess overlap between octopaminergic, serotonergic, and glutamatergic neurons of the male reproductive system utilized pairwise combinations of GAL4 and LexA drivers specific for each neurotransmitter. Pairing *TRH-GAL4* and *Tdc2-LexA* together with *UAS-6XGFP* and *LexAop-6XmCherry* reporters revealed no overlap in either the SVs (Figure 3, A-F), ED (Figure 3, G-L), or AGs (Figure 3, M-R). These results are consistent with the split-GAL4 result above of no intersection between octopaminergic and serotonergic neurons of the male reproductive system, although both neuron types are often tightly fasciculated, especially in the SVs. Pairing *vGlut-*

LexA with *TRH-GAL4* revealed a high degree of overlap in the SVs (Figures 3S1, A-F), partial overlap in the ED (Figures 3S1, G-L), and near complete overlap in the AGs (Figures 3S1, M-R). Pairing *vGlut-LexA* with *Tdc2-GAL4* revealed significant overlap in the SVs (Figures 3S2, A-F), majority overlap in the ED (Figures 3S2, G-L), and limited overlap in the AGs (Figures 3S2, M-R). The results of the split-GAL4 intersectional strategy and the GAL4/LexA overlap strategy are entirely consistent with each other. Taken together, they demonstrate that the Drosophila internal male reproductive system receives input from two distinct and nonoverlapping motor-neuron populations, one population that co-expresses octopamine and glutamate (OGNs) and another distinct population that co-expresses serotonin and glutamate (SGNs). The SV receives roughly equal innervation from both classes, the AG is innervated more extensively by SGNs, and the ED is innervated more extensively by OGNs.

OGNs are *fru* +/*dsx* + while SGNs are *fru*+/*dsx* -

Neurons that innervate the male reproductive tract are expected to be sexually dimorphic (BILLETER AND GOODWIN 2004; YAMAMOTO 2007; SIWICKI AND KRAVITZ 2009; VERHULST AND VAN DE ZANDE 2015). To determine whether they express the canonical sex-determination genes *fruitless* (*fru*) and/or *doublesex* (*dsx*), *fru-GAL4* and *vGlut-LexA* were paired with *UAS-6XGFP* and *LexAop-6XmCherry*. This experiment revealed complete overlap: every vGlut-positive neuron in the reproductive system—both OGNs and SGNs—was also *fru*-positive (Fig. 3S3, A–C). To examine *dsx* expression, the octopaminergic driver *Tdc2-AD* was combined with *dsx-GAL4-DBD*. The resulting pattern (dense terminals in the SVs and ED, sparse arbors in the AGs; Fig. 3S3, D) matched that of *Tdc2-GAL4* alone, indicating that all OGNs are *dsx*-positive. In contrast, pairing the serotonergic *TRH-AD* with *dsx-GAL4-DBD* produced no signal in the reproductive tract (Fig. 3S3, E), showing that SGNs are *dsx*-negative. Together, these experiments establish that OGNs are *fru*+/*dsx*+, whereas SGNs are *fru*+/*dsx*–, underscoring a molecular distinction between the two neuromodulatory inputs to the male reproductive system.

Non-overlapping expression of TβH and Tdc2 with 5-HT confirms exclusivity of OGNs and SGNs

Several predictions follow from the finding that non-overlapping sets of OGNs and SGNs innervate the male reproductive system. Among these are that the neurotransmitter synthesis enzymes for OA, Tyramine-β-hydroxylase (TβH), and Tyrosine decarboxylase 2 (Tdc2) should be exclusively expressed in the OGNs along with the sole Drosophila vesicular glutamate transporter (vGlut), while 5-HT should be exclusively expressed in the SGNs along with vGlut-40XV5. To test these predictions, vGlut-40XV5 expression was separately assessed in combination with TβH or Tdc2. 5-HT expression, visualized with an anti-5-HT antibody, was also included in this analysis to distinguish SGNs. As predicted, extensive vGlut-40XV5 expression was observed throughout the male reproductive system except for the testes (Figures 4, A and G) with a sharp boundary of neuronal innervation at the testicular duct (arrows, Figure 4, A). Also as predicted, TβH-GFP and Tdc2 were observed in the male reproductive system with expression patterns similar to that of *Tdc2-GAL4* (Figures 4, B and H, respectively).

197 Pairwise combinations of overlapping expression of vGlut-40XV5, 5-HT, and either TβH
198 (Figures 4, D-F) or Tdc2 (Figures 4, J-L) are also shown.
199 Higher resolution images of vGlut-40XV5, TβH-GFP, Tdc2, and 5-HT in the male
200 reproductive system allow an assessment of overlapping expression. In the SV, broad
201 robust expression was observed for vGlut-40XV5 (Figures 4S1, A, G, M, and S) and 5-
202 HT (Figures 4S1, C, I, O, and U), with somewhat more restricted expression for TβH-
203 GFP (Figure 4S1, B and H) and Tdc2 (Figure 4S1, N, T). Pairwise overlapping
204 expression is also shown for vGlut-40XV5 and 5-HT with TβH-GFP (Figures 4S1, D-F
205 and J-L) and Tdc2 (Figures 4S1, P-R and V-X). In the highest resolution images,
206 coincident expression is evident between vGlut-40XV5 with TβH-GFP (Figure 4S1, J)
207 and vGlut-40XV5 with Tdc2 (Figure 4WS1, V). Consistent with results above,
208 exclusivity of expression is apparent between TβH-GFP and 5-HT (Figure 4S1, L) and
209 between Tdc2 and 5-HT (Figure 4S1, X), although the tight fasciculation of OGNs and
210 SGNs is evident.
211 Similar results were obtained in higher resolution images of the ED and AGs
212 although the extent of innervation of the different amines varies between these tissues
213 with more OGNs than SGNs in the ED and the reciprocal in the AGs. In higher
214 resolution images of the ED, strong extensive expression was observed for vGlut-
215 40XV5 (Figures 4S2, A, G, M, and S) with moderately less expression for TβH-GFP
216 (Figure 4S2, B and H) and Tdc2 (Figure 4S2, N, T), with significantly less expression of
217 5-HT (Figures 4S2, C, I, O, and U. Pairwise overlapping expression is also shown for
218 vGlut-40XV5 and 5-HT with TβH-GFP (Figures 4S2, D-F and J-L) and Tdc2 (Figures
219 4S2, P-R and V-X). In the highest resolution images, coincident expression is evident
220 between vGlut-40XV5 with TβH-GFP (Figure 4S2, J) and vGlut-40XV5 with Tdc2
221 (Figure 4S2, V). As in the SV, exclusivity of expression is apparent between TβH-GFP
222 and 5-HT (Figure 4S2, L) and between Tdc2 and 5-HT (Figure 4S2, X), also with tight
223 fasciculation of the OGNs and SGNs.
224 In higher resolution images of the AGs, robust widespread expression was observed
225 for vGlut-40XV5 (Figures 4S3, A, G, M, and S) and 5-HT (Figures 4S3, C, I, O, and U,
226 with no expression of TβH-GFP (Figure 4S3, B and H), and sparse expression of Tdc2
227 (Figure 4S3, N, T). Pairwise overlapping expression is also shown for vGlut-40XV5 and
228 5-HT with TβH-GFP (Figures 4S3, D-F and J-L) and Tdc2 (Figures 4S3, P-R and V-X).
229 In the highest resolution images, coincident expression is evident between vGlut-40XV5
230 and Tdc2 (Figure 4S3, V). As in the SV and ED, exclusivity of expression is apparent
231 between Tdc2 and 5-HT (Figure 4S3, X).
232 The expression of vGlut-40XV5, TβH-GFP, and 5-HT was also assessed at the
233 junction of the SVs and AGs with the ED. vGlut-40XV5 innervation of both the SV and
234 AG is particularly dense (Figure 4S4, A). Significant expression of TβH-GFP and 5-HT
235 was also observed (Figure 4S4, B and C, respectively). Pairwise overlapping
236 expression for vGlut-40XV5, TβH-GFP, and 5-HT is also shown (Figure 4S4, D-F).
237 These experiments showing no overlap in expression of TβH-GFP and Tdc2 with 5-HT
238 provide additional support to the exclusivity of OGNs and SGNs. Collectively, these
239 findings confirm that octopaminergic vGlut-positive and serotonergic vGlut-positive
240 motor neurons form distinct, nonoverlapping populations that differentially innervate the

241 Drosophila male reproductive tract, underscoring strict transmitter exclusivity within this
242 circuit.
243
244 **Expression of vGlut and vMAT in both OGNs and SGNs further confirms multi-**
245 **neurotransmitter usage**
246 Co-labeling of vGlut-40XV5 with TβH / Tdc2 in OGNs and with 5-HT in SGNs implies
247 both neuron types are multi-transmitter and predicts they will express not only vGlut but
248 also the sole Drosophila monoamine vesicular transporter vMAT known to package both
249 OA and 5-HT (DESHPANDE *et al.* 2020). Since OGNs and SGNs often fasciculate tightly
250 together, co-conditional expression of vGlut and vMAT was implemented to visualize
251 expression separately in each population. This was achieved using either the *TRH-*
252 *GAL4* or *Tdc2-GAL4* drivers in combination with the *B2RT-STOP-B2RT-vGlut-40XMYC*,
253 *RSRT-STOP-RSRT-6XV5-vMAT*, *UAS-B2* and *UAS-R* recombinase transgenes. Using
254 the *TRH-GAL4* driver to restrict conditional expression to SGNs, as predicted, both
255 vGlut-40XMYC (Figures 5, A, E) and 6XV5-vMAT (Figures 5, B, F) were detected in the
256 SV. Tdc2 expression was also included in this experiment (Figures 5, C and G) as was
257 a *UAS-CD8-mCherry* reporter to outline SGNs (Figures 5, D and H). A high degree of
258 overlap was observed between vGlut-40XMYC and 6XV5-vMAT (Figure5, I) with no
259 overlap between Tdc2 and the other markers (Figures 5, J-L).
260 In a reciprocal experiment in the SV using the *Tdc2-GAL4* driver and 5-HT
261 immunostaining, both vGlut-40XMYC (Figure 5, M and Q) and 6XV5-vMAT (Figure 5, N
262 and R) were detected with a mostly overlapping distribution (Figure 5, U). 5-HT
263 immunostaining was in close proximity but did not overlap with any of the other markers
264 (Figure 5, V-X). It is also notable that the morphology of the SGNs is distinct from the
265 OGNs with the SGNs being larger and more extensively branched compared to the
266 OGNs (SGNs-Figures 5, D and H; OGNs-Figures 5, P and T), suggesting SGNs may
267 assert more regulatory control of SV muscle activity than OGNs.
268 Similar results were obtained in these co-conditional experiments for the ED and
269 AGs. With the *TRH-GAL4* experiment, vGlut-40XMYC (Figure 5S1, A and E) and 6XV5-
270 vMAT (Figure 5S1, B and F) were both present with a highly overlapping distribution
271 (Figure 5S1, I). Tdc2 did not overlap with any of the other markers (Figure 5S1, J-L).
272 With the *Tdc2-GAL4* experiment, vGlut-40XMYC (Figure 5S1, M and Q) and 6XV5-
273 vMAT (Figure 5S1, N and R) were both observed in a highly overlapping distribution
274 (Figures 5S1, U). 5-HT immunostaining did not overlap with any of the other markers
275 (Figures 5S1, V-X). Note that morphological differences between the SGNs and OGNs
276 in the ED are not as easily distinguished as in the SV.
277 With the *TRH-GAL4* experiment in the AGs, both vGlut-40XMYC (Figures 5S2, A and
278 E) and 6XV5-vMAT (Figures 5S2, B and F) are present in a largely overlapping
279 distribution (Figure 5S2, I). As with the SV and ED, Tdc2 expression did not overlap
280 with any of the other markers (Figures 5S2, J-L). With the *Tdc2-GAL4* experiment in
281 the AG, both vGlut-40XMYC (Figures 5S2, M and Q) and 6XV5-vMAT (Figures 5S2, N
282 and R) are present in an overlapping configuration (Figure 5S2, U). The distribution of
283 5-HT is distinct from any of the other markers (Figure 5S2, V-X). In the AGs the
284 morphology of the SGNs (Figures 5S2, D and H) is distinct from that of the OGNs
285 (Figures 5S2, P and T).

Since OGNs and SGNs are intermingled in tightly fasciculated neuron bundles, we used intersectional labeling to visualize the glutamate transporter vGlut-40XV5 and the monoamine transporter 6XV5-vMAT in each class separately. Together, the results show that both vesicular transporters are expressed in OGNs and SGNs in an overlapping distribution while the OGNs and SGNs remain anatomically distinct throughout the male reproductive tract.

Expansion microscopy reveals prominent co-occurrence of vGlut and vMAT on ED synaptic vesicles of both OGNs and SGNs

Although there is apparent overlap between vGlut-40XMYC and 6XV5-vMAT in both SGNs and OGNs it is not possible to resolve whether they reside on the same or different synaptic vesicles using standard microscopy methods. This constraint is due to the ~250nm diffraction limit of light at visible wavelengths (ABBE 1873). To overcome this limitation, expansion microscopy was performed on EDs using co-conditional expression of vGlut-40XMYC and 6XV5-vMAT separately in SGNs and OGNs as above. The protocol utilized in these experiments reported 10X expansion in a single round (DAMSTRA et al. 2023) and this agreed well with our empirically determined expansion factor of 10.47X based on the size comparison of nuclei area in muscles of the unexpanded and expanded EDs (Figure 5S5, A and B, respectively). In a representative example of expanded SGNs, 6XV5-vMAT (Figure 5S3, A) and vGlut-40XMYC (Figure 5S3, B) revealed a significantly overlapping distribution (Figure 5S3, C). To quantify the co-occurrence of vGlut-40XMYC and 6XV5-vMAT the BIOP JACop ImageJ plug-in was used to calculate a Mander's co-efficient, a metric that calculates the fraction of one signal that co-occurs with another. The output of the BIOP JACop plug-in revealed substantial co-occurrence of 6XV5-vMAT and vGlut-40XMYC (Figures 5S3, D-I) including a graphical representation (Figure 5S3, J). For the SGNs, the numerical Mander's coefficients for 6XV5-vMAT co-occurrence with vGlut-40XMYC were 67.9% and vGlut-40XMYC co-occurrence with 6XV5-vMAT were 57.2% (Figure 5S3, K).

Expanded OGNs yielded similar results. In a representative example, 6XV5-vMAT (Figure 5S4, A) and vGlut-40XMYC (Figure 5S4, B) exhibited substantial overlap (Figure 5S4, C). The output of the BIOP JACop plug-in also revealed majority co-occurrence in image (Figure 5S4, D-I) and graphical form (Figure 5S4, J). For the OGNs, the numerical values of the Mander's coefficients were 67.4% for 6XV5-vMAT co-occurrence with vGlut-40XMYC and 75.6% for vGlut-40XMYC co-occurrence with 6XV5vMAT (Figure 5S4, K).

The results of the expansion microscopy experiments indicate that in both SGNs and OGNs the majority of ED synaptic vesicles are positive for both vGlut-40XMYC and 6XV5-vMAT and thereby they co-release glutamate and either OA (OGNs) or 5-HT (SGNs). This demonstration of a neurotransmitter co-release mechanism may be a conserved strategy for synchronizing rapid gland and muscle activity during copulation that has general implications across species for how co-transmitter neurons mediate complex motor behaviors.

OGNs and SGNs express synaptic markers common to other neuromuscular junctions

In addition to providing information on whether a given synapse is primarily excitatory or modulatory, identifying vesicular transporters and synaptic markers allows mapping of active release sites to determine how pre- and post-synaptic specializations align. Such information is essential for (i) elucidating how each neurotransmitter influences muscle contractility and secretory function, and (ii) predicting how synaptic efficacy might change during prolonged copulation or in response to neuromodulatory feedback. To further characterize the synapses of the neurons innervating the male reproductive system immunostaining was performed with vGlut-40XMYC, 6XV5-vMAT, and either of three well-established Drosophila synaptic markers including Synapsin (Syn)-synaptic vesicles, Bruchpilot (Brp)-active zones, and Discs-large (Dlg-Drosophila homolog of mammalian PSD-95)-post-synaptic density. In the SV, strong Syn staining was observed (Figures 6, C and F) that exhibited extensive co-localization with vGlut-40XMYC (Figure 6, H) and 6XV5-vMAT (Figure 6, I). Similar results were obtained in the ED and AGs. Abundant Syn expression was observed (Figure 6, C' and F') that exhibited near precise overlap with vGlut-40XMYC (Figure 6, H') and 6XV5-vMAT (Figure 6H, I'). For the AG, robust Syn expression was observed (Figures 6A, C'' and F'') that co-localized strongly with vGlut-40XMYC (Figure 6A, H'') and 6XV5-vMAT (Figure 6A, I''). It is notable that a significantly higher density of Syn expression was observed in the SV (Figure 6A, F) compared with the AGs (Figure 6A, F') and ED (Figure 6A. F''), presumably indicating greater neurotransmitter output.

The active zone marker Brp exhibited strong expression in the SV (Figure 6S1, C and G) that overlapped almost entirely with 6XV5-vMAT. Brp expression in the ED and AG was noticeably sparser as compared to the SV. The sparse Brp expression in the ED (Figure 6S1, K and O) overlapped with 6XV5-vMAT. Similarly, in the AGs, Brp expression was sparse and overlapped with 6XV5-vMAT (Figure 6S1, S and W).

The post-synaptic density marker Dlg was expressed broadly throughout the male reproductive system (Figure 6S2, C). In the SV, the bulk of Dlg expression is predominantly in the epithelial cells with lower levels of expression in the muscles (Figure 6S2, G and K) and no preferential post-synaptic accumulation (Figures 6S2, H and L). Similar results were observed in the ED and AGs. In the ED at the level of the muscle Dlg expression is diffuse (Figure 6S2, O) and does not accumulate post-synaptically opposite synapses in the muscles (Figure 6S2, P). In the AGs, Dlg expression is also diffuse in the muscles (Figure 6S2, T) and does not accumulate post-synaptically opposite synapses in the muscle (Figure 6C, U). Images of Dlg expression in the epithelial layer of the ED (Figure 6C, Q) and AG (Figure 6C, V) reveal apparent membrane localization in a honeycomb pattern. The lack of post-synaptic accumulation of Dlg opposite the synapses of SGNs and OGNs in the male reproductive system is reminiscent of larval type II OGNs and distinct from larval type I glutamatergic neurons that exhibit prominent post-synaptic concentration of Dlg (Parnas et al. 2001). It is also notable that there is no vGlut-40XMYC that does not co-localize with 6XV5-vMAT, indicating there are no neurons innervating the SVs, AGs, or ED that uses glutamate as their sole small molecule neurotransmitter. The absence of synapses with post-synaptic Dlg accumulation, a characteristic of type I glutamate-only larval neurons, also supports this assertion. Defining the molecular architecture of these synapses is critical for understanding how they package, release, and receive neurotransmitters to shape the strength and specificity of communication between motor neurons and target organs.

377
378 **LDCVs are present in OGNs and SGNs**
379 In addition to synaptic transmission via synaptic vesicles, neurons are also known to
380 communicate using neuropeptides released via Large Dense Core Vesicles (LDCVs).
381 To determine whether neurons innervating the male reproductive system contain
382 LDCVs, immunostaining was performed with the LDCV marker IA2-GFP (Yu et al. 2025)
383 in combination with vGlut-40XMYC and 6XV5-vMAT. Abundant IA2-GFP expression
384 was observed throughout the male reproductive system (Figure 6S3, C). In the SVs,
385 IA2-GFP (Figure 6S3, F and L) localizes to the same pre-synaptic regions of the
386 neurons as vGlut-40XMYC (Figures 6S3, D and J) and 6XV5-vMAT (Figures 6S3, E and
387 K). In the highest resolution images, there appears to be some overlap between IA2-
388 GFP and vGlut-40XMYC (Figure 6S3, N) as well as between IA2-GFP and 6XV5-vMAT
389 (Figure 6S3, O), but a substantial fraction of IA2-GFP distributes in close proximity to,
390 but is distinct from, vGlut-40XMYC and 6XV5-vMAT. This distribution pattern is not
391 entirely surprising as it is consistent with the prior observation that vesicular
392 neurotransmitter transporters have been detected on LDCVs (Yu et al. 2025).
393 Similar results were observed in the ED and AGs. In the ED, prominent IA2-GFP
394 expression was evident (Figures 6S4, C and I) that partially co-localized with vGlut-
395 40XMYC (Figures 6S4, E and K) and 6XV5-vMAT (Figures 6S4, F and L). Considerable
396 IA2-GFP expression was also apparent in the AGs (Figures 6S4, O and U) that partially
397 overlapped with vGlut-40XMYC (Figures 6S4, Q and W) and 6XV5-vMAT (Figures 6S4,
398 R and X). This finding of pronounced expression of IA2-GFP throughout the pre-
399 synaptic terminals of neurons innervating the male reproductive system suggest
400 substantial LDCVs are present in both SGNs and OGNs, and that these neurons are
401 thus communicating not just via small molecule neurotransmitters inside synaptic
402 vesicles but also by neuropeptides contained within LDCVs.
403
404 **No cholinergic or GABAergic transmission at OGN or SGN synapses**
405 Although to our knowledge there have been no motor neurons reported in Drosophila
406 that use acetylcholine or GABA as a neurotransmitter, to rule out these possibilities for
407 the male reproductive system, Drosophila containing genome-edited 7XMYC-vAChT
408 and 9XV5-vGAT were immunostained for their corresponding epitope tags. Not
409 unexpectedly, no expression of 7XMYC-vAChT was observed in the SVs, ED, or AGs
410 (Figures 6S5, C, G, and K, respectively). Similarly, no expression of 9XV5-vGAT was
411 observed in the SVs, ED, or AGs (Figures 6S5, D, H, and L, respectively), indicating
412 that neither acetylcholine nor GABA are used as neurotransmitters in the OGNs and
413 SGNs of the Drosophila internal male reproductive system.
414
415 **GAL4 drivers for OA, 5-HT, and glutamate receptors express in the muscles of**
416 **male reproductive organs**
417 Given that OGNs and SGNs innervate the male reproductive system, an obvious
418 prediction that follows is that neurotransmitter receptors for glutamate, OA, and 5-HT
419 should be expressed in the muscles of the male reproductive system. As a first step in
420 testing this prediction, GAL4 drivers for each of these neurotransmitters were paired
421 with the *UAS-CD8-mCherry* reporter and assessed for expression. As it is well
422 established that the GluRIIA-E/kainate type glutamate receptors mediate synaptic

transmission at Drosophila NMJs (DiAntonio 2006; He and Dickman 2025), GAL4 drivers for all five were assessed. GAL4 drivers for GluRIIA, GluRIID, and GluRIIE showed no expression in the male reproductive system, but they also exhibited no expression in other adult or larval muscles where they are known to be expressed. These results suggest that the GAL4 drivers for these three GluRII receptors are simply non-functional and are therefore non-informative. However, GluRIIB-GAL4 and GluRIIC-GAL4 exhibited broad expression in the musculature of the male reproductive system (Figures 7, A and B, respectively). This suggests glutamate is used for signaling throughout the male reproductive system, consistent with the widespread expression of vGlut in pre-synaptic terminals.

OA receptor GAL4 drivers for OAMB, OAα2R, Oct-TyrR, OAβ1R, OAβ2R, and OAβ3R were assessed for expression in the male reproductive system. OAMB-GAL4 exhibited expression in the muscles of the SVs and ED, as well as epithelial cells of the AGs (Figure 7S1, A). OAα2R-GAL4 displayed strong expression in the muscles of the SVs, weak expression in the muscles of the AGs, and no expression in the ED (Figure 7S1, B). Oct-TyrR-GAL4 showed strong expression in non-muscle cells of the distal AG, muscle expression in the AGs, ED, and ejaculatory bulb, expression in the testes, but no expression in the muscles of the SVs (Figure 7S1, C). OAβ2R-GAL4 exhibited strong expression in the epithelial cells of the ED, muscle expression in the SVs, ED, and ejaculatory bulb, expression in the testes, but no muscle expression in the AGs (Figure 7S1, E). OAβ1R-GAL4 and OAβ3R-GAL4 exhibited broad expression in the neurons innervating the male reproductive system (Figures 7S1, D and F, respectively) but no muscle expression, suggesting they are not mediating OA signaling in the muscles. OAβ3R-GAL4 also displayed expression in the testes. These results suggest OA receptors play a prominent role in the functioning of the male reproductive system and differentially mediate OA signaling in specific parts of the male reproductive system based on their restricted, non-uniform expression patterns.

5-HT receptor GAL4 drivers for 5-HT1A, 5-HT2A, 5-HT-1B, 5-HT2B, and 5-HT7 were also assessed for expression in the male reproductive system. 5-HT1A-GAL4, 5-HT1B-GAL4, and 5-HT2B-GAL4 exhibited broad expression in the neurons innervating the male reproductive system, but no muscle expression (Figures 7S2, A, C, and D, respectively), suggesting these receptors are not mediating 5-HT signaling in the muscles. 5-HT2A exhibited expression specifically in the epithelial cells of the SVs (Figure 7S2, B). 5-HT7 showed substantial expression in neurons, but most strikingly, strong expression in the muscles of the distal SVs, including the sphincter region, with a discrete boundary of expression (arrows, Figure 7S2, E).

GluRIIA is expressed in the SVs and AGs, but not the ED

While informative for determining cellular expression, GAL4 driven reporters for genes of interest do not provide critical mechanistic information about the subcellular distribution of the corresponding proteins. To gain further insight into the role of OA, 5-HT, and glutamate receptors in the function of the male reproductive system the expression patterns of several receptors were assessed using epitope-tagging. To determine the subcellular distribution of the ionotropic GluRII/kainate-type glutamate receptors known to mediate fast excitatory glutamatergic transmission at other Drosophila NMJs (DiAntonio 2006; He and Dickman 2025), the expression of a

469 previously characterized genome-edited GluRIIA-GFP fly strain in which GFP has been
470 inserted near the carboxy-terminus of GluRIIA at its endogenous genomic location was
471 evaluated in the male reproductive system. In the SV, GluRIIA-GFP (Figure 8, B and E)
472 exhibited punctate expression that paralleled, but was complementary to, that of the
473 glutamatergic synaptic vesicle marker vGlut-40XV5 (Figure 8, A and D). This
474 distribution of GluRIIA-GFP is not unlike its distribution at the NMJ of third instar larva,
475 optimally localized post-synaptically to bind glutamate released from pre-synaptic
476 terminals (Beckers *et al.* 2024). Surprisingly, no GluRIIA-GFP was observed in the ED
477 (Figures 8, H and K) despite abundant expression of vGlut-40XV5 (Figures 8, G and J).
478 Expression of GluRIIA-GFP in the AGs (Figures 8, N and Q) was similar to that in the
479 SVs in that it closely paralleled vGlut-40XV5 expression (Figure 8, M and P) but was
480 complementary to it. Finding GluRIIA-GFP expression in the SVs and AGs, but not the
481 ED, and the expression of GluRIIB in all three tissues based on the *GluRIIB-GAL4*
482 expression pattern, suggest the SVs and AGs use a mixture of glutamate receptors
483 containing one or the other of the mutually exclusive GluRIIA or GluRIIB subunits in
484 combination with the common GluRIIC, D, and E subunits, while all glutamate receptors
485 in the ED solely utilize GluRIIB. As GluRII receptors containing GluRIIA generate higher
486 currents than those that contain GluRIIB (DiAntonio et al. 1999), the lower GluRIIB
487 currents are apparently sufficient for a functional ED.
488
489 **OA receptors exhibit distinct expression patterns in the muscles, neurons, and**
490 **epithelial cells of the male reproductive system**
491 OA receptors are modulatory G-protein coupled receptors (GPCRs) that mediate
492 slower-acting but longer-lasting effects than ionotropic receptors. To visualize
493 expression of the OA receptors OAMB, OAα2R, and OAβ2R, CRISPR/Cas9 genome
494 editing was used to create conditional alleles of each receptor fused at their carboxy
495 termini to a multimerized epitope tag for enhanced detection sensitivity. These genome
496 edits are at the endogenous genomic location of each gene and their expression is thus
497 under the control of their complete endogenous regulatory regions. For visualizing
498 expression in the male reproductive system, germline inversion or excision variants
499 were generated that converted conditional expression to constitutive expression.
500 OAMB-10XV5 exhibited strong expression in the epithelial cells of the ED and AGs
501 with limited expression in muscles (Figure 8S1, A). Co-immunostaining with the
502 synaptic vesicle marker Synapsin was conducted to visualize pre-synaptic terminals
503 (Figure 8S1, B). In the SVs, higher resolution images revealed low level expression of
504 OAMB-10XV5 in muscles as well as obvious expression in pre-synaptic neurons
505 (Figures 8S1, D and G) that largely overlapped with Syn (Figures 8S1, F and I). OAMB-
506 10XV5 was similarly distributed in the ED with low-level expression in muscle and
507 clearly discernible expression in pre-synaptic neurons (Figure 8S1, J) based on
508 substantial overlap with Syn (Figure 8S1, L).
509 Strong OAMB-10XV5 expression was also observed in the epithelial cells of the ED
510 in a honeycomb pattern (Figure 8S1, M and P) reminiscent of Dlg and presumably
511 associated with the plasma membrane. OAMB-10XV5 expression in the epithelial cells
512 of the AGs was similar to its expression in the epithelial cells of the ED with prominent
513 signal in a honeycomb pattern (Figure 8S2, A and D). OAMB-10XV5 also exhibited low-
514 level expression in the muscles of the AG and expression in the pre-synaptic neurons

515 (Figure 8S2, G) by virtue of significant overlap with Syn (Figure 8S2, I). Prominent
516 OAMB-10XV5 expression was also observed in the ejaculatory bulb. Low-level
517 expression of OAMB-10XV5 was detected in the muscles of the ejaculatory bulb as was
518 expression in the pre-synaptic neurons (Figure 8S2, J and M) as evidenced by mostly
519 overlapping expression with Syn (Figure 8S2, L and O). In the non-muscular portion of
520 the ejaculatory bulb, OAMB-10XV5 expression was readily discernable in the epithelial
521 cells in a honeycomb pattern (Figure 8S2, J and P).
522 OAα2R-20XV5 exhibited strong expression in the muscles of both the SVs and
523 more distal regions of the proximal ED near where it connects with the ejaculatory bulb,
524 as well as lower-level expression in the AGs (Figure 8S3, A). Higher resolution images
525 of OAα2R-20XV5 in the SV indicate expression is restricted to the muscle (Figure 8S3,
526 G) as there is no apparent overlap with Syn (Figure 8S3, I). A cross-section of the SV
527 muscle reveals OAα2R-20XV5 is localized to the membrane of the muscle (Figure 8S3,
528 J), as would be expected for a GPCR. In the AGs, OAα2R-20XV5 is expressed in the
529 muscles (Figure 8S3, M and P) as well as in the pre-synaptic neurons as evidenced by
530 co-localization with Syn (Figure 8S3, O and R). OAα2R-20XV5 expression ends
531 abruptly just after the SVs fuse into the sphincter that regulates the movement of sperm
532 into the ED (Figure 8S4, A and D). OAα2R is expressed in the pre-synaptic neurons
533 innervating the sphincter with little to no expression in the sphincter muscles (Figure
534 8S4, C and F). In the proximal region of the anterior ED prominent OAα2R-20XV5
535 expression is observed throughout the innervating neurons with little to no OAα2R-
536 20XV5 in the muscles (Figures 8S4, G, I, J, and L). In contrast, in the distal region of
537 the anterior ED, robust expression of OAα2R-20XV5 is detected in the muscles (Figures
538 8S4, M, P, and S) but not in the pre-synaptic neurons (Figures 8E, O, R, and U). This
539 complementary pattern of OAα2R-20XV5 in neurons but not muscles in the proximal ED
540 and muscles but not neurons in the distal ED suggests these different regions of the ED
541 are exhibiting a differential response to OA. As in the SV, OAα2R-20XV5 localizes to
542 the membrane of the muscles as evident in a cross-sectional image (Figure 8E, S).
543 Interestingly in this region, Syn expression is inside the muscles of the ED (Figure 8E,
544 T), potentially suggesting the muscles are being stimulated from the inside, or
545 alternatively, that the neurons are stimulating the underlying epithelial cells. As pre-
546 synaptic neuronal expression of adrenoreceptors in mammals has been shown to be
547 release-inhibiting (Brown and Gillespie 1957; Starke 1972), including in the urinary
548 bladder (Somogyi and de Groat 1990) and vas deferens (O'Connor et al. 1999;
549 Scheibner et al. 2001), OAα2R expression in the pre-synaptic neurons of the internal
550 male reproductive system may also function via inhibitory auto-reception.
551 OAβ2R-40XV5 exhibits strong expression in the epithelial cells of the ED, the
552 muscles of the ejaculatory bulb, the muscles of the SVs near the point of fusion, the
553 testes, with lower-level muscle expression in the SVs, ED, and AGs (Figure 8S5, A).
554 Higher resolution images of the SV reveal obvious expression in the muscle (Figure
555 8S5, D and G) but not in the pre-synaptic neurons as there is no apparent overlap with
556 Syn (Figures 8S5, F and I). A cross-sectional image of the SV reveals OAβ2R-40XV5 is
557 localized to the plasma membrane of muscle cells (Figure 8S5, J). In higher resolution
558 images of the ED, moderate levels of OAβ2R-40XV5 are present in the muscles
559 (Figures 8S5, M and P) but not in the innervating pre-synaptic neurons as there is no

560 obvious overlap with Syn (Figures 8S5, O and R). At the junction where the SVs fuse
561 into a single duct, OAβ2R-40XV5 expression is strong prior to fusion but drops off
562 abruptly at the point of full fusion (arrow, Figure 8S6, A). The strongest levels of
563 OAβ2R-40XV5 expression throughout the entire male reproductive system is in what
564 appears to be the epithelial cells that line the ED (Figure 8S6, A). A cross-section of the
565 ED reveals the distribution of OAβ2R-40XV5 in epithelial cells is exclusively at the
566 apical surface (Figure 8S6, D). Also notable, there is another boundary of OAβ2R-
567 40XV5 expression in the SVs somewhat prior to fusion (solid arrow, Figure 8S6, G).
568 Higher resolution images of OAβ2R-40XV5 expression at the point of SV fusion shows
569 the sharp dip in expression at the point of full fusion (arrow, Figure 8S6, J). A cross-
570 sectional image also reveals the drop in expression and membrane localization of
571 OAβ2R-40XV5 in the muscle (Figure 8S6, M). Similar to the proximal anterior ED, the
572 more distal region of the anterior ED exhibits strong expression in the muscles, and
573 especially the underlying epithelial cells (Figures 8S7, A and D), In the AGs, OAβ2R-
574 40XV5 expression is manifest in the muscles (Figures 8S7, G and J) but does not
575 overlap with the pre-synaptic neurons as evidenced by the lack of overlap with Syn
576 (Figures 8S7, I and L). Prominent OAβ2R-40XV5 expression was also observed in the
577 ejaculatory bulb (Figure 8S7, M and P). As β2 adrenoreceptors relax bladder muscles
578 in mice (WUEST et al. 2009), OAβ2R may relax muscles in the male reproductive
579 system.
580 Octopamine receptor expression in the internal organs of the male reproductive tract
581 was predicted based on the dense OGN innervation of these tissues. Although OA
582 receptor presence in these muscles aligns with their role in modulating contractile
583 strength and rhythm, the organ-specific differences in receptor subtype abundance
584 could only be established empirically. Epithelial expression implies that octopamine
585 influences non-neuronal functions such as protein secretion or barrier permeability, but
586 the precise cellular responses remain to be defined. Mapping OAMB, OAα2R, and
587 OAβ2R to discrete muscle, neuronal, and epithelial compartments provides mechanistic
588 information about how octopamine fine-tunes contraction, secretion, and presynaptic
589 feedback across the male reproductive tract, offering an evolutionary framework for
590 adrenergic control of fertility and pinpointing cell-specific targets for modulating
591 reproductive output.
592
593 **5-HT7 is widely expressed in the male reproductive system but most prominently**
594 **in the sphincter region**
595 Since the *5-HT7-GAL4* reporter delineates a sharp posterior boundary in the SV,
596 endogenous 5-HT7 receptor expression was evaluated to pinpoint where 5-HT may
597 directly modulate reproductive tract motility. To assess the expression pattern of the 5-
598 HT7 receptor, a 20XV5 tag was added to the carboxy-terminus by CRISPR/Cas9
599 genome editing at its endogenous genomic location. 5-HT7-20XV5 localizes to the
600 muscles of the SV just before and after the junction, the epithelial cells of the AGs, and
601 the ejaculatory bulb (Figures 8S8, A). Higher resolution images of the SV reveal low
602 level expression in muscles (Figures 8S8, D and G), as well as expression in the pre-
603 synaptic neurons innervating the male reproductive system as evidenced by co-
604 localization with Syn (Figures 8S8, F and I). In the ED, 5-HT7-20XV5 is expressed in
605 the muscles (Figures 8S8, J and M), but unlike the SV, it is not expressed the pre-

606 synaptic neurons as it does not appear to co-localize with Syn (Figures 8S8, L and O).
607 Expression levels of 5-HT7-20XV5 increase in the SV near the point of fusion and are
608 maximal from just before the junction all the way to the terminus in the ED (Figure 8S9,
609 A). Expression levels of 5-HT7-20XV5 appear to increase at a discrete boundary point
610 on the SVs prior to fusion (arrow, Figure 8S9, D). This boundary of increasing
611 expression at this same region of the SV is highly reminiscent of OAβ2R-40XV5 (Figure
612 8S6, G). A higher resolution image of the sphincter region of the SV post-fusion reveals
613 high levels of 5-HT7-20XV5 expression (Figure 8S9, G) but not in the innervating pre-
614 synaptic neurons based on the absence of co-localization with Syn (Figure 8S9, I). A
615 cross-section of this same region reveals the 5-HT7-20XV5 protein localizes to muscle
616 membranes (Figure 8S9, J). A high-resolution image of the terminus of the sphincter
617 confirms 5-HT7-20XV5 expression extends all the way to the end (Figure 8S9, M). This
618 observation of 5-HT7-20XV5 expression throughout the fused sphincter region of the
619 SV contrasts with that of OAα2R-20XV5 (Figure 8S4, D) and OAβ2R-40XV5 (Figure
620 8S6, A), both of which end at the point of full SV fusion and suggests 5-HT plays a more
621 important role than OA in sphincter regulation. 5-HT7-20XV5 expression is also
622 elevated in the muscles at the terminus of the AGs (Figure 8S9, P). In the AGs, 5-HT7-
623 20XV5 is most prominently expressed in the underlying epithelial cells (Figures 8S10, A
624 and D). An AG cross-section reveals 5-HT7-20XV5 localizes exclusively to the apical
625 surface of the epithelial cells (Figure 8S10, G), highly reminiscent of OAβ2R-40XV5
626 localization to the apical surface of epithelial cells of the ED (Figure 8S6, D). Nearer the
627 surface of the AGs, low-level expression of 5-HT7-20XV5 is detected in the muscle
628 (Figure 8S10, J) and obvious expression is observed in the innervating pre-synaptic
629 neurons based on overlapping expression with Syn (Figure 8S10, L). 5-HT7-20XV5
630 expression was also observed in the ejaculatory bulb (Figures 8S10, M). Interestingly,
631 none of the OA or serotonin receptors exhibited preferential accumulation in the post-
632 synaptic muscle opposite the pre-synaptic terminals, as observed for GluRIIA. This
633 observation implies volume transmission may play a significant role in modulating
634 muscle activity in the male reproductive system. Neurotransmitter signaling via volume
635 transmission has previously been proposed for the Drosophila female reproductive
636 system based on expression patterns of OA receptors(ROHRBACH *et al.* 2024a).
637
638 **SGNs are essential for male fertility but OGNs are dispensable**
639 Having established that both OGNs and SGNs innervate the male reproductive
640 system an obvious question follows: what are their roles in male fertility? It has
641 previously been reported that OA-deficient flies are male fertile and female sterile
642 (MONASTIRIOTI et al. 1996; COLE et al. 2005). However, in Tβh and Tdc2 mutant flies
643 that fail to synthesize OA, glutamate signaling in the OGNs innervating the male
644 reproductive system is still intact. To determine if simultaneously silencing the OGNs
645 innervating the male reproductive system for both glutamate and OA signaling causes
646 sterility, *Tdc2-GAL4-DBD* was combined with *AbdB-AD* and *UAS-BONT-C* to block all
647 synaptic transmission in these neurons. This intersectional combination results in the
648 silencing of only the Tdc2 neurons in the posterior VNC by virtue of the restricted
649 expression of the AbdB-AD hemidriver to the posterior few segments of the VNC. The
650 result was the same as eliminating OA signaling alone, males were fertile, and females
651 were sterile (Table 1), thus establishing that neither OA nor glutamate signaling is

652 required for fertility in the OGNs innervating the male reproductive system. The
653 observed female sterility validates the silencing function of the UAS-BONT-C transgene.
654 To assess the requirement of the SGNs innervating the male reproductive system for
655 fertility, flies containing TRH-DBD, AbdB-AD, and UAS-BONT-C were generated. Both
656 males and females of this genotype were sterile (Table 1). The observation that
657 females were also sterile, while no serotonergic innervation of the female reproductive
658 system has been reported, suggests the male sterility is due to 5-HT neurons common
659 to both males and females, and thus the male sterility cannot be unambiguously
660 attributed to the SGNs innervating the male reproductive system.
661 In an attempt to identify a split-GAL4 combination that more specifically targets
662 SGNs innervating the male reproductive system, several dozen hemi-drivers that
663 express in neurons whose cell bodies are located in the most posterior region of the
664 VNC were screened for male sterility in combination with UAS-BONT-C and either *TRH-*
665 *AD* or *TRH-GAL4-DBD*, as appropriate. One line, *VT019028-GAL4-DBD* was identified
666 that resulted in male sterility and female fertility, suggesting silencing of male-specific
667 sexually dimorphic neurons, and not neurons common to both males and females, were
668 responsible for the male sterility. The *TRH-AD*/*VT019028-GAL4-DBD* driver in
669 combination with a *UAS-His2A-GFP* nuclear reporter results in expression in sparse
670 neurons in the brain and VNC as well as around two dozen neurons at the posterior tip
671 of the VNC (Figure 9, A). Female flies of the same genotype exhibited a similar sparse
672 pattern of expression in the brain and VNC with the exception that there were noticeably
673 fewer His2A-GFP expressing neurons at the tip of the VNC (Figure 9, B). The neurons
674 most likely responsible for male sterility are those unique to males. The *VT019028-*
675 *GAL4-DBD* driver was also assessed for fertility in combination with *AbdB-AD* and *UAS-*
676 *BONT-C* with the same result of male sterility and female fertility (Table 1). The
677 expression patterns of *VT019028-GAL4-DBD* with *AbdB-AD* in combination with *UAS-*
678 *His2A-GFP* reveals restricted expression to the tip of the ventral nerve cord with
679 noticeably more neurons in the male (Figure 9A, C and D). These results with *AbdB-AD*
680 narrow the neurons responsible for the male sterility to the tip of the VNC. The
681 expression patterns of 5-HT and Tdc2 in these immunostains are also shown (Figures
682 9, E-H, and I-L, respectively).
683 To determine if any of the *VT019028-GAL4-DBD* neurons intersecting with *TRH-AD*
684 or *AbdB-AD* are serotonergic or octopaminergic, higher resolution images of the tip of
685 the VNC were examined. In the full confocal stack image, Three His2A-GFP neurons
686 are clearly visible that overlap with 5-HT (Figure 9S1, D). However, it has previously
687 been shown that there are both dorsal (~10 neurons) and ventral (~9 neurons) clusters
688 of serotonergic neurons innervating the male reproductive system (BILLETER et al.
689 2006b) and some neurons may thus be obscured from a dorsal perspective. A partial
690 stack containing the dorsal cluster reveals the same three neurons (Figure 9S1, I).
691 However, a ventral view of these neurons shows a fourth neuron overlapping with 5-HT
692 (Figure 9S1, K). A partial stack of the ventral cluster reveals three His2A-GFP neurons
693 overlapping with 5-HT (Figure 9S1, O). There also appears to be one or two Tdc2
694 neurons overlapping with His2A-GFP. However, examination of three-dimensional
695 images revealed they are only in close proximity but not overlapping.
696 Similar results were obtained with *VT019028-GAL4-DBD* neurons intersecting with
697 *AbdB-AD*. Four His2A-GFP neurons overlap with 5-HT in a full confocal stack view

698 (Figure 9S2, D). These four neurons are visible in the dorsal serotonergic cluster
699 (Figure 9S2, I), while three additional His2A-GFP neurons overlapping with 5-HT are
700 apparent in the ventral serotonergic neuron cluster (Figure 9S2, N). One His2A-GFP
701 neuron appears to overlap with Tdc2 (Figure 9S2, E), but this apparent overlap is not
702 reproduced in the dorsal (Figure 9S2, J) or ventral (Figure 9S2. O) partial stacks. The
703 innervation of *VT019028-GAL4-DBD* neurons with *TRH-AD* and *AbdB-AD* visualized
704 with the *UAS-CD8-mCherry* reporter is similarly broad in the SVs, ED, and AGs (Figure
705 9S3, A and B, respectively). Taken together, these results strongly suggest synaptic
706 transmission in the SGNs included in the *VT019028-GAL4-DBD* intersections with *TRH-*
707 *AD* and *AbdB-AD* that innervate the male reproductive organs are required for male
708 fertility, although a role for the small number of other interneurons at the tip of the VNC
709 in common between both combinations cannot be excluded.
710 To rule out the possibility that the male sterility observed in the *VT019028-GAL4-*
711 *DBD* intersections with *UAS-BONT-C* and either *TRH-AD* and *AbdB-AD* is due to failure
712 to mate, mating assays were performed where single males and single females of the
713 different genotypes were placed together in a well of a 12-well plate and videotaped.
714 The mating success rates of *VT019028-GAL4-DBD*/*TRH-AD* and *VT019028-GAL4-*
715 *DBD*/*AbdB-AD* were 81.25% (n=16) and 57.9% (n=28), respectively. These results
716 demonstrate the observed male sterility is not due to failure to copulate.
717 In these mating assays, mating duration was also assessed along with several
718 control genotypes. Mean mating durations for *VT019028-GAL4-DBD*/*TRH-AD* and
719 *VT019028-GAL4-DBD*/*AbdB-AD* were 28.74 and 24.75 minutes, respectively (Figure
720 10, A). This was not significantly different from *Canton-S* wildtype controls (26.91), and
721 other controls missing one or more of the components necessary for silencing *AbdB-*
722 *AD*, *UAS-BONT-C* (27.07) and *UAS-BONT-C* alone (28.75) (Figures 10, B and C).
723 These results are in line with previously reported mating durations for Drosophila
724 (CRICKMORE AND VOSSHALL 2013). Interestingly, silencing all 5-HT neurons (*TRH-GAL4-*
725 *DBD* ∩ *AbdB-AD*) or all OA neurons (*TRH-GAL4-DBD* ∩ *AbdB-AD*) innervating the
726 male reproductive system resulted in statistically significant reductions in mating
727 duration, 19.11 (Figure 10B, D) and 21.8 (Figure 10B, E), respectively.
728 To assess the distribution of sperm in the reproductive system during mating by
729 *VT019028-GAL4-DBD*/*TRH-AD* > *UAS-BONT-C* sterile males, a Protamine-GFP
730 reporter that fluorescently labels sperm nuclei was incorporated into the genotype. For
731 this experiment, control and experimental males were placed in petri dishes with virgin
732 females, separated 10 minutes after the initiation of mating, immediately dissected, and
733 the isolated male reproductive systems video recorded using a stereofluorescent
734 microscope. In the control males, ProtB-GFP sperm were readily visible in the ED
735 (Figure 10S1, A, Video 1). In contrast, in the experimental males, no ProtB-GFP sperm
736 were observed (Figure 10S1, B, Video 2). These results demonstrate that the male
737 sterility is due to a failure of the sphincter that regulates the flow of sperm between the
738 SV and ED to open and thus the defect is with the emission phase of ejaculation.
739
740 **Glutamate signaling in OGNs and SGNs is dispensable for male fertility**
741 In the *VT019028-GAL4-DBD*/*TRH-AD* > *UAS-BONT-C* sterile males, 5-HT and
742 glutamate signaling are both abolished due to the BONT-C blockade of synaptic
743 transmission. To determine if glutamate signaling alone is required in these neurons, a

conditional allele of vGlut was incorporated into this genotype such that specifically glutamate signaling was eliminated while serotonergic signaling remained intact. These males were determined to be fertile. To ascertain whether there were changes in the level of fertility, fertility assays were conducted on 5-day post-eclosion males. No changes in fertility as compared to controls were observed (Figure 10S2, A). Immunostaining the AGs of control and experimental flies confirmed the effectiveness of the conditional vGlut allele by the presence of vGlut in control flies and its absence in experimental flies (Figure 10S3, A and D, respectively). As glutamate has been shown to promote neuron survival as neurons age (SHEN et al. 2018; BUCK et al. 2023), to determine if fertility might be altered in older males, the same 5-day old males used in the previous fertility experiment were held in isolation from females until they were 30 days post-eclosion and the experiment was repeated. While there was not unexpectedly a modest decrease in fertility with age, no differences in fertility were apparent between the control and experimental genotypes (Figure 10S2, B). These results establish that glutamatergic signaling is not required in *VT019028-GAL4-DBD*/*TRH-AD* neurons for fertility. To determine if more extensive elimination of glutamate signaling in the OGNs and SGNs would alter fertility, glutamate was specifically eliminated in both classes of neurons. No reductions in fertility were observed in 5-day post-eclosion males (Figure 10S2, A). These results indicate glutamate is not required in either OGNs or SGNs for fertility.

The sphincter region of the SV initiates ED peristaltic waves

Neuron-independent peristaltic waves are known to occur spontaneously in the male ED of Drosophila that persist even when all nerves innervating the male reproductive system have been severed (NORVILLE et al. 2010). To gain a better understanding of the muscle activity occurring during these waves in both the ED and throughout the rest of the male reproductive system, a fly strain was generated that expressed the Ca++ sensor GCAMP8m specifically in muscles under control of the myosin heavy chain promoter (*MHC-GCAMP8m*). This fly strain allows visualization of the changes in Ca++ levels that occur in the muscles during these peristaltic waves. As expected, waves of fluorescence are visualizable coincident with peristaltic waves of muscle contractions in the ED (video 3). These peristaltic waves originate not in the ED but in the sphincter region of the SV just prior to and after the point of SV fusion (video 4), although the region of the SV prior to the fusion point that is involved in initiation varies (video 5). Muscle contractions in other regions of the male reproductive system are also apparent. These contractions are weak and seemingly random in the SV (video 6), AG (video 7), and testes (video 8), but occasionally in the AG strong coordinated contractions are observed (video 9). Together, these imaging data reveal that the seminal-vesicle sphincter acts as an autonomous pacemaker, launching neuron-independent peristaltic waves that drive ejaculatory-duct motility.

Discussion

The male reproductive tract of flies and mammals have obvious morphological differences, yet they share many essential anatomical features and a common organizational logic. During copulation Drosophila males deliver seminal fluid and

~4000-6000 sperm to females during a tightly choreographed ~20-minute window (Kaufman 1942; Gilbert 1981). This involves the emission of sperm and seminal fluid from their sites of origin into the ED where they mix and are subsequently expelled into the female reproductive tract. Despite the critical importance of ejaculation, its neuronal mechanisms have remained poorly defined, hindering broader insights into the neural logic of male fertility. Here we close this gap by demonstrating that two distinct yet intermingled classes of amine/glutamate neurons, OGNs and SGNs, coordinate the ejaculatory sequence that ensures successful reproduction. Their transmitter pairs confer the capacity to co-release both fast excitatory and slower acting aminergic modulatory neurotransmitters. Differential expression of ionotropic glutamate receptors and aminergic metabotropic neurotransmitter receptors combine in post-synaptic muscle across the male reproductive system to confer an additional level of complexity to coordinately regulate fluid secretion, organ contractility, and directional sperm movement, to the end of optimizing male fertility.

This system can serve as a genetically tractable model to gain general insights into how multi-transmitter neurons coordinate and modulate interrelated action sequences critical for complex organ function. Lessons learned from this system may have implications for understanding how males of Drosophila and other species adapt their reproductive strategies to a dynamic environment. Additionally, understanding the mechanisms by which this system operates has the potential to identify neuromodulation strategies for male infertility and prostate cancer as multi-transmitter sympathetic and parasympathetic neurons innervating human male reproductive organs have been implicated in these conditions (Burnstock 2009; Magnon *et al.* 2013; Burnstock 2014; Drobnis and Nangia 2017; Dwivedi *et al.* 2021).

Mechanisms of multi-transmitter neuron-mediated transfer of sperm and seminal fluid

Movement of sperm and seminal fluid through the male reproductive tract requires an alternating series of coordinated muscle contractions and relaxations. Based on the observed co-packaging of vMAT and vGlut in the majority of synaptic vesicles in the ED of both the OGNs and SGNs, combined with the observed non-uniform distribution of neurotransmitter receptors for OA, 5-HT, and glutamate in neurons and muscles, potential pre- and post-synaptic mechanisms for regulating the activity of the muscles of the internal male reproductive system are possible.

Pre-synaptic expression of the α-type OA receptors OAMB and OAα2R may facilitate alternating bursts of action potential-dependent neurotransmitter release by diminishing pre-synaptic neurotransmitter release via an auto-receptive mechanism. As α-type adrenergic and noradrenergic receptors have been consistently shown to inhibit neurotransmitter release in multiple rodent species in both the peripheral and central nervous system including the vas deferens, heart, and brain when expressed in pre-synaptic neurons (Starke 1972; Trendelenburg et al. 1994; Miyazaki et al. 1998; Scheibner et al. 2001; Trendelenburg et al. 2003), the presence of OAMB and OAα2R in the pre-synaptic terminals of neurons innervating the internal male reproductive organs may have the effect of suppressing neurotransmitter output from pre-synaptic terminals and shortening the duration of muscle contractions. Thus, pre-

835 synaptic expression of OAMB and OAα2R may have the effect of increasing the cycling
836 frequency of muscle contractions and relaxations.
837 As glutamate is acting via post-synaptic GluRII-type receptors, its effect will almost
838 certainly be excitatory with the result of eliciting fast muscle contractions. In contrast,
839 the functional consequences of OA and 5-HT are not so clear cut. Either of these
840 amines could enhance muscle contractions or facilitate muscle relaxation, depending on
841 the neurotransmitter receptor(s) receiving the signal. In muscles of the mammalian
842 prostate and lower urinary tract, α-type adrenergic and noradrenergic receptors have
843 been demonstrated to augment muscle contractions while β-type receptors have been
844 found to facilitate muscle relaxation (HONDA et al. 1985; MICHEL AND VRYDAG 2006;
845 WUEST et al. 2009). In contrast, OAMB and OAβ2R have been shown to enhance
846 muscle relaxation and contraction, respectively in the Drosophila female reproductive
847 system (DESHPANDE et al. 2022).
848 5-HT7 receptors are known to promote smooth muscle relaxation in the urinary tract,
849 gut, oviduct, and blood vessels of mammals (CARTER et al. 1995; LEUNG et al. 1996;
850 PRINS et al. 1999; INOUE et al. 2003; RECIO et al. 2009; CHANG CHIEN et al. 2015;
851 MATSUMOTO-MIYAI et al. 2015). Although muscle contraction receives preferential focus,
852 muscle relaxation is also critically important for the execution of motor programs
853 (GOULDING et al. 2014; WONG AND LANGE 2014; GOWDA et al. 2018; HIRAMOTO et al.
854 2021) and 5-HT7 most likely plays a role in mediating muscle relaxation in the internal
855 male reproductive system. An additional confounding factor is that OAα2R has been
856 shown to respond not just to OA but also to 5-HT (QI et al. 2017). The observations of
857 the presence of both muscle contraction enhancing, and muscle relaxation promoting,
858 OA and 5-HT receptors in the same muscles of the internal male reproductive organs
859 indicates the mechanisms of neuronal regulation of their activity are complex and may
860 even involve synergistic effects that can only be established empirically.
861
862 **A potential timing mechanism mediated by multi-transmitter neurons**
863 Pre-synaptic release of glutamate acting on post-synaptic ionotropic GluRII-type
864 glutamate receptors will cause near immediate, short-term, contraction of muscles. At
865 least in the ED, our results show that the majority of synaptic vesicles co-package either
866 OA or 5-HT along with glutamate, and thus simultaneous co-release is being used as a
867 mechanism of neurotransmitter signaling. The amines OA or 5-HT acting on post-
868 synaptic metabotropic OA and 5-HT receptors will have the effect of either prolonging
869 the length of, or augmenting the relaxation of, muscles, dependent on the specific
870 aminergic neurotransmitter receptors involved. These latter effects will be delayed
871 relative to the glutamate-induced fast muscle contractions due to the discrepancy in the
872 time course of action between ionotropic and metabotropic receptors. Thus, co-
873 releasing a fast-acting excitatory neurotransmitter acting through an ionotropic receptor
874 simultaneous with a modulatory aminergic neurotransmitter acting through slower acting
875 GPCRs in the same multi-transmitter neuron may create a sequential timing mechanism
876 whereby fast glutamate-mediated muscle contractions always precede either amine-
877 mediated prolonging of muscle contraction or facilitation of muscle relaxation. A single
878 neuron co-releasing one fast and one slow neurotransmitter may thus have the
879 advantage over two distinct neurons separately releasing these transmitters in that the

former can more effectively synchronize, and at the same time, stagger events that require precise timing.

Potential for adaptation to environment

The complexity of neuronal control of male reproductive function revealed in this investigation exposes a variety of possibilities for adaptive regulation to dynamic environmental conditions. Polygynous Drosophila males are well-established to alter the quantity and quality of their ejaculate based on environmental circumstances, especially the level of competition with other males (BRETMAN et al. 2009; MOATT et al. 2014), but also due to nutrient availability (MACARTNEY et al. 2021) and the presence of pathogens (LIAO et al. 2024). The male reproductive system may adapt to environmental conditions by tuning octopamine and serotonin signaling, adjusting the levels of their biosynthetic enzymes, the vesicular monoamine transporter vMAT, or relevant receptors to alter the amount of sperm and seminal fluid released during copulation. A potential mechanism for altering OA and/or 5-HT levels is extra-synaptic volume transmission whereby the level of OA or 5-HT secreted into the hemolymph in locations anatomically distant from the male reproductive system. Thus, global levels of OA and 5-HT in the hemolymph could be adjusted based on environmental conditions and this signal could then impact the male reproductive system to optimize ejaculate quality and quantity. Finally, the presence of OAMB and 5-HT7 on epithelial cells suggest the potential for the regulation of the quality of seminal fluid as the expression of these receptors implies, they could differentially alter gene expression in the epithelial cells in response to changing levels of OA and 5-HT. The results of this study create a foundation for mechanistic investigations into the molecular basis by which male reproductive resources are adaptively modulated.

Potential for signaling via neuropeptides

The broad abundant expression of the LDCV reporter IA2 in the neurons innervating the internal organs of the male reproductive system suggests a significant role for neuropeptide signaling since neuropeptides are known to be packaged into LDCVs (PELLETIER AND LECLERC 1979; KREINER et al. 1986). Bolstering the prospect of this possibility, numerous neuropeptides across evolutionary distant insect species have been shown to alter the frequency and/or amplitude of the spontaneous peristaltic waves in the ED of male insect reproductive systems (MARCINIAK et al. 2017; CIZMAR et al. 2019; LANGE et al. 2023). Multiple neuropeptides have also been implicated in the function of the internal male reproductive organs of mammals, including humans, (SEGAWA et al. 1978; ALLEN et al. 1982; TAINIO 1995). Given these considerations, it thus seems likely that neuropeptides outside the scope of this investigation also play a role in regulating Drosophila male reproduction.

The SV/ED junction is a control center

Immediately proximal to the ED, SVs fuse into a single duct that forms the sphincter regulating sperm flow from the SV to the ED during mating. The differential expression patterns of OAα2R, OAβ2R, and 5-HT7 in this region of the SV is intriguing. The extent of OAα2R and OAβ2R expression ends very shortly after the merge, at precisely the point where full SV fusion occurs and there is no longer a partition separating the ducts

(BAIRATI 1968). Only 5-HT7 expression extends into the fully fused SV that constitutes the sphincter separating the SV from the ED. This expression pattern implies a prominent role for 5-HT7 in sphincter regulation. Previous reports of 5-HT7 mediating relaxation of smooth muscle in the mammalian gut (CARTER et al. 1995; PRINS et al. 1999), urinary bladder neck (RECIO et al. 2009), cardiovascular system (LEUNG et al. 1996; CHANG CHIEN et al. 2015), lymphatic system (CHAN AND VON DER WEID 2003), and oviduct (INOUE et al. 2003) raises the possibility it may function to relax the sphincter muscles during copulation to permit sperm flow. Additionally, expression of OAβ2R and the likely relaxation-promoting 5-HT7 receptors increases sharply in the SV just prior to the point of fusion. Perhaps not coincidentally, this limit of expression corresponds with the distal-most extent of sperm localization in the SV where relaxation of the SV muscles must also occur for sperm to move along the duct to the ED. It is also notable, as revealed in the Ca++ imaging experiments, that the sphincter region is the site of initiation of the peristaltic waves of muscle contractions that are promulgated through the ED. The SV/ED junction is thus a critical control center for both regulation of sperm flow into the ED during mating and initiating neuron-independent peristaltic waves in the ED.

Molecular continuity of neurotransmitter signaling between males and females?

The expression of 5-HT7 and OAβ2R on the apical surface of the epithelial cells lining the AG and ED, respectively, is surprising because it implies that levels of 5-HT and OA are fluctuating in the lumen of these organs. The origin of these neurotransmitters is not obvious but if OA and 5-HT are present in the lumen of the AG and ED, another intriguing possibility is that these neurotransmitters are transferred to the female at mating for signaling in order to modulate female behavior and/or reproductive activity. A recent study detailed the molecular continuity of proteins in the seminal fluid of males functionally interacting with proteins in the female reproductive tract (MCCULLOUGH et al. 2022). The potential presence of OA and 5-HT in the lumen of the AG and ED raises the possibility that this molecular continuity could extend to neurotransmitters in male seminal fluid signaling to neurotransmitter receptors in the female reproductive tract to convey information such as health, internal state, or environmental conditions to regulate female reproductive output. A detailed examination of the expression patterns of OA receptors in the female reproductive tract indicates this is indeed a possibility, at least for OA signaling (ROHRBACH *et al.* 2024b).

Materials and methods

Fly strains

Stocks from the Bloomington Drosophila Stock Center (NIH P40OD018537) were used in this study. *Tdc2-GAL4* (COLE et al. 2005) RRID:BDSC_9313, *GluRIIA-GAL4* RRID:BDSC_84637, *GluRIID-GAL4* RRID:BDSC_84638, and *TRH-GAL4* RRID:BDSC_84694 (DENG et al. 2019)
vGlut-GAL4 RRID:BDSC_60312, *vGlut-GAL4-DBD* (DIAO et al. 2015)
Tdc2-AD (DIONNE et al. 2018) RRID:BDSC_601902
TRH-GAL4-DBD RRID:BDSC_70371
TRH-AD RRID:BDSC_70975

GluRIIB-GAL4 RRID:BDSC_60333 and *GluRIIE-GAL4* RRID:BDSC_60332 (DIAO et al. 2015)
Oct-TyrR-GAL4 RRID:BDSC_77735 and *GluRIIC-GAL4* RRID_83268 (LEE et al. 2018)
GluRIIA-GFP RRID:BDSC_99517 (BECKERS et al. 2024)
5-HT1A-GAL4 RRID:BDSC_84588, *5-HT1B-GAL4* RRID:BDSC_84589 , *5-HT2A-GAL4* RRID:BDSC_84590, *5-HT2B-GAL4* RRID:BDSC_84591, and *5-HT7-GAL4* RRID:BDSC_84592 (DENG et al. 2019)
TβH-GFP RRID:BDSC_80113 (LI-KROEGER et al. 2018)
fru-GAL4 RRID:BDSC_66696
UAS-CD8-mCherry RRID:BDSC_27392
ProtB-GFP (MANIER et al. 2010) RRID:BDSC_58406
AbdB-AD (DIAO et al. 2024)
vGlut-AD (GAO et al. 2008)
IA2-GFP (YU et al. 2025)
UAS-BONT-C (HAN et al. 2022)
dsx-GAL4-DBD (SHIRANGI et al. 2016)
vGlut-40XV5 and *vGlut-40XMYC* (STOWERS 2025)
B2RT-7XMYC-vAChT (TISON et al. 2020)
RSRT-9XV5-vGAT (CERTEL et al. 2022)
OAMB-GAL4, *OAα2R-GAL4*, *OAβ1R-GAL4*, *OAβ2R-GAL4*, *OAβ3R-GAL4* (MCKINNEY et al. 2020)
FRT-F3 OAMB-10XV5 (BAKSHINSKA et al. 2025)
B3RT-Tdc2-LexA, *B3RT-vGlut-LexA*, *RSRT-STOP-RSRT-6XV5-vMAT*, *UAS-B3* and *20XUAS-R* (SHERER et al. 2020)
20XUAS-B2 (WILLIAMS et al. 2019)
13LexAop-6XmCherry (SHEARIN et al. 2014)

Stocks original to this report

Tdc2-GAL4-DBD (*JK65C*)
B3RT-Tdc2-LexA germline excision
B3RT-vGlut-LexA germline excision
RSRT-6XV5-vMAT germline excision
FRT-F3-OAα2R-20XV5
FRT-F3-OAα2R-20XV5 germline inversion
B2RT-STOP-B2RT-OAβ2R-40XV5
B2RT-OAβ2R-40XV5 germline excision
5-HT7-20XV5
MHC-GCAMP8m (*VK27*)

Entry clones

The *R4-GAL4-DBD-R3* entry clone contains a 640bp insert encoding the GAL4 DNA binding domain. The *L1-MHC-5'Reg-R5* entry clone contains 5254bp of upstream regulatory sequence from the Drosophila Myosin Heavy Chain (MHC) gene. The *L5-GCAMP8m-L2* entry clone contains a 1276bp insert encoding GCAMP8m (ZHANG et al. 2023). Entry clones were generated as previously described (PETERSEN AND STOWERS 2011).

1018
1019 **Expression clones**
1020 *Tdc2-GAL4-DBD* was constructed by combining entry clones *L1-Tdc2-5'Reg-L4* and *L3-*
1021 *Tdc2-3'Reg-L2* (SHEARIN et al. 2013) with the *R4-GAL4-DBD-R3* entry clone and the
1022 destination vector *pDESTP10* (SHEARIN et al. 2013). *MHC-GCAMP8m* was assembled
1023 by combining entry clones *L1-MHC-5'Reg-R5* and *L5-GCAMP8m-L2* with *pDESTP10-*
1024 *SPEC*. *pDESTP10-Spec* is a derivative of *pDESTP10* in which AmpR was replaced
1025 with SpecR.
1026
1027 **Donor plasmid assembly**
1028 Donor plasmids were assembled starting with gene synthesis of the homology arms
1029 (Synbio). The gene synthesis also included recombinase target sites and mutations in
1030 the PAM sites associated with the guide RNAs. Homology arms typically extended
1031 ~750bp beyond the cut sites of the guide RNAs. STOP cassettes were added via
1032 Gibson cloning. Multimerized epitope tags (STOWERS 2025) were added via *Asc I*/*Not I*
1033 restriction enzyme cloning. The *OAα2R-FRT-F3-20XV5* donor plasmid contained a pair
1034 of *FRT-F3* sites appropriately arranged for conditional expression of OAα2R-20XV5
1035 after inversion/excision by FLP recombinase (FISHER *et al.* 2017) with the 20XV5 fused
1036 to the carboxy-terminus. The *OAβ2R-B2RT-STOP-B2RT-40XV5* donor plasmid
1037 contained B2 recombinase target sites flanking a STOP cassette such that OAβ2R-
1038 40XV5 was expressed after excision of the STOP cassette with 40XV5 fused to the
1039 carboxy-terminus. The 5-HT7-20XV5 donor plasmid contained a 20XV5 multimerized
1040 epitope tag fused to the carboxy-terminus but was not designed for conditional
1041 expression.
1042
1043 **Guide RNA plasmid assembly**
1044 Guide RNAs were assembled in the *pCFD4* double-guide RNA plasmid as previously
1045 described (PORT *et al.* 2014). Two double guide RNA plasmids were used with each
1046 donor construct for genome editing. The guide RNA plasmids and the guide RNAs they
1047 contain are as follows: *pCFD4-OAα2RGd12*-TCTAAATCAATATCAGTG and
1048 AACATAAACATCCTAAAA; *pCFD4-OAα2R-Gd34*-ACCTGTAACAGCACACAT and
1049 GGCATGTATCAGCACTAC; *pCFD4-OAβ2R-Gd56*-ATAAATGAGATTATACTC and
1050 CATGCATCTGGAATTTAT; *pCFD4-OAβ2R-Gd78*-CGGCGGGCGGATCCCGCC and
1051 AGGATGGCAGGGAGTCGA; *pCFD4-5-HT7-Gd56*-TGGGCGATGAGAGGCACG and
1052 TGGGCGATGAGAGGCACG; *pCFD4-5-HT7-Gd78*-CCACGAGGACCTCCATTC and
1053 GGGTCTTCCCTAGGTTTC.
1054
1055 **Genome editing**
1056 For each genome edit, the donor plasmid was injected together with both *pCFD4* guide
1057 RNA plasmids into the *nos-Cas9 attP40* fly strain by Rainbow Transgenic Flies. Adult
1058 flies that were injected as embryos were crossed to 3rd chromosome balancer stocks.
1059 Candidate progeny males from this first cross containing the *TM6b* balancer
1060 chromosome were crossed to yw; n-syb-GAL4, UAS-FLP/TM6c (*OAα2R-FRT-F3-*
1061 *20XV5*, *yw*; *20XUAS-B2*; *n-syb-GAL4* (*OAβ2R-B2RT-STOP-B2RT-40XV5*) or *yw*;
1062 *Ly*/*TM6c* (*5-HT7-20XV5*) fly strain and larval progeny were screened by

immunostaining. Males whose progeny exhibited positive immunostaining were subsequently crossed to a third chromosome balancer stock to establish stable lines.

Germline excision/inversion

Germline inversion of *OAα2R-FRT-F3-20XV5* was accomplished by crossing to *yw*; *nos-GAL4*; *UAS-FLP*. Males containing all three genetic components were crossed to a third chromosome balancer stock. Individual progeny males from this cross were crossed a second time to the third chromosome balancer stock and non-Tb larva were screened by anti-V5 immunostaining to identify germline excisions. A similar strategy was used with *OAβ2R-B2RT-STOP-B2RT-40XV5* for a germline excision except the initial cross was to *yw*; *nos-GAL4*; *UAS-B2*. *vGlut-LexA* was generated by crossing *B3RT-vGlut-LexA* to *yw*: *nos-GAL4*; *UAS-B3*. Progeny from this cross containing all three genetic components were crossed to a second chromosome balancer stock. Single progeny males were then crossed to a *13XLexAop-6XmCherry* reporter and larva were screened for expression in the ventral nerve cord to identify germline excision positives. A similar strategy was used to create *B3RT-Tdc2-LexA* starting with *B3RT-Tdc2-LexA* (McKinney et al. 2020). *RSRT-6XV5-vMAT* was generated by crossing *RSRT-STOP-RSRT-6XV5-vMAT* with *yw*; *nos-GAL4*; *UAS-R*. Progeny from this cross containing all three genetic components were crossed to a second chromosome balancer stock. Single progeny males were crossed to the second balancer a second time and larval progeny were subjected to anti-V5 immunostaining to identify germline excisions.

Immunostaining

Male reproductive systems were dissected in PBS and fixed in 4% paraformaldehyde for 30 minutes with rotation. After 2X brief washes with PBS, they were incubated in PBS containing 2% Triton-X 100 and 2% BSA (PBSTB) for at least two hours with rotation. Subsequently, they were incubated in primary antibodies PBSTB for one hour with rotation, followed by overnight incubation at 4°C without rotation to prevent tissue damage. After 3X 5-minute washes in PBSTB, male reproductive systems were incubated for 2-3 hours in PBSTB with secondary antibodies with rotation. After three 5-minute washes in PBS, they were incubated in PBS containing Phalloidin 405 for one hour. After two 5-minute washes in PBSTB and one 5-minute wash in PBS, male reproductive systems were mounted on glass slides in Vectashield Plus (Vector Laboratories, Cat. #H-1900) using a coverslip that was glued on the edges with clear nail polish.

Primary antibodies and dilution factors: The SYN (3C11) mAb 1:20 (Klagges et al. 1996). Brp nc82 mAb 1:40 (deposited at the DSHB by Eric Buchner), Dlg 4F3 mAb 1:40 (Parnas *et al.* 2001), were obtained from the Developmental Studies Hybridoma Bank, created by the NICHD of the NIH and maintained at The University of Iowa, Department of Biology, Iowa City, IA 52242. Mouse anti-V5 SV5-P-K (Novus NBP2-52703) 1:200; rat anti-V5 SV5-P-K (Novus NBP2-81037) 1:200, rabbit anti-V5 SV5-P-K (Novus NBP2-52653) 1:200; Human anti-V5 (Novus NBP2-81035) 1:200; rat anti-MYC 9E10 (Novus NBP2-81020) 1:200, rabbit anti-MYC 9E10 (Novus NBP2-52636), mouse anti-MYC 4A6; (Millipore Sigma) 1:200, mouse anti-vGlut 1:10 (Banerjee et al. 2021), mouse anti-

GFP 3E6 (Thermo-Fisher A11120) 1:200; Rabbit anti-GFP (Thermo-Fisher G10362); rat anti-mCherry 16D7 (ThermoFisher-M11217) 1:200, rabbit anti-Tdc2 pab0822-P, Covalab) 1:500; rat anti-5-HT YC5 (Abcam ab6336) 1:300.

Secondary antibodies and dilution factors: Goat anti-Mouse Alexa 405 (Thermo-Fisher A31553) 1:400; Goat anti-Mouse Alexa 488 (Jackson Immunoresearch 115-545-166) 1:400; Donkey anti-Rat Alexa 488 (Jackson Immunoresearch 712-546-153) 1:400, Goat anti-Rabbit Alexa 488 (Thermo-Fisher A32731) 1:400, Goat anti-Mouse Alexa 568 (Thermo Fisher A11031) 1:400, Goat anti-Rabbit Alexa 568 (Thermo Fisher A11036)1:400, Donkey anti-Rat Alexa 568 (Thermo-Fisher A78946) 1:400; Goat anti-Mouse Alexa 647 (Thermo-Fisher A32728) 1:400; Goat anti-Rabbit Alexa 647 (Thermo-Fisher A32733) 1:400; Goat anti-Rat Alexa 647 (Thermo-Fisher A48265 1:400); Donkey anti-Human Alexa 790 (Jackson Immunoresearch 709-655-149) 1:400. Muscles were stained with Phalloidin iFluor405 (Abcam AB176752) 1:800.

Confocal microscopy was performed using a Leica Stellaris DMI8 inverted confocal scanning light microscope in the microscopy facility at the Montana State University Center for Biofilm Engineering.

Expansion microscopy

The Ten-fold Robust Expansion Microscopy (TREx) protocol was used to expand the male ED (ED) (DAMSTRA et al. 2023). Briefly, Drosophila male reproductive systems were dissected and fixed for at least thirty minutes in 4% paraformaldehyde. The ED's were then dissected out and immunostained as described above. Tissues were then incubated in Acryloyl-X solution, 1:100 dilution (Invitrogen, catalog #2604348), overnight, at room temperature and protected from light. The next day, the ED's were rinsed in PBS and incubated in TRex solution at 4 C, for 45-60 minutes. 0.15% ammonium persulfate and 0.15% TEMED was added and the TREx mixture was quickly transferred to chamber slides. TREx mixture with ED's were placed in wells (1 ED per well), coverslipped and allowed to polymerize at 37 C for at least 45 minutes. After gel polymerization, each gel-ED was trimmed to eliminate excess gel. Gel-ED's were incubated in proteinase K (Biolabs, catalog #P81075, 800U/ml) 1:100 solution, overnight at room temperature. Expansion of gel-ED's was done the following day. Three washes in water were performed, at least 20 minutes per wash. DAPI (Thermofisher Scientific, catalog# D1306), 2ug/ml, was added in the first wash to aid in tissue visualization. After the third wash, hydrogel-ED's were trimmed again and placed in chamber slides. 1 hydrogel-ED per well and coverslipped. Imaged expanded ED's in upright confocal (Leica Stellaris 8 DIVE) equipped with a ×40 NA = 0.8 water objective. z Stack- images were deconvoluted using the Lightning confocal function and 3D images were generated for each image. ED's typically expanded approximately tenfold.

Colocalization Analysis

Digitally deconvolved- 3D images of expanded EDs were analyzed using ImageJ software (SCHINDELIN et al. 2012). To exclude background in an unbiased manner, we thresholded all images by using the Otsu threshold and calculated Manders' coefficients by using the BIOP JACop.plugin. A scatter plot of green and red pixel intensities

(associated with each of the two markers, Vmat and Vglut) was generated by using the colocalization function. Manders' coefficient ranges from 0 to 1, indicating no or complete colocalization. Prior to doing the colocalization analysis of each image, a region of interest (ROI) was traced using the stain from the CD8 marker. This ROI corresponded to an axon terminal.

Mating assays

Mating assays involved placing single 3–7-day old virgin males with single 3-7-day old virgin females in the same well of a 12 well tissue culture plate without anesthesia. The wells of the 12 well plates were half-filled with agarose. Flies were videotaped for three hours. Mating assays were conducted at 25C and 50% humidity in a room dedicated to behavioral assays. Mating was scored by viewing the videos and scorers were blind to the genotypes.

Fertility assays

The fertility assays involved placing single 5 day old or 30-day old virgin males with four 3-7-day old virgin females in fresh vials without anesthesia for six hours. After six hours the males were removed and the four females returned to the vials for 72hrs at which point the females were removed. Six days after removal of the females the pupae on the walls of the vials were counted. The counting was done blind to the genotypes. Fly culturing for all stages of the fertility assays were conducted at 25C and 50% in an incubator.

Animal use

All experiments involving *Drosophila melanogaster* were conducted in accordance with approved protocols and standard laboratory practices. *Drosophila melanogaster* is not considered a vertebrate animal and accordingly does not require Montana State University Institutional Animal Care and Use Committee (IACUC) approval.

Data availability

All plasmids and their complete sequences are available upon request. Fly strains original to this publication will be deposited at the Bloomington Drosophila Stock Center or made available upon request.

Acknowledgements

Stocks obtained from the Bloomington Drosophila Stock Center (NIH P40OD018537) were used in this study. Antibodies used in this study were obtained from the Developmental Studies Hybridoma Bank created by the NICHD of the NIH and maintained at The University of Iowa, Department of Biology. This work used a Leica Stellaris DMI8 inverted confocal scanning light microscope in the Center for Biofilm Engineering-Bioimaging and Analytical Cores, RRID:SCR_026519, which is supported by Montana State University. This work was supported by National Institutes of Health (NIH) grant 2R01GM115510 to SJC and RSS.

Figure Legends

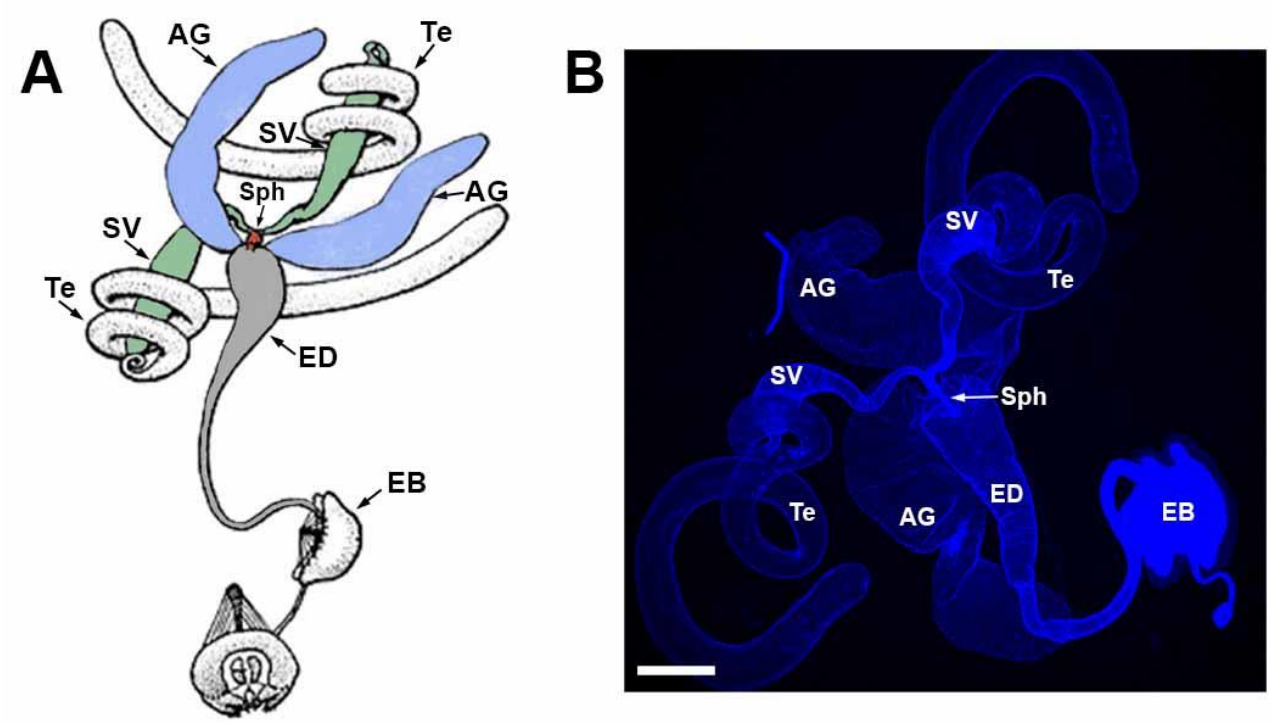

Figure 1. The Drosophila male reproductive system. A) schematic diagram showing paired testes, SVs (green), and AGs (purple), and a singular sphincter (red), ED (gray), and ejaculatory bulb. B) actual male reproductive system. Te-testes, SV-seminal vesicle, AG-accessory gland, Sph-sphincter, ED-ejaculatory duct, EB-ejaculatory bulb. Scale bar: 200μm.

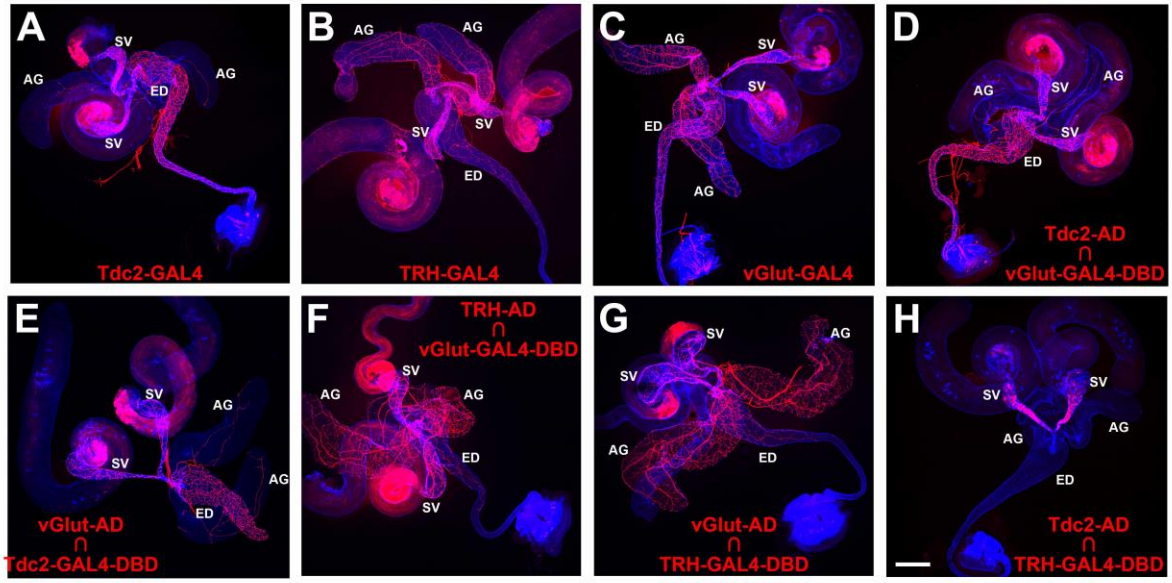

Figure 2. Gal4 and Split-GAL4 expression patterns in the Drosophila male reproductive system. A) *Tdc2-GAL4*; B) *TRH-GAL4*; C) vGlut-GAL4; D) Tdc2-AD ∩ *vGlut-GAL4-*

1211 *DBD*; E) *vGlut-AD* ∩ *Tdc2-GAL4-DBD*; F) *TRH-AD* ∩ *vGlut-GAL4-DBD*; G) *vGlut-AD* ∩
1212 *TRH-GAL4-DBD*; H) *Tdc2-AD* ∩ *TRH-GAL4-DBD*. Scale bar: 200μm.
1213
1214 **Figure 3.** Expression of *TRH-GAL4* and *Tdc2-LexA* in the Drosophila male
1215 reproductive system. A, D, G, J, M, P) *TRH-GAL4*, *UAS-6XGFP*; B, E, H, K, N, Q)
1216 *Tdc2-LexA*, *LexAop-6XmCherry*. C, F, I, L, O, R) overlay. Scale bars: O-50μm; R-
1217 10μm.

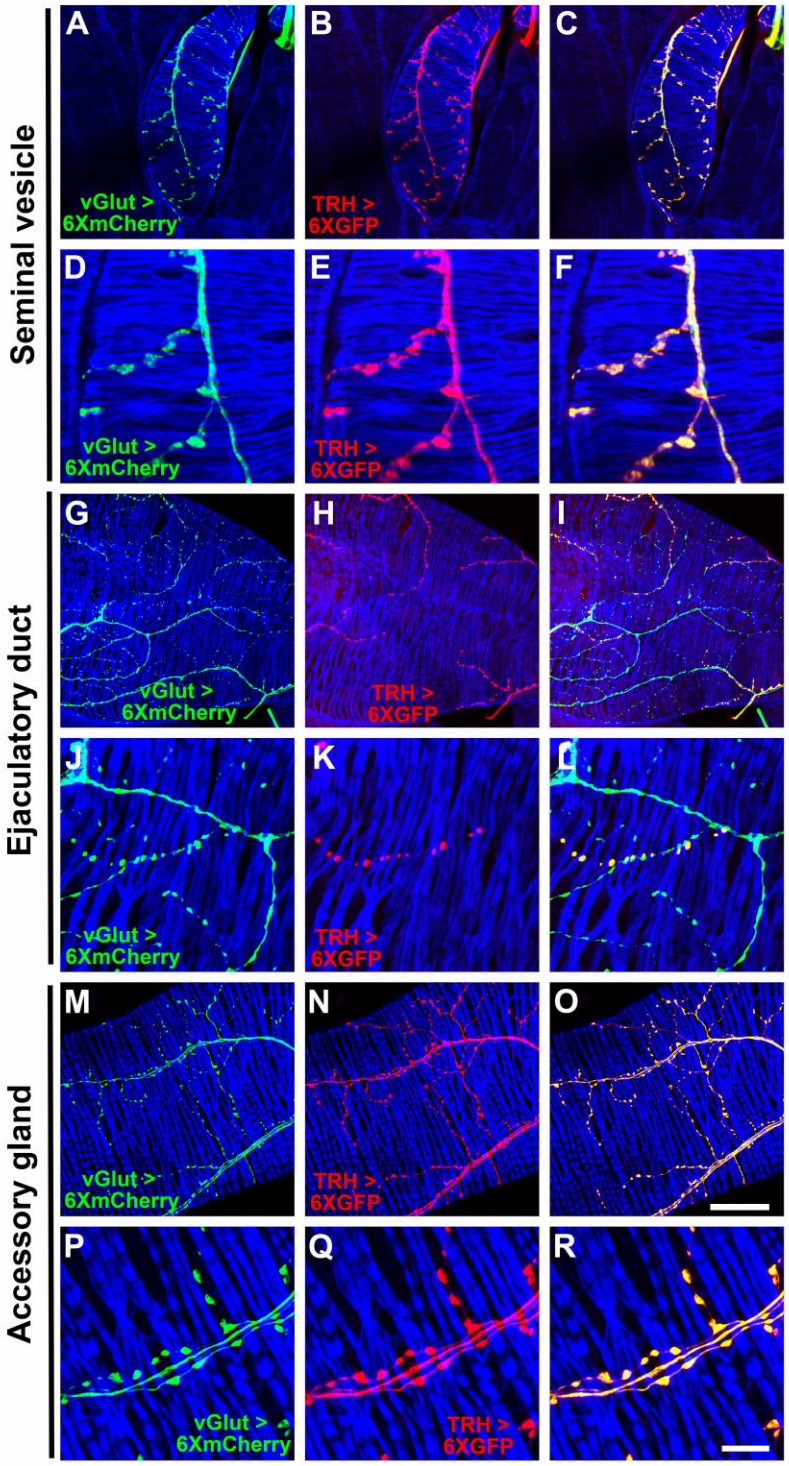
Seminal vesicle
Ejaculatory duct
Accessory gland
A
B
C
D
E
F
G
H
I
J
K
L
M
N
O
P
Q
R
vGlut >
6XmCherry
TRH >
6XGFP

1218

1219 **Figure 3S1.** Expression of *vGlut-LexA* and *TRH-GAL4* in the Drosophila male
1220 reproductive system. A, D, G, J, M, P) *vGlut-LexA*, *LexAop-6XmCherry*; B, E, H, K, N,
1221 Q) *TRH-GAL4*, *UAS-6XGFP*. C, F, I, L, O, R) overlay. Scale bars: O-50μm; R-10μm.

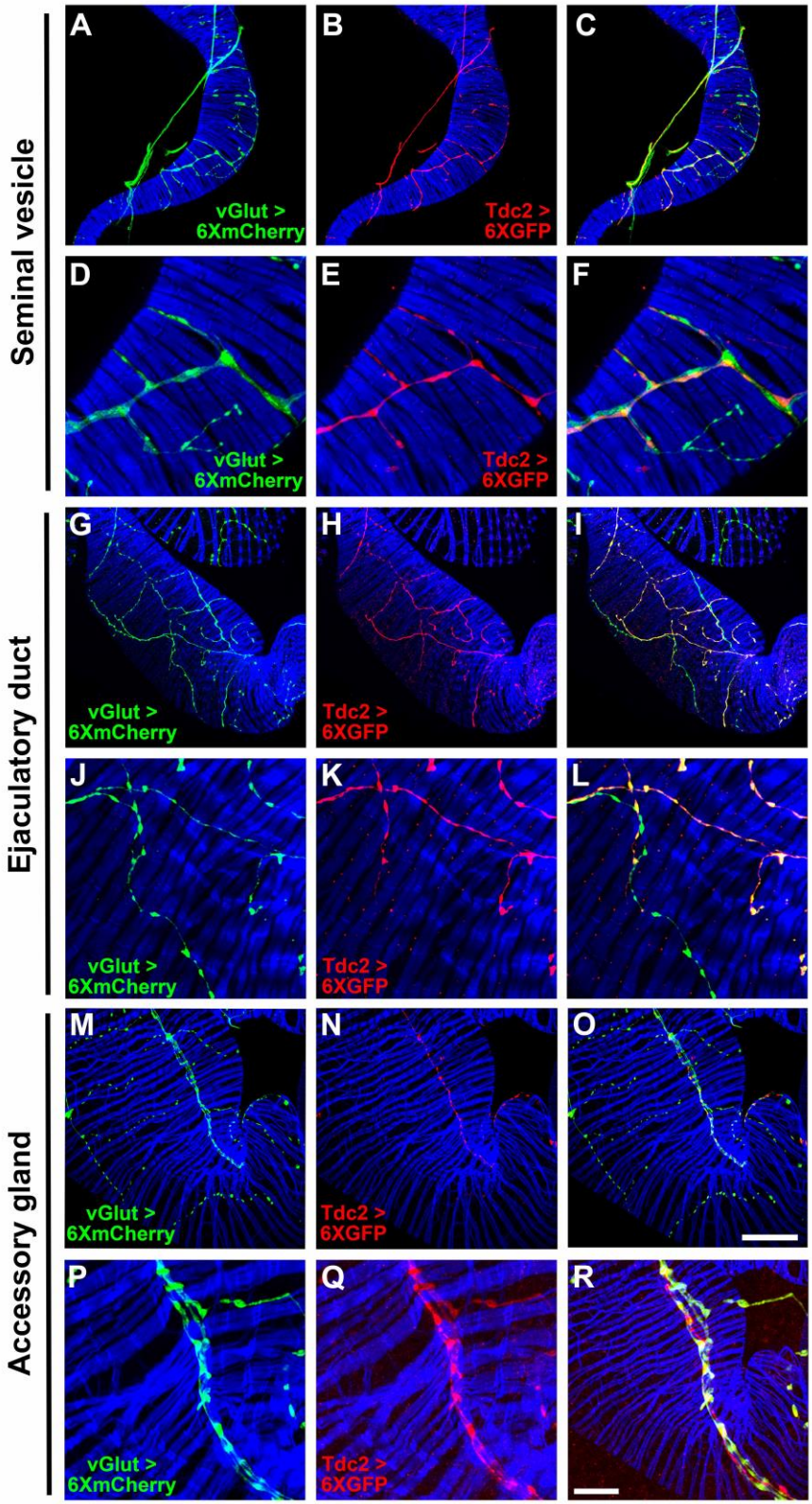
Seminal vesicle
Ejaculatory duct
Accessory gland
A
B
C
D
E
F
G
H
I
J
K
L
M
N
O
P
Q
R
vGlut >
6XmCherry
Tdc2 >
6XGFP

1222

1223 **Figure 3S2.** Expression of *vGlut-LexA* and *Tdc2-GAL4* in the Drosophila male
1224 reproductive system. A, D, G, J, M, P) *vGlut-LexA*; B, E, H, K, N, Q) *Tdc2-GAL4*,
1225 *LexAop-6XmCherry*. C, F, I, L, O, R) overlay. Scale bars: O-50μm; R-10μm.

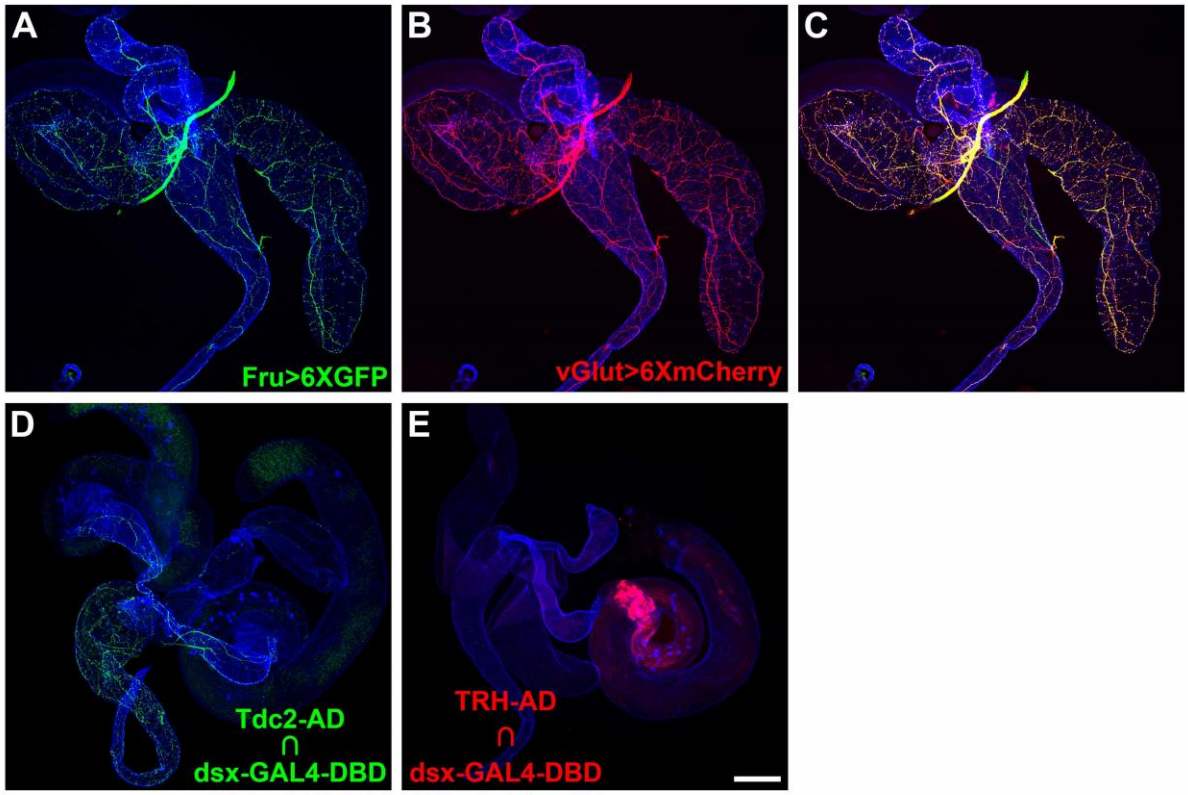

1226
1227 **Figure 3S3.** Fruitless and Doublesex expression in the Drosophila male reproductive
1228 system. A) *fru-GAL4*, *UAS-6XGFP*; B) *vGlut-LexA*, *LexAop-6XmCherry*; C) overlay; D)
1229 Tdc2-AD ∩ dsx-GAL4; E) TRH-AD ∩ dsx-GAL4. Scale bar: 200μm.

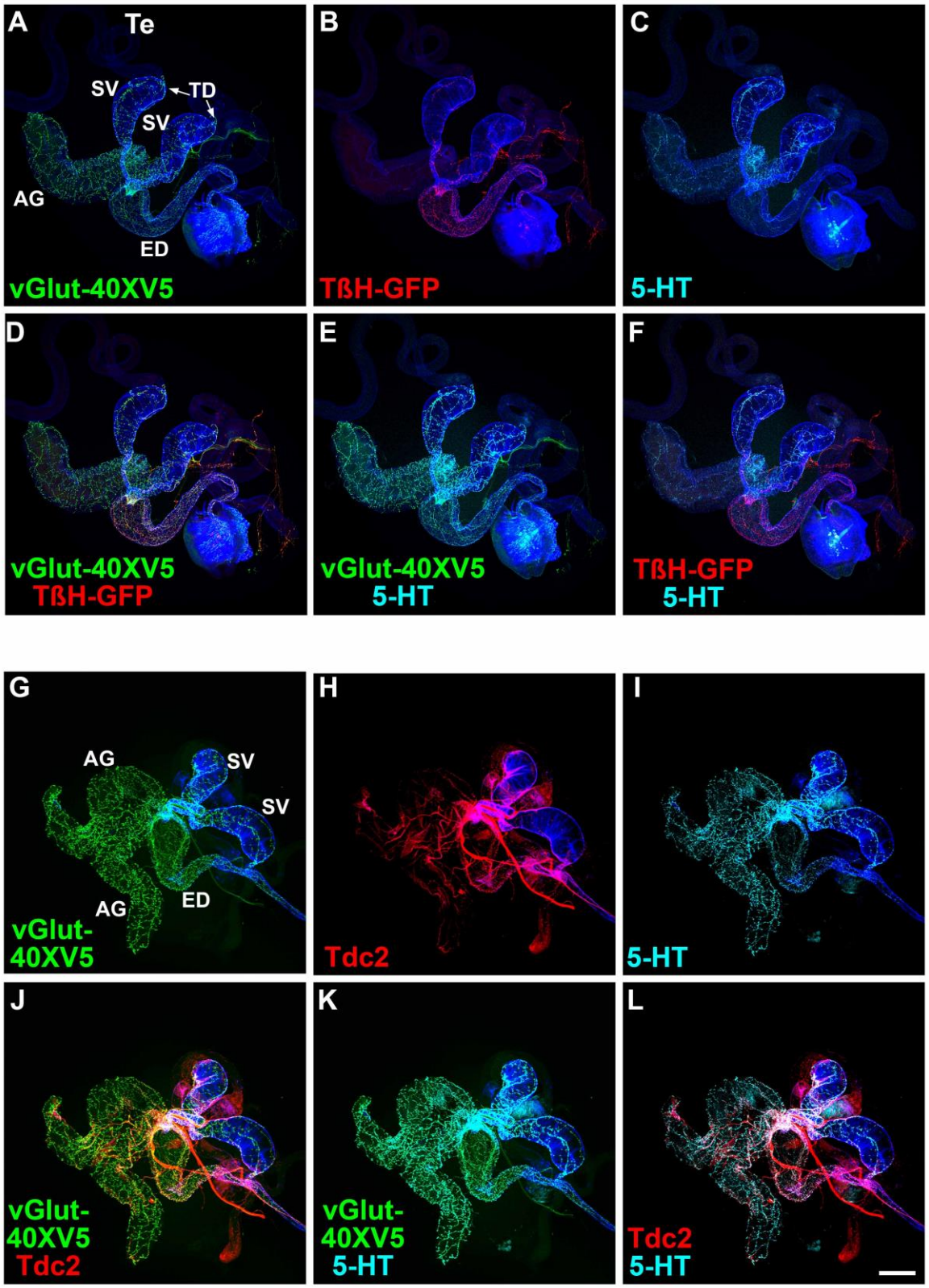
A
Te
SV
TD
SV
AG
ED
vGlut-40XV5
B
TßH-GFP
C
5-HT
D
vGlut-40XV5
TßH-GFP
E
vGlut-40XV5
5-HT
F
TßH-GFP
5-HT
G
AG
SV
SV
AG
ED
vGlut-
40XV5
H
Tdc2
I
5-HT
J
vGlut-
40XV5
Tdc2
K
vGlut-
40XV5
5-HT
L
Tdc2
5-HT

1230

1231 **Figure 4.** Expression of vGlut, TβH-GFP, Tdc2, and 5-HT in the Drosophila male
1232 reproductive system. A) vGlut-40XV5; B) TβH-GFP; C) 5-HT; D) vGlut-40XV5, TβH-
1233 GFP overlay; E) vGlut-40XV5, 5-HT overlay; F) TβH-GFP, 5-HT overlay. G) vGlut-
1234 40XV5; H) Tdc2; I) 5-HT; J) vGlut-40XV5, Tdc2 overlay; K) vGlut-40XV5, 5-HT overlay;
1235 L) Tdc2, 5-HT overlay. Scale bar: 200μm.

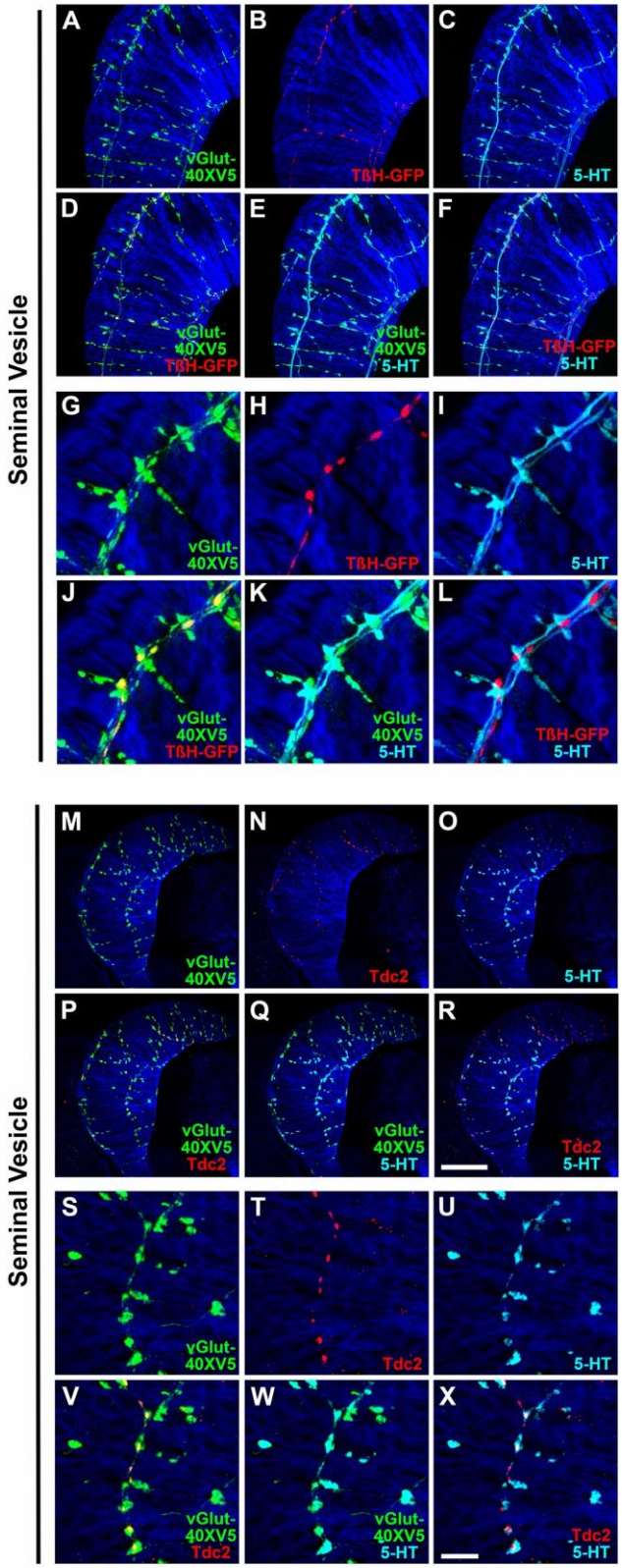
Seminal Vesicle
A
vGlut-
40XV5
B
TßH-GFP
C
5-HT
D
vGlut-
40XV5
TßH-GFP
E
vGlut-
40XV5
5-HT
F
TßH-GFP
5-HT
G
vGlut-
40XV5
H
TßH-GFP
I
5-HT
J
vGlut-
40XV5
TßH-GFP
K
vGlut-
40XV5
5-HT
L
TßH-GFP
5-HT
Seminal Vesicle
M
vGlut-
40XV5
N
Tdc2
O
5-HT
P
vGlut-
40XV5
Tdc2
Q
vGlut-
40XV5
5-HT
R
Tdc2
5-HT
S
vGlut-
40XV5
T
Tdc2
U
5-HT
V
vGlut-
40XV5
Tdc2
W
vGlut-
40XV5
5-HT
X
Tdc2
5-HT

1236

1237 **Figure 4S1.** Expression of vGlut, TβH-GFP, Tdc2, and 5-HT in the SV of the Drosophila
1238 male reproductive system. A, G) vGlut-40XV5; B, H) TβH-GFP; C, I) 5-HT; D, J) vGlut-
1239 40XV5, TβH-GFP overlay; E, K) vGlut-40XV5, 5-HT overlay; F, L) TβH-GFP, 5-HT
1240 overlay; M, S) vGlut-40XV5; N, T) Tdc2; O, U) 5-HT; P, V) vGlut-40XV5, Tdc2 overlay;
1241 Q, W) vGlut-40XV5, 5-HT overlay; R, X) Tdc2, 5-HT overlay. Scale bars: R-50μm; X-
1242 10μm.

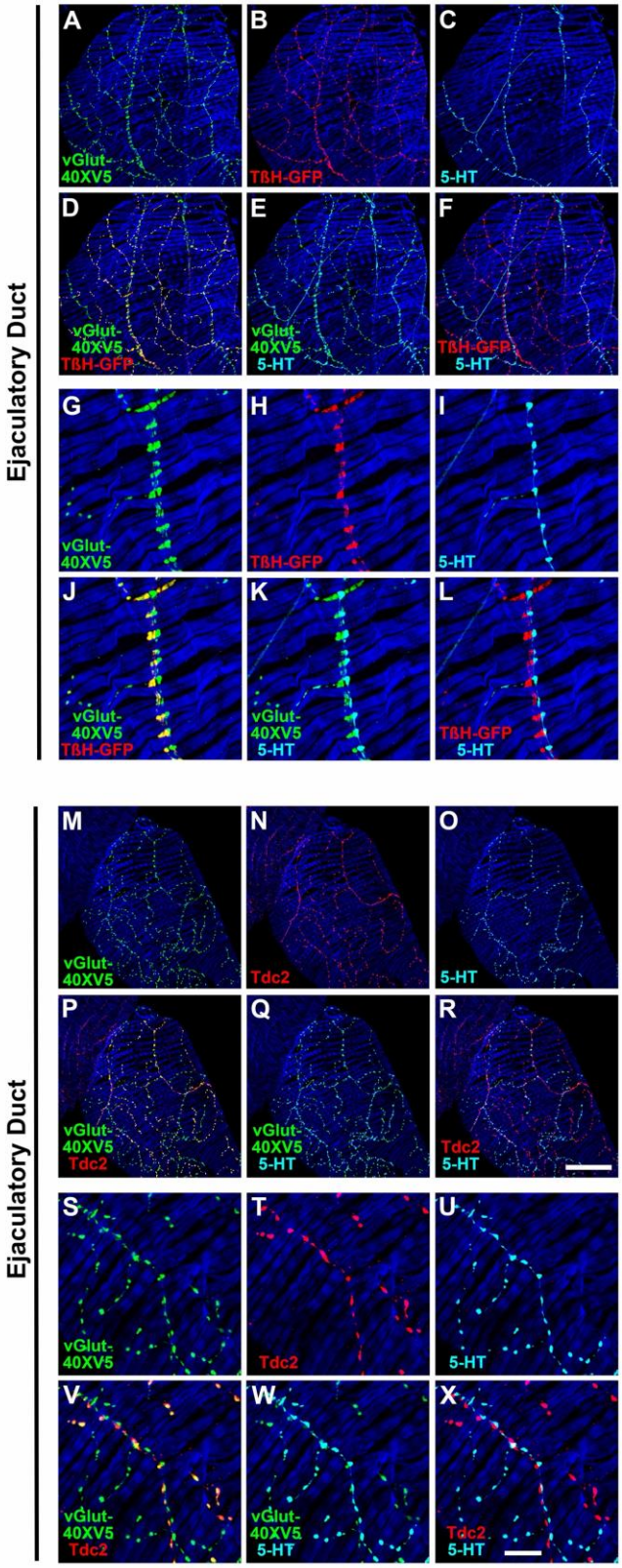
Ejaculatory Duct
A
vGlut-
40XV5
B
TßH-GFP
C
5-HT
D
vGlut-
40XV5
TßH-GFP
E
vGlut-
40XV5
5-HT
F
TßH-GFP
5-HT
G
vGlut-
40XV5
H
TßH-GFP
I
5-HT
J
vGlut-
40XV5
TßH-GFP
K
vGlut-
40XV5
5-HT
L
TßH-GFP
5-HT
Ejaculatory Duct
M
vGlut-
40XV5
N
Tdc2
O
5-HT
P
vGlut-
40XV5
Tdc2
Q
vGlut-
40XV5
5-HT
R
Tdc2
5-HT
S
vGlut-
40XV5
T
Tdc2
U
5-HT
V
vGlut-
40XV5
Tdc2
W
vGlut-
40XV5
5-HT
X
Tdc2
5-HT

1243

1244 **Figure 4S2.** Expression of vGlut, TβH-GFP, Tdc2, and 5-HT in the ED of the Drosophila
1245 male reproductive system. A, G) vGlut-40XV5; B, H) TβH-GFP; C, I) 5-HT; D, J) vGlut-
1246 40XV5, TβH-GFP overlay; E, K) vGlut-40XV5, 5-HT overlay; F, L) TβH-GFP, 5-HT
1247 overlay; M, S) vGlut-40XV5; N, T) Tdc2; O, U) 5-HT; P, V) vGlut-40XV5, Tdc2 overlay;
1248 Q, W) vGlut-40XV5, 5-HT overlay; R, X) Tdc2, 5-HT overlay. Scale bars: R-50μm; X-
1249 10μm.

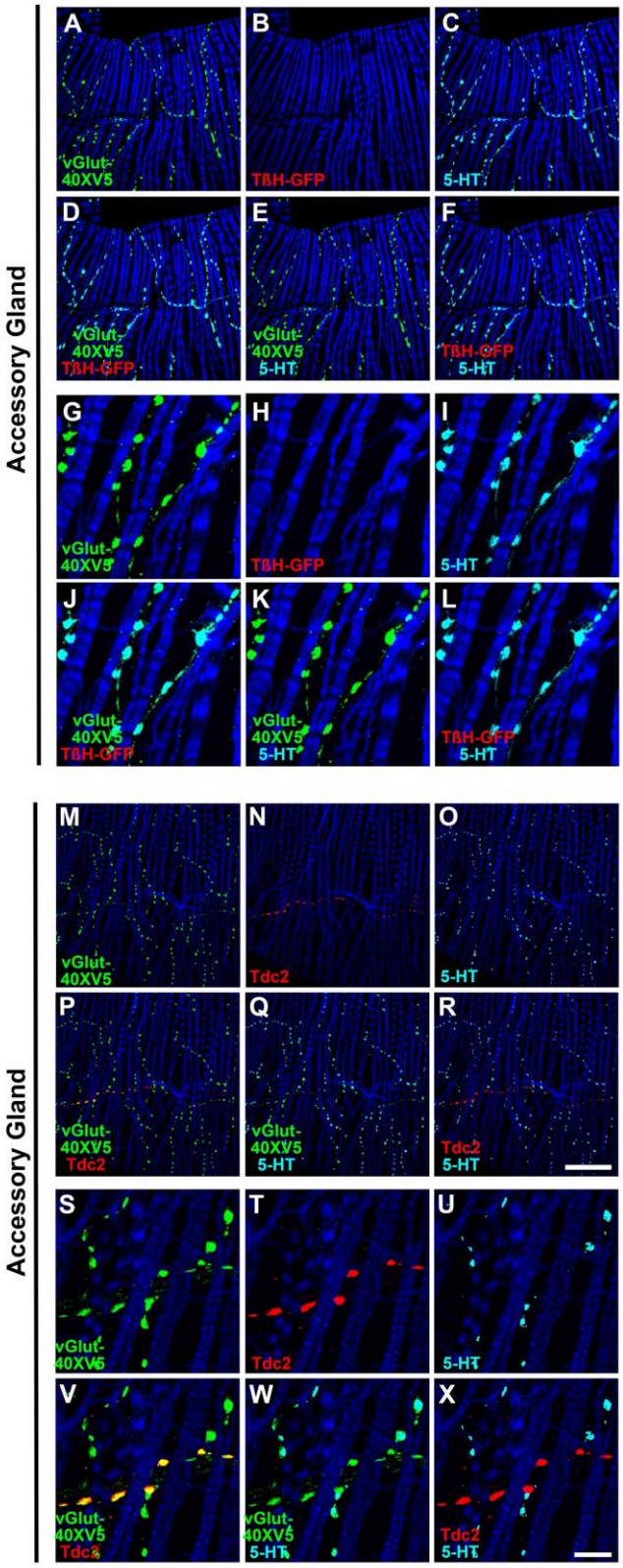
Accessory Gland
A
vGlut-
40XV5
B
TβH-GFP
C
5-HT
D
vGlut-
40XV5
TβH-GFP
E
vGlut-
40XV5
5-HT
F
TβH-GFP
5-HT
G
vGlut-
40XV5
H
TβH-GFP
I
5-HT
J
vGlut-
40XV5
TβH-GFP
K
vGlut-
40XV5
5-HT
L
TβH-GFP
5-HT
Accessory Gland
M
vGlut-
40XV5
N
Tdc2
O
5-HT
P
vGlut-
40XV5
Tdc2
Q
vGlut-
40XV5
5-HT
R
Tdc2
5-HT
S
vGlut-
40XV5
T
Tdc2
U
5-HT
V
vGlut-
40XV5
Tdc2
W
vGlut-
40XV5
5-HT
X
Tdc2
5-HT

1250

1251 **Figure 4S3.** Expression of vGlut, TβH-GFP, Tdc2, and 5-HT in the AG of the Drosophila
1252 male reproductive system. A, G) vGlut-40XV5; B, H) TβH-GFP; C, I) 5-HT; D, J) vGlut-
1253 40XV5, TβH-GFP overlay; E, K) vGlut-40XV5, 5-HT overlay; F, L) TβH-GFP, 5-HT
1254 overlay; M, S) vGlut-40XV5; N, T) Tdc2; O, U) 5-HT; P, V) vGlut-40XV5, Tdc2 overlay;
1255 Q, W) vGlut-40XV5, 5-HT overlay; R, X) Tdc2, 5-HT overlay. Scale bars: R-50μm; X-
1256 10μm.

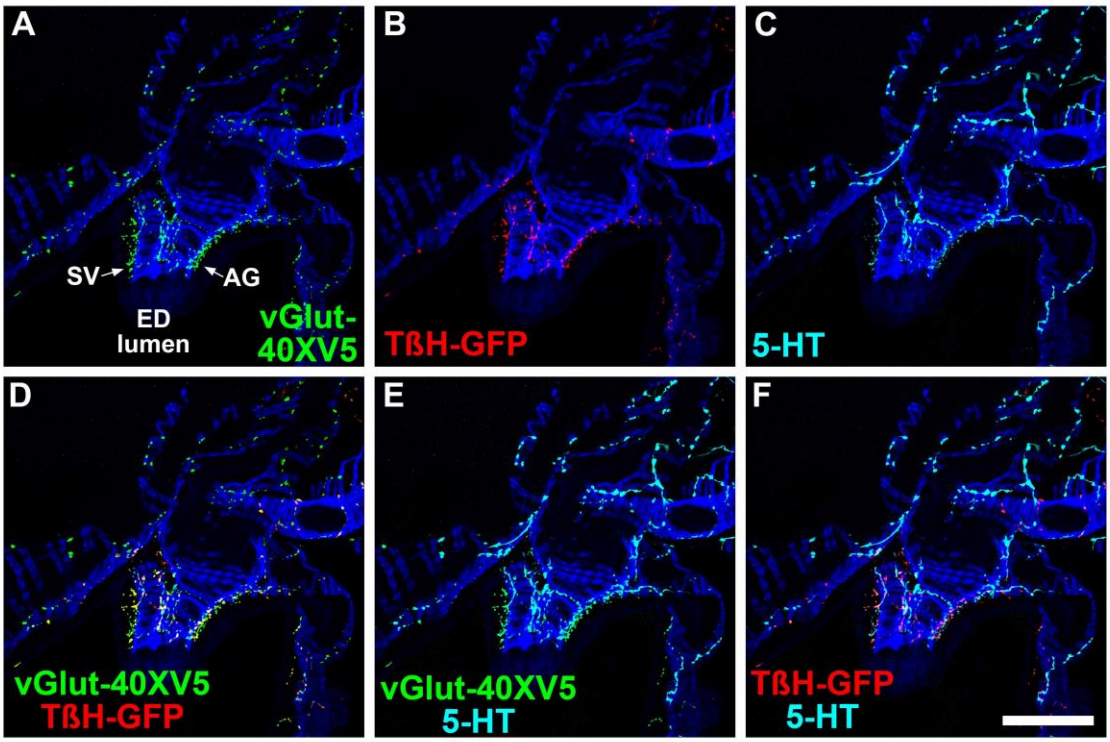

1257
1258 **Figure 4S4.** Expression of vGlut, TβH-GFP, and 5-HT at the junction of the SV and
1259 AGs with the ED of the Drosophila male reproductive system. A) vGlut-40XV5; B) TβH-
1260 GFP; C) 5-HT; D) vGlut-40XV5, TβH-GFP overlay; E) vGlut-40XV5, 5-HT overlay; F)
1261 TβH-GFP, 5-HT overlay. A) vGlut-40XV5; B) Tdc2; C) 5-HT; D) vGlut-40XV5, Tdc2
1262 overlay; E) vGlut-40XV5, 5-HT overlay; F) Tdc2, 5-HT overlay. Scale bar: 50μm.

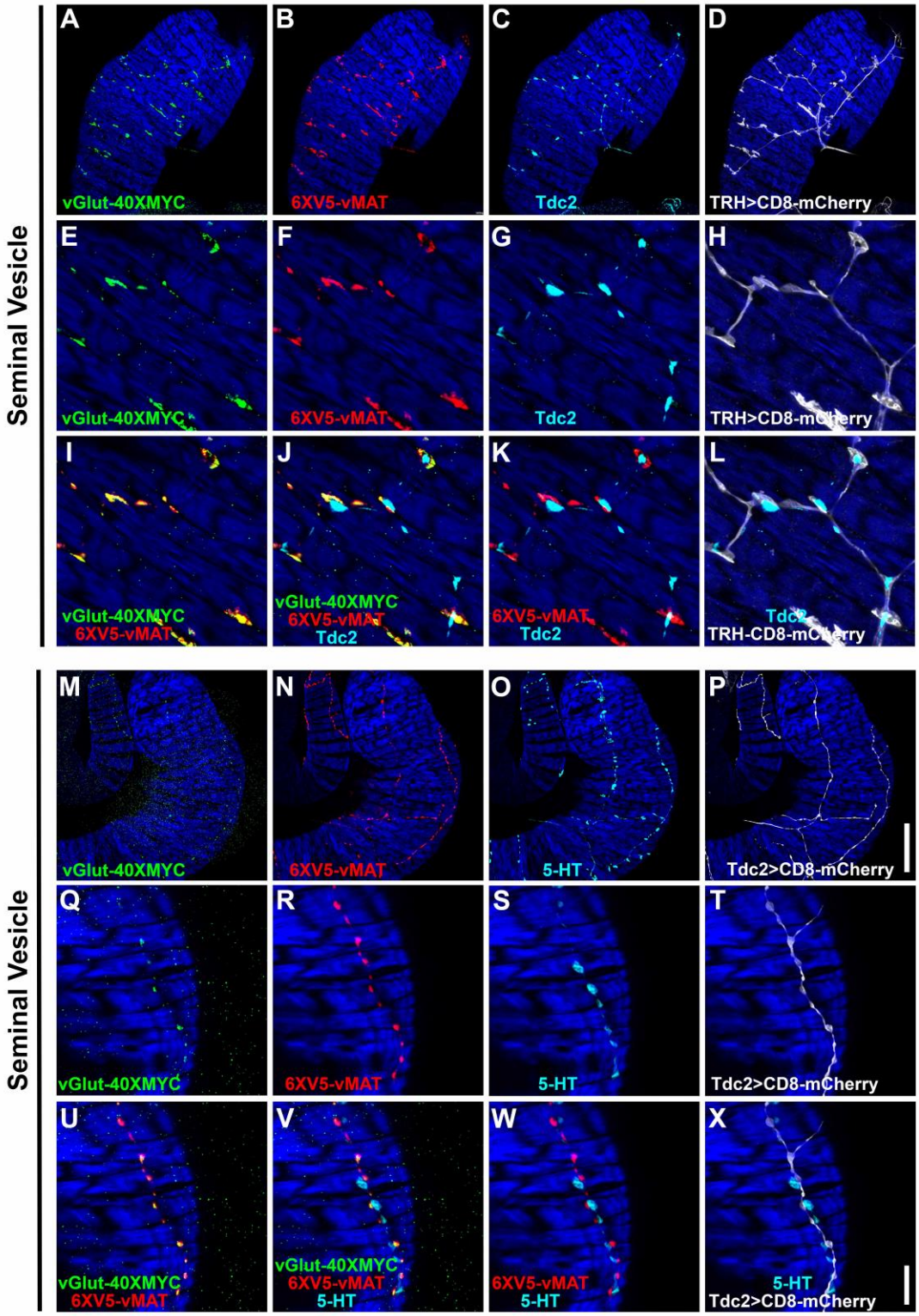
Seminal Vesicle
A
vGlut-40XMYC
B
6XV5-vMAT
C
Tdc2
D
TRH>CD8-mCherry
E
vGlut-40XMYC
F
6XV5-vMAT
G
Tdc2
H
TRH>CD8-mCherry
I
vGlut-40XMYC
6XV5-vMAT
J
vGlut-40XMYC
6XV5-vMAT
Tdc2
K
6XV5-vMAT
Tdc2
L
Tdc2
TRH-CD8-mCherry
Seminal Vesicle
M
vGlut-40XMYC
N
6XV5-vMAT
O
5-HT
P
Tdc2>CD8-mCherry
Q
vGlut-40XMYC
R
6XV5-vMAT
S
5-HT
T
Tdc2>CD8-mCherry
U
vGlut-40XMYC
6XV5-vMAT
V
vGlut-40XMYC
6XV5-vMAT
5-HT
W
6XV5-vMAT
5-HT
X
5-HT
Tdc2>CD8-mCherry

1263

1264 **Figure 5.** Co-conditional expression of vGlut-40XMYC and 6XV5-vMAT in the SV of
1265 serotonergic (TRH) or octopaminergic (Tdc2) neurons of the Drosophila male
1266 reproductive system. A-D) 63X. A) vGlut-40XMYC; B) 6XV5-vMAT; C) Tdc2; D)
1267 TRH>CD8-mCherry. E-L) 63X zoom 4X. E) vGlut-40XMYC; F) 6XV5-vMAT; G) Tdc2;
1268 H) TRH>CD8-mCherry; I) vGlut-40XMYC, 6XV5-vMAT overlay; J) vGlut-40XMYC,
1269 6XV5-vMAT, Tdc2 overlay; K) 6XV5-vMAT, Tdc2 overlay; L) Tdc2, TRH>CD8-mCherry
1270 overlay. M-P) 63X. M) vGlut-40XMYC; N) 6XV5-vMAT; O) 5-HT; P) Tdc2>CD8-
1271 mCherry. Q-X) 63X zoom 4X. Q) vGlut-40XMYC; R) 6XV5-vMAT; S) 5-HT; T)
1272 Tdc2>CD8-mCherry; U) vGlut-40XMYC, 6XV5-vMAT overlay; V) vGlut-40XMYC, 6XV5-
1273 vMAT, 5-HT overlay; W) 6XV5-vMAT, 5-HT overlay; X) Tdc2, Tdc2>CD8-mCherry
1274 overlay. Scale bars: P-50μm; X-10μm.

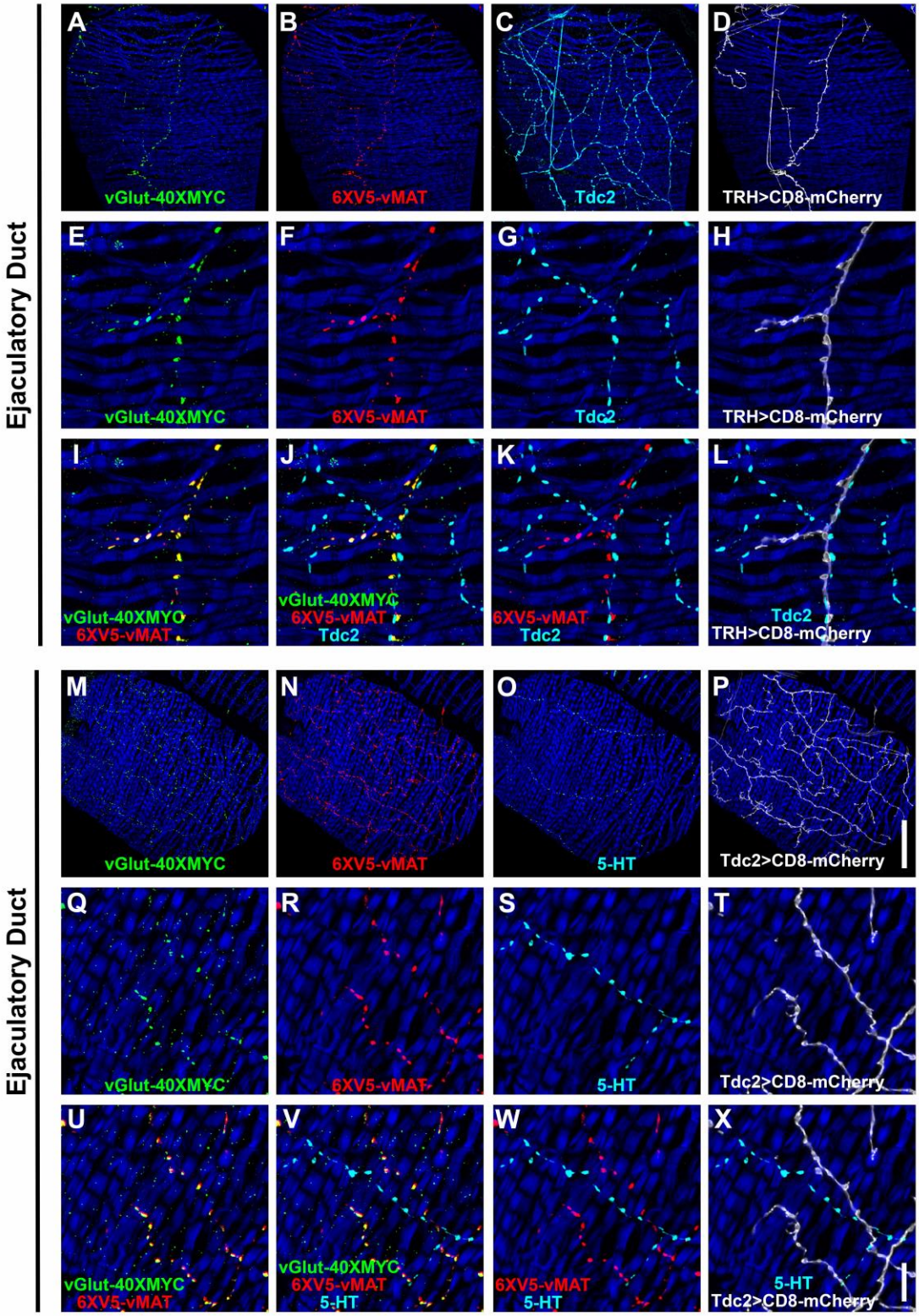
Ejaculatory Duct
A
vGlut-40XMYC
B
6XV5-vMAT
C
Tdc2
D
TRH>CD8-mCherry
E
vGlut-40XMYC
F
6XV5-vMAT
G
Tdc2
H
TRH>CD8-mCherry
I
vGlut-40XMYC
6XV5-vMAT
J
vGlut-40XMYC
6XV5-vMAT
Tdc2
K
6XV5-vMAT
Tdc2
L
Tdc2
TRH>CD8-mCherry
Ejaculatory Duct
M
vGlut-40XMYC
N
6XV5-vMAT
O
5-HT
P
Tdc2>CD8-mCherry
Q
vGlut-40XMYC
R
6XV5-vMAT
S
5-HT
T
Tdc2>CD8-mCherry
U
vGlut-40XMYC
6XV5-vMAT
V
vGlut-40XMYC
6XV5-vMAT
5-HT
W
6XV5-vMAT
5-HT
X
5-HT
Tdc2>CD8-mCherry

1275

1276 **Figure 5S1.** Co-conditional expression of vGlut-40XMYC and 6XV5-vMAT in the ED of
1277 serotonergic (TRH) or octopaminergic (Tdc2) neurons of the Drosophila male
1278 reproductive system. A-D) 63X. A) vGlut-40XMYC; B) 6XV5-vMAT; C) Tdc2; D)
1279 TRH>CD8-mCherry. E-L) 63X zoom 4X. E) vGlut-40XMYC; F) 6XV5-vMAT; G) Tdc2;
1280 H) TRH>CD8-mCherry; I) vGlut-40XMYC, 6XV5-vMAT overlay; J) vGlut-40XMYC,
1281 6XV5-vMAT, Tdc2 overlay; K) 6XV5-vMAT, Tdc2 overlay; L) Tdc2, TRH>CD8-mCherry
1282 overlay. M-P) 63X. M) vGlut-40XMYC; N) 6XV5-vMAT; O) 5-HT; P) Tdc2>CD8-
1283 mCherry. Q-X) 63X zoom 4X. Q) vGlut-40XMYC; R) 6XV5-vMAT; S) 5-HT; T)
1284 Tdc2>CD8-mCherry; U) vGlut-40XMYC, 6XV5-vMAT overlay; V) vGlut-40XMYC, 6XV5-
1285 vMAT, 5-HT overlay; W) 6XV5-vMAT, 5-HT overlay; X) Tdc2, Tdc2>CD8-mCherry
1286 overlay. Scale bars: P-50μm; X-10μm.

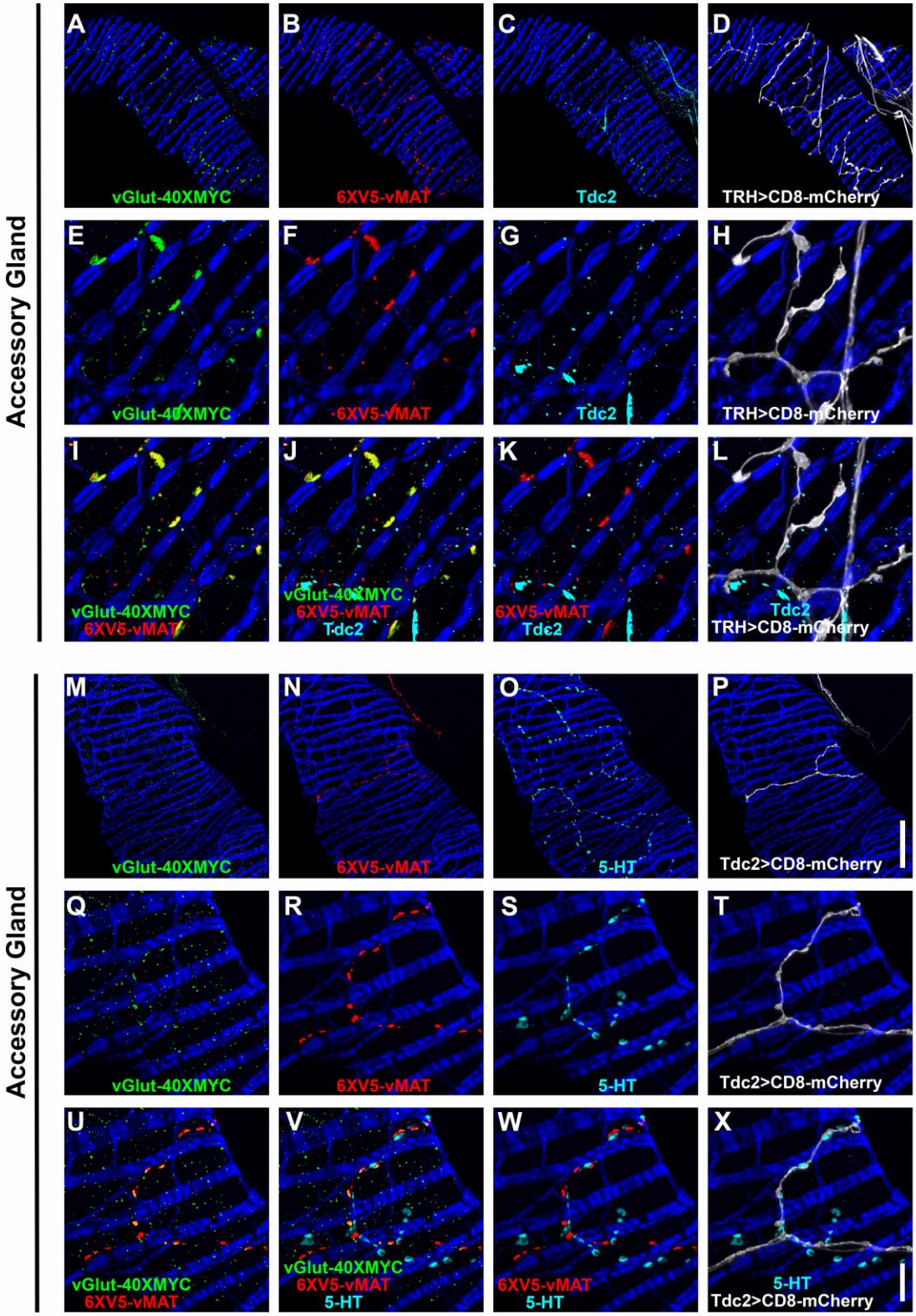
Accessory Gland
A
vGlut-40XMYC
B
6XV5-vMAT
C
Tdc2
D
TRH>CD8-mCherry
E
vGlut-40XMYC
F
6XV5-vMAT
G
Tdc2
H
TRH>CD8-mCherry
I
vGlut-40XMYC
6XV5-vMAT
J
vGlut-40XMYC
6XV5-vMAT
Tdc2
K
6XV5-vMAT
Tdc2
L
Tdc2
TRH>CD8-mCherry
Accessory Gland
M
vGlut-40XMYC
N
6XV5-vMAT
O
5-HT
P
Tdc2>CD8-mCherry
Q
vGlut-40XMYC
R
6XV5-vMAT
S
5-HT
T
Tdc2>CD8-mCherry
U
vGlut-40XMYC
6XV5-vMAT
V
vGlut-40XMYC
6XV5-vMAT
5-HT
W
6XV5-vMAT
5-HT
X
5-HT
Tdc2>CD8-mCherry

1287

Figure 5S2. Co-conditional expression of vGlut-40XMYC and 6XV5-vMAT in the AG of serotonergic (TRH) or octopaminergic (Tdc2) neurons of the Drosophila male reproductive system. A-D) 63X. A) vGlut-40XMYC; B) 6XV5-vMAT; C) Tdc2; D) TRH>CD8-mCherry. E-L) 63X zoom 4X. E) vGlut-40XMYC; F) 6XV5-vMAT; G) Tdc2; H) TRH>CD8-mCherry; I) vGlut-40XMYC, 6XV5-vMAT overlay; J) vGlut-40XMYC, 6XV5-vMAT, Tdc2 overlay; K) 6XV5-vMAT, Tdc2 overlay; L) Tdc2, TRH>CD8-mCherry overlay. M-P) 63X. M) vGlut-40XMYC; N) 6XV5-vMAT; O) 5-HT; P) Tdc2>CD8-mCherry. Q-X) 63X zoom 4X. Q) vGlut-40XMYC; R) 6XV5-vMAT; S) 5-HT; T) Tdc2>CD8-mCherry; U) vGlut-40XMYC, 6XV5-vMAT overlay; V) vGlut-40XMYC, 6XV5-vMAT, 5-HT overlay; W) 6XV5-vMAT, 5-HT overlay; X) Tdc2, Tdc2>CD8-mCherry overlay. Scale bars: P-50μm; X-10μm.

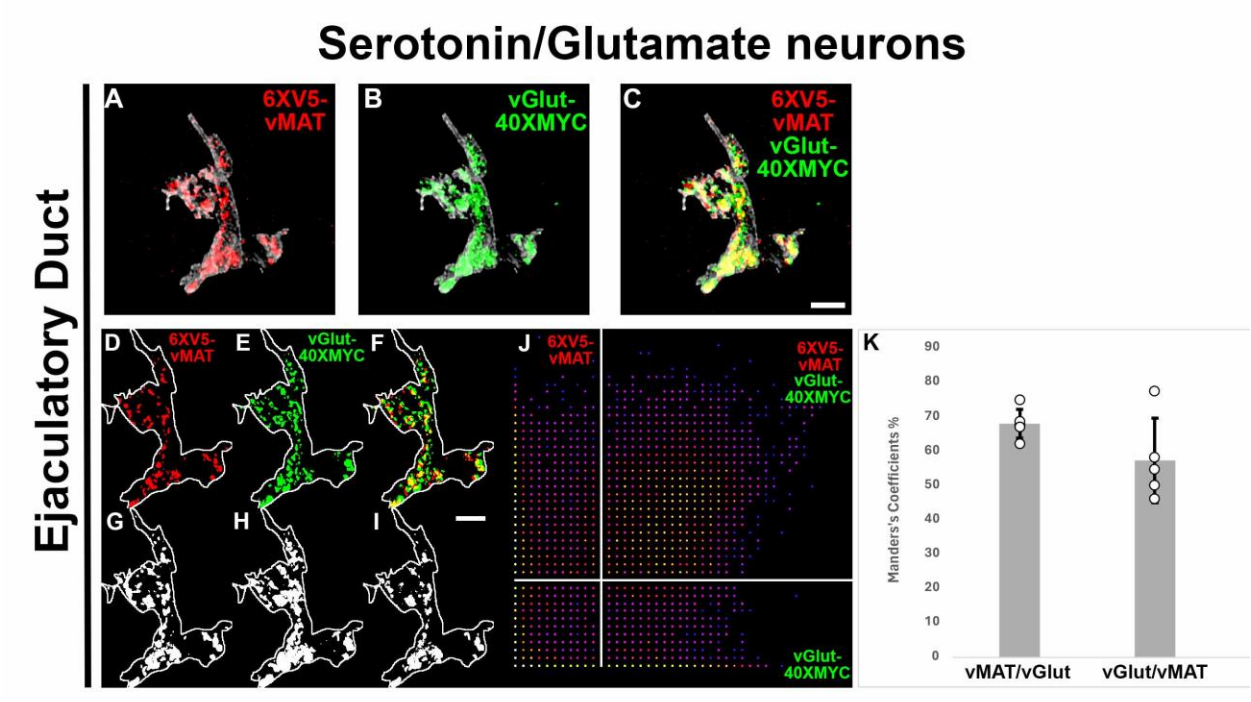

Figure 5S3. Co-conditional expression of vGlut-40XMYC and 6XV5-vMAT in serotonergic neurons of the Drosophila ED using expansion microscopy. A, D) 6XV5-vMAT; B, E) vGlut-40XMYC; C, F) overlay. A-C) 6XV5-vMAT and vGlut-40XMYC expression above the threshold intensity values. D-F) Complete 6XV5-vMAT and vGlut-40XMYC expression. G) Mander's plot of 6XV5-vMAT and vGlut-40XMYC. Vertical line indicates intensity threshold value for 6XV5-vMAT. Horizontal line indicates intensity threshold value for vGlut-40XMYC. H) Mander's coefficients. Grayscale signal in A-C) denotes the CD8-mCherry plasma membrane marker. Scale bars: 500nm. Scale bars have been corrected by 10X to reflect the empirically determined 10.5X expansion factor.

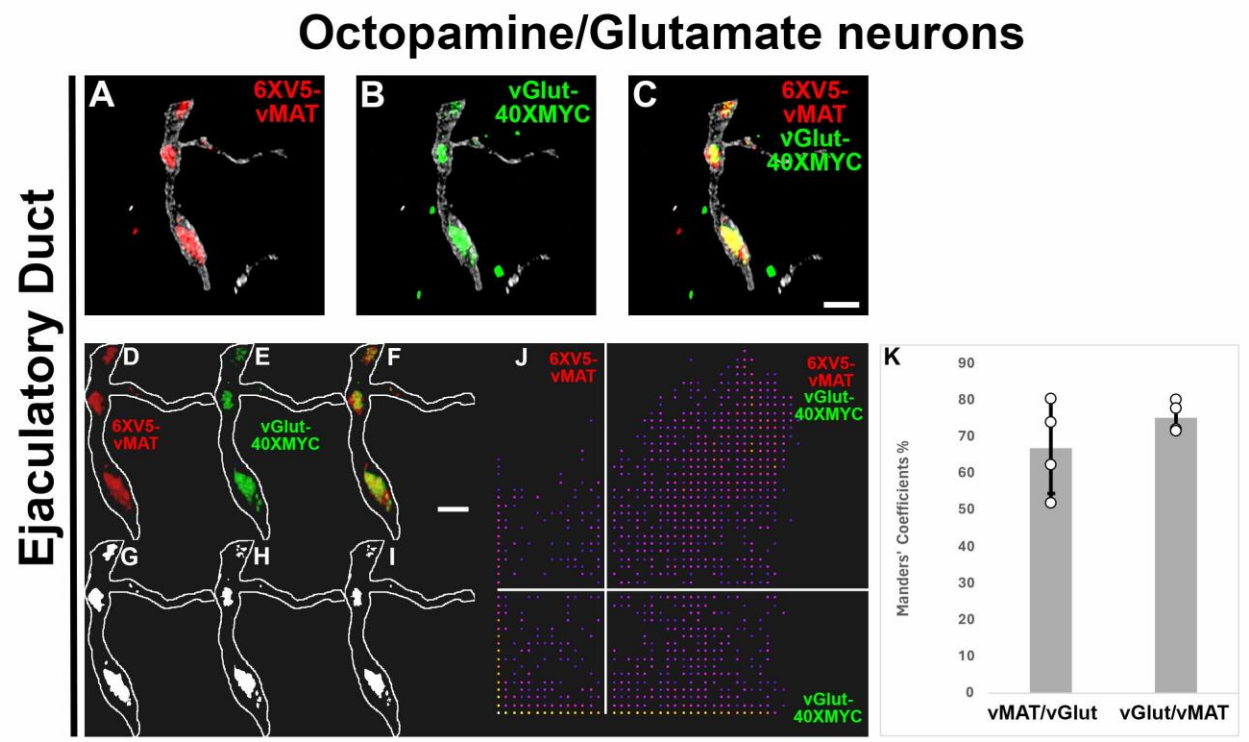

Figure 5S4. Co-conditional expression of vGlut-40XMYC and 6XV5-vMAT in octopaminergic neurons of the Drosophila ED using expansion microscopy. A, D) 6XV5-vMAT; B, E) vGlut-40XMYC; C, F) overlay. A-C) 6XV5-vMAT and vGlut-40XMYC expression above the threshold intensity values. D-F) Complete 6XV5-vMAT and vGlut-40XMYC expression. G) Mander's plot of 6XV5-vMAT and vGlut-40XMYC. Vertical line indicates intensity threshold value for 6XV5-vMAT. Horizontal line indicates intensity threshold value for vGlut-40XMYC. H) Mander's coefficients. Grayscale signal in A-C) denotes the CD8-mCherry plasma membrane marker. Scale bars: 500nm. Scale bars have been corrected by 10X to reflect the empirically determined 10.5X expansion factor.

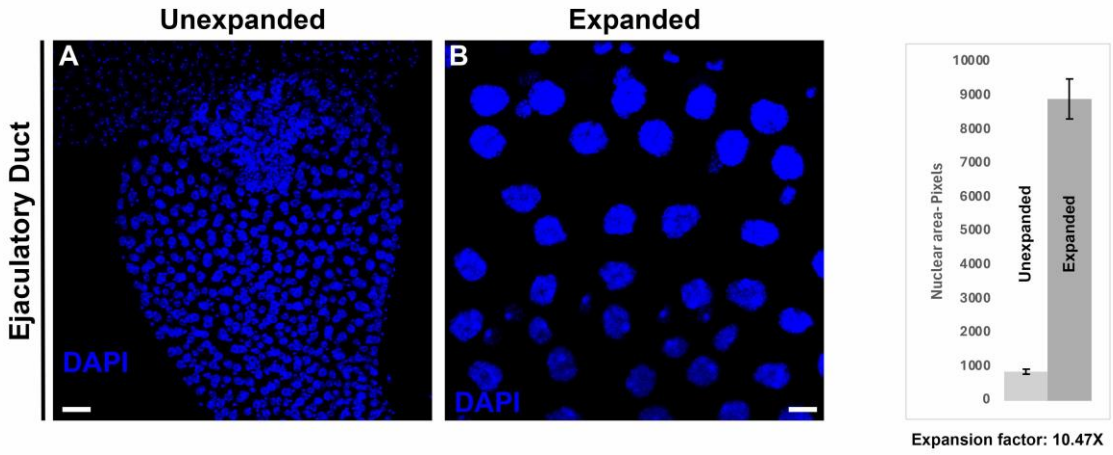

1322 **Figure 5S5.** Nuclei of unexpanded and expanded EDs. A) DAPI-stained nuclei from an
1323 unexpanded ED. B) DAPI-stained nuclei of an expanded ED. C) Bar graph plot of
1324 nuclei area (mean ± SE-black bars). For the experiment shown the calculated
1325 expansion factor (post-ExM nuclear area/pre-ExM nuclear area) was 10.47, p-value <
1326 0.00001. Fij/ImageJi open-source software was used to segment images and calculate
1327 nuclear area. Scale bars: 25um.

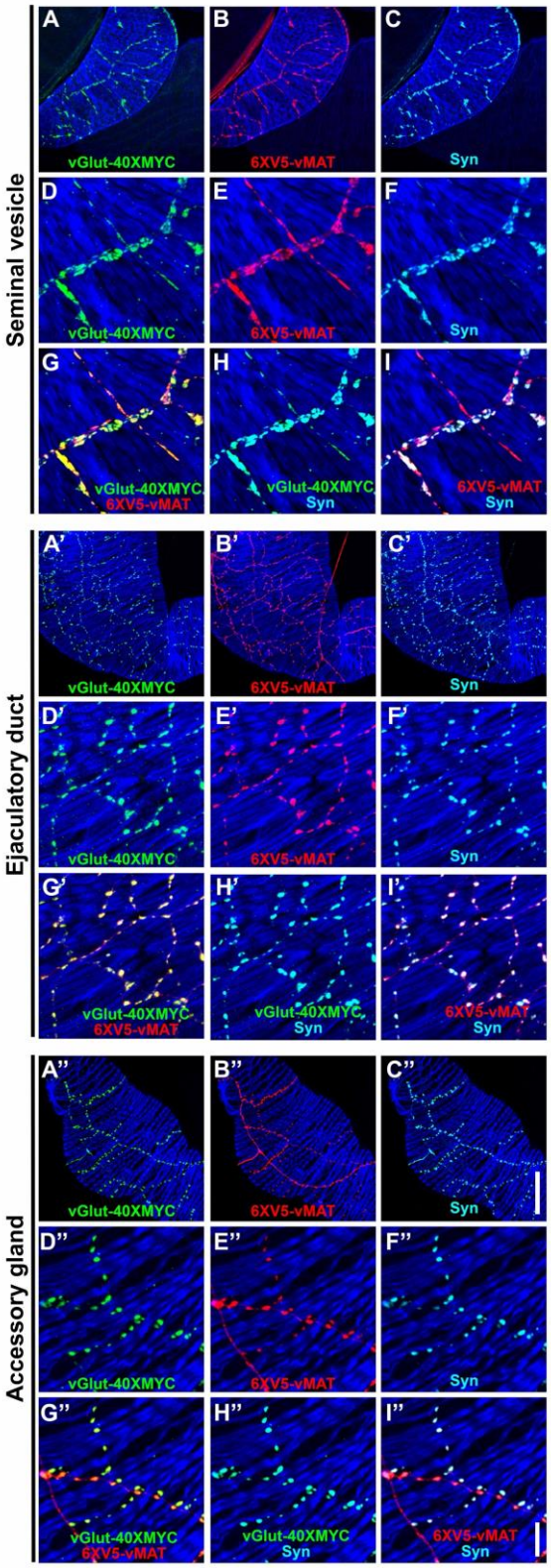
Seminal vesicle
Ejaculatory duct
Accessory gland
A
B
C
D
E
F
G
H
I
A'
B'
C'
D'
E'
F'
G'
H'
I'
A''
B''
C''
D''
E''
F''
G''
H''
I''
vGlut-40XMYC
6XV5-vMAT
Syn

1328

1329 **Figure 6.** Expression of the synaptic vesicle marker Synapsin in combination with
1330 vGlut-40XMYC and 6XV5-vMAT in the SV, ED, and AG of the Drosophila male
1331 reproductive system. A-I) SV. A) vGlut-40XMYC; B) 6XV5-vMAT; C) Synapsin; D)
1332 vGlut-40XMYC; E) 6XV5-vMAT; F) Synapsin; G) vGlut-40XMYC, 6XV5-vMAT overlay;
1333 H) vGlut-40XMYC, Synapsin overlay; I) 6XV5-vMAT, Synapsin overlay. A'-I') ED. A')
1334 vGlut-40XMYC; B') 6XV5-vMAT; C') Synapsin; D') vGlut-40XMYC; E') 6XV5-vMAT; F')
1335 Synapsin; G') vGlut-40XMYC, 6XV5-vMAT overlay; H') vGlut-40XMYC, Synapsin
1336 overlay; I') 6XV5-vMAT, Synapsin overlay. A''-I'') AG. A'') vGlut-40XMYC; B'') 6XV5-
1337 vMAT; C'') Synapsin; D'') vGlut-40XMYC; E'') 6XV5-vMAT; F'') Synapsin; G'') vGlut-
1338 40XMYC, 6XV5-vMAT overlay; H'') vGlut-40XMYC, Synapsin overlay; I'') 6XV5-vMAT,
1339 Synapsin overlay. Scale bars: C''-50μm; I''-10μm.

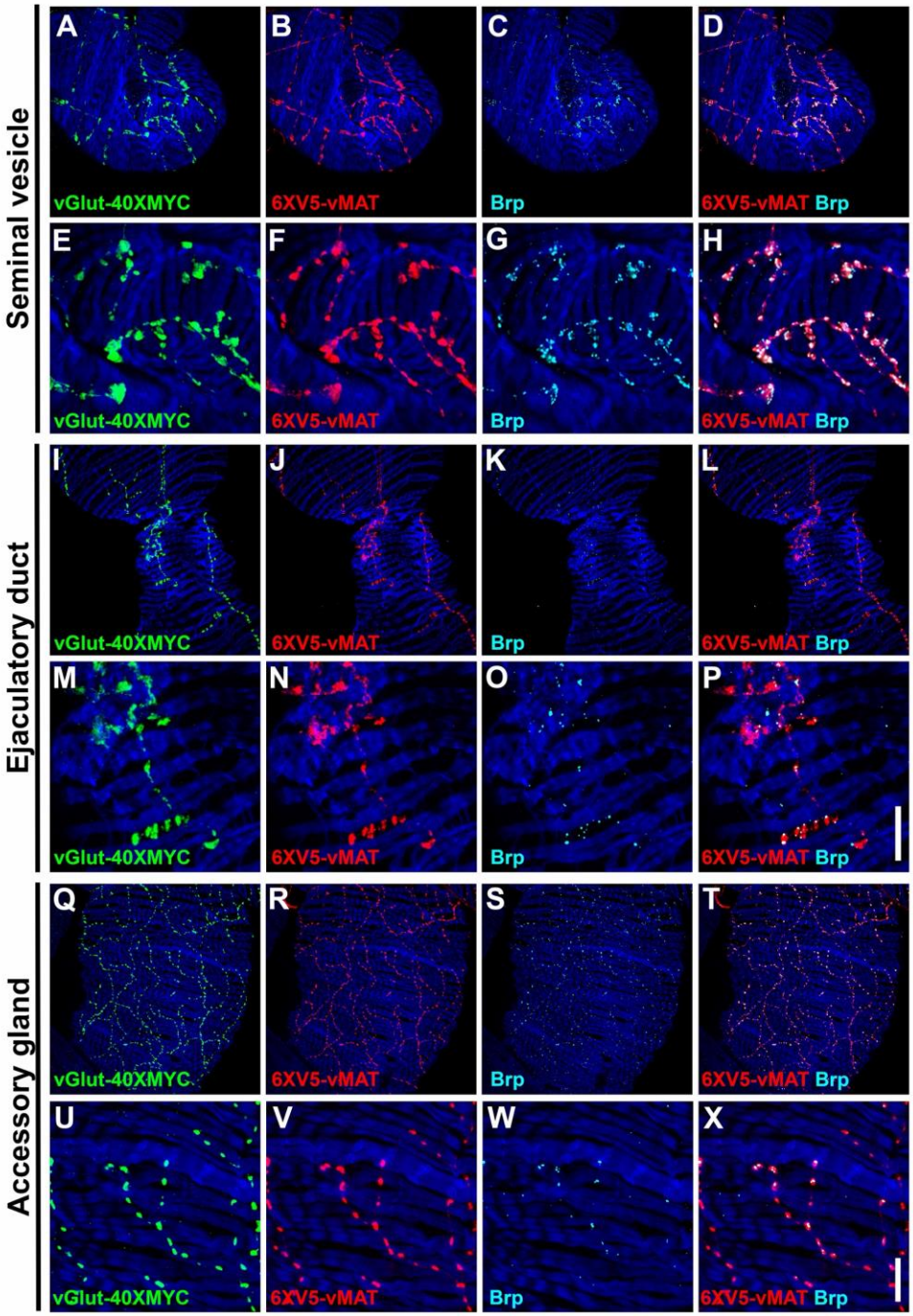
Seminal vesicle
Ejaculatory duct
Accessory gland
A
B
C
D
E
F
G
H
I
J
K
L
M
N
O
P
Q
R
S
T
U
V
W
X
vGlut-40XMYC
6XV5-vMAT
Brp
6XV5-vMAT Brp

1340

1341 **Figure 6S1.** Expression of the active zone marker Brp in combination with vGlut-
1342 40XMYC and 6XV5-vMAT in the SV, ED, and AG of the Drosophila male reproductive
1343 system. A-H) SV. A) vGlut-40XMYC; B) 6XV5-vMAT; C) Brp; D) 6XV5-vMAT, Brp
1344 overlay; E) vGlut-40XMYC; F) 6XV5-vMAT; G) Brp; H) 6XV5-vMAT, Brp overlay. I-P)
1345 ED. I) vGlut-40XMYC; J) 6XV5-vMAT; K) Brp; L) 6XV5-vMAT, Brp; M) vGlut-40XMYC;
1346 N) 6XV5-vMAT; O) Brp; P) 6XV5-vMAT, Brp overlay. I-P) AG. Q) vGlut-40XMYC; R)
1347 6XV5-vMAT; S) Brp; T) 6XV5-vMAT, Brp; U) vGlut-40XMYC; V) 6XV5-vMAT; W) Brp; X)
1348 6XV5-vMAT, Brp overlay. Scale bars: P-50μm; X-10μm.
1349

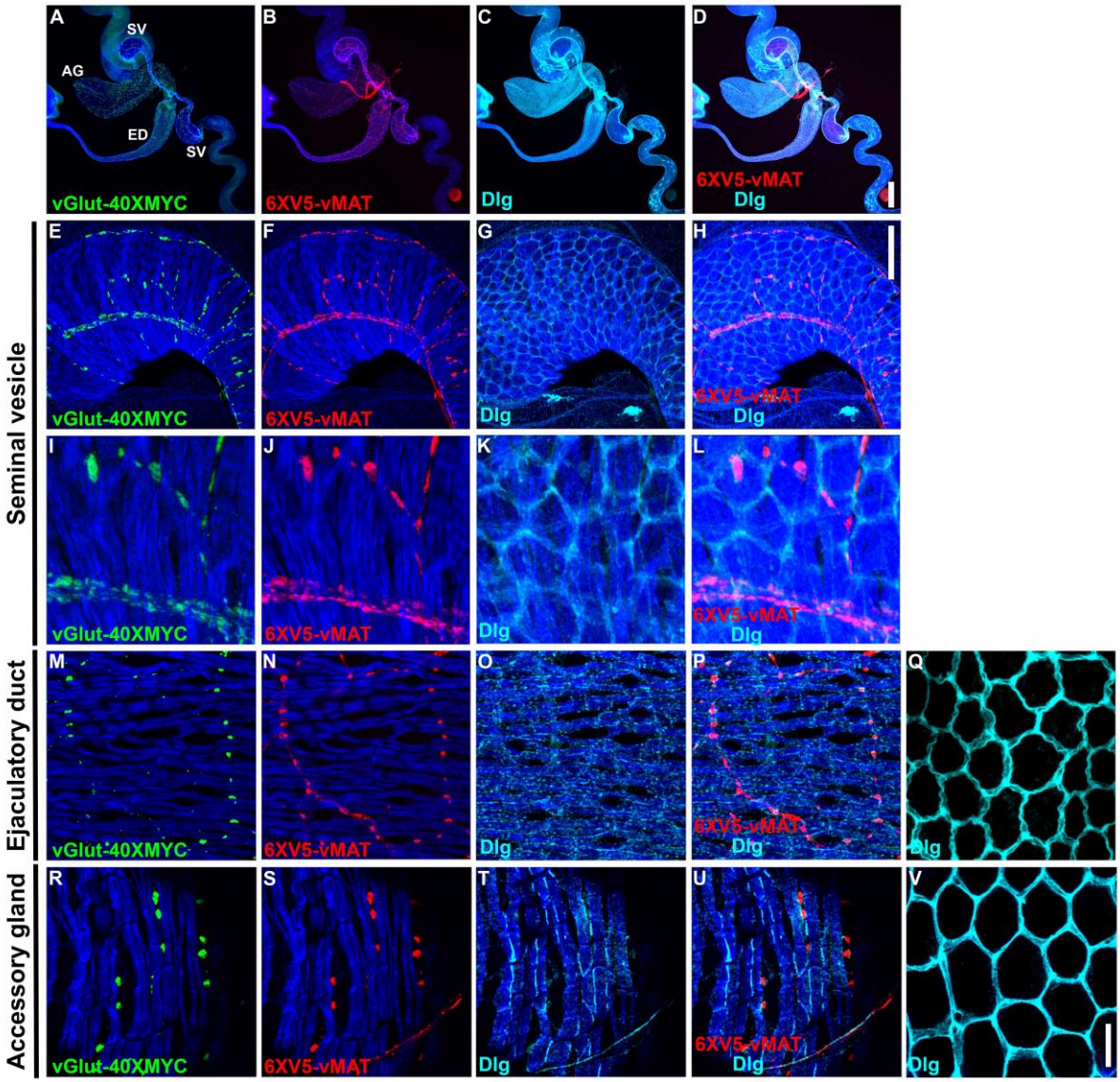

1350
1351 **Figure 6S2.** Expression of the post-synaptic density marker Dlg in combination with
1352 vGlut-40XMYC and 6XV5-vMAT in the SV, ED, and AG of the Drosophila male
1353 reproductive system. A-D) Complete reproductive system. A) vGlut-40XMYC; B) 6XV5-

1354 vMAT; C) Dlg; D) 6XV5-vMAT, Dlg overlay; E-L) SV. E) vGlut-40XMYC; F) 6XV5-vMAT;
1355 G) Dlg; H) 6XV5-vMAT, Dlg overlay; I) vGlut-40XMYC; J) 6XV5-vMAT; G) Dlg; H) 6XV5-
1356 vMAT, Dlg overlay. I-P) ED. I) vGlut-40XMYC; K) 6XV5-vMAT; L) Dlg; M-P) ED muscle
1357 surface. M) vGlut-40XMYC; N) 6XV5-vMAT; O) Dlg; P) 6XV5-vMAT, Dlg overlay Q) Dlg
1358 in the ED epithelial cells. R-U) AG muscle surface. R) vGlut-40XMYC; S) 6XV5-vMAT;
1359 T) Dlg; U) 6XV5-vMAT, Dlg overlay; V) Dlg in AG epithelial cells. Scale bars: D-200μm;
1360 H-50μm; V-10μm.

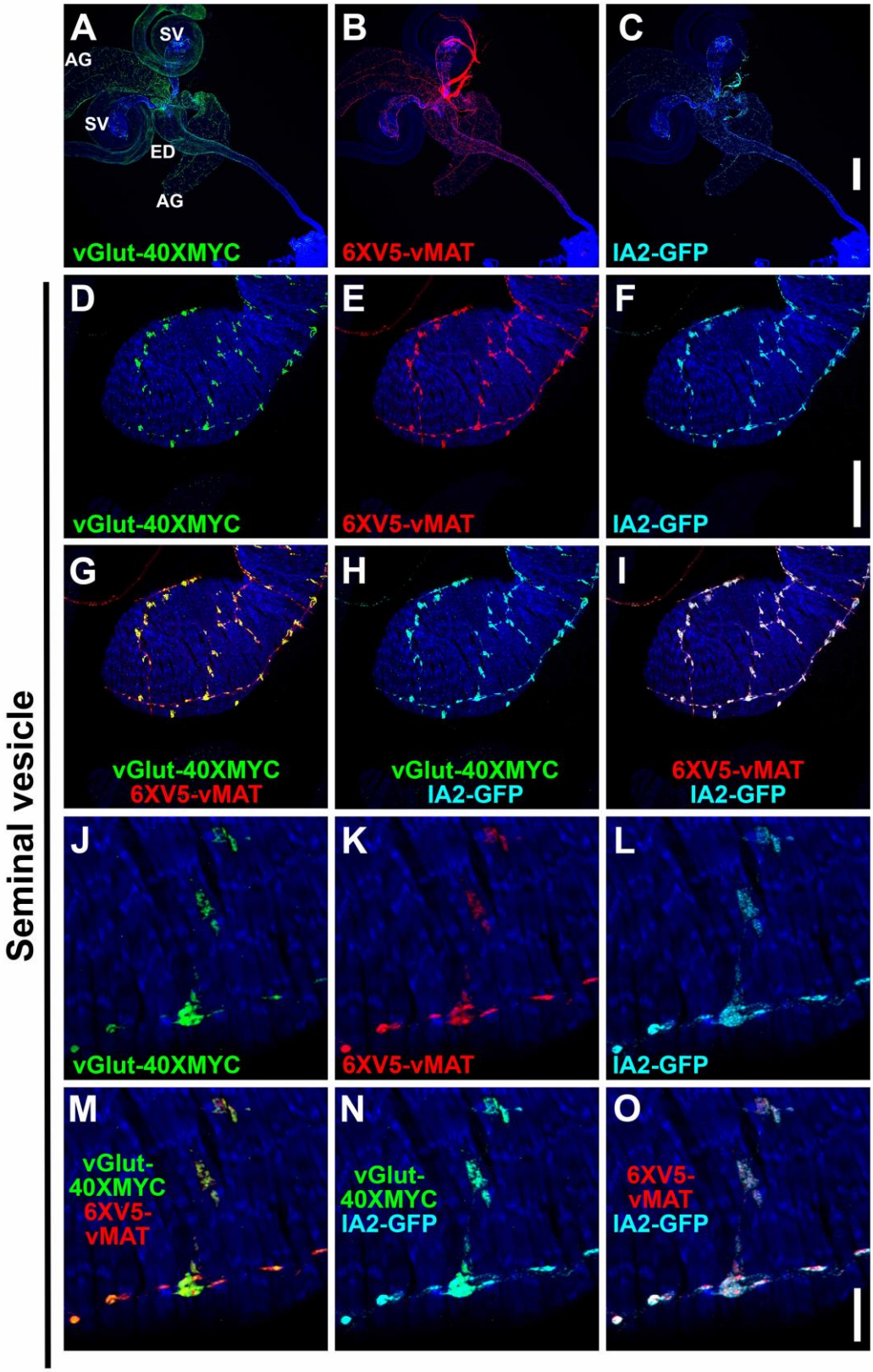
A
SV
AG
SV
ED
AG
vGlut-40XMYC
B
6XV5-vMAT
C
IA2-GFP
Seminal vesicle
D
vGlut-40XMYC
E
6XV5-vMAT
F
IA2-GFP
G
vGlut-40XMYC
6XV5-vMAT
H
vGlut-40XMYC
IA2-GFP
I
6XV5-vMAT
IA2-GFP
J
vGlut-40XMYC
K
6XV5-vMAT
L
IA2-GFP
M
vGlut-
40XMYC
6XV5-
vMAT
N
vGlut-
40XMYC
IA2-GFP
O
6XV5-
vMAT
IA2-GFP

1361

1362 **Figure 6S3.** Expression of the large core dense vesicle marker IA2-GFP in combination
1363 with vGlut-40XMYC and 6XV5-vMAT in the SV of the Drosophila male reproductive
1364 system. A-C) Complete reproductive system. A) vGlut-40XMYC; B) 6XV5-vMAT; C)
1365 IA2-GFP; D-O) SV. D, J) vGlut-40XMYC; E, K) 6XV5-vMAT; F, L) IA2-GFP; G, M)
1366 vGlut-40XMYC, 6XV5-vMAT overlay; H, N) vGlut-40XMYC, IA2-GFP overlay; I, O)
1367 6XV5-vMAT, IA2 overlay. Scale bars: C-200μm; F-50μm; O-10μm.

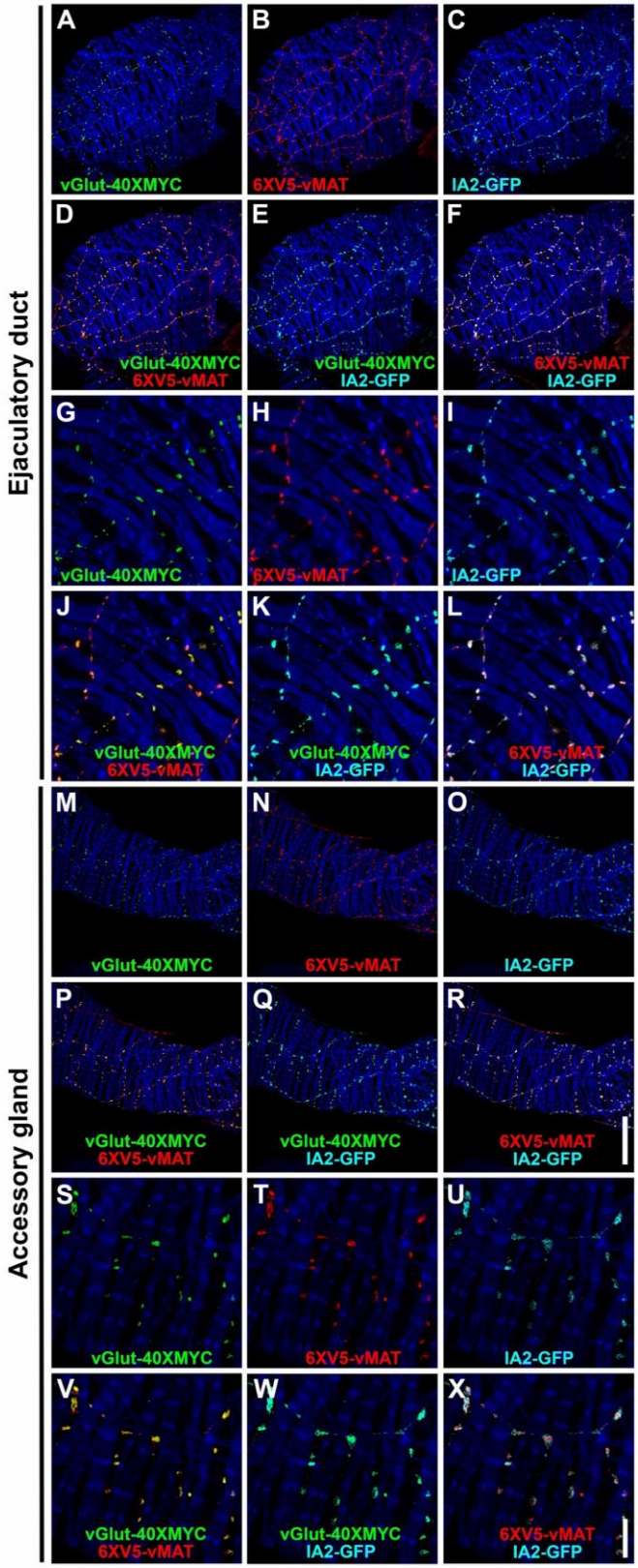
Ejaculatory duct
Accessory gland
A
vGlut-40XMYC
B
6XV5-vMAT
C
IA2-GFP
D
vGlut-40XMYC
6XV5-vMAT
E
vGlut-40XMYC
IA2-GFP
F
6XV5-vMAT
IA2-GFP
G
vGlut-40XMYC
H
6XV5-vMAT
I
IA2-GFP
J
vGlut-40XMYC
6XV5-vMAT
K
vGlut-40XMYC
IA2-GFP
L
6XV5-vMAT
IA2-GFP
M
vGlut-40XMYC
N
6XV5-vMAT
O
IA2-GFP
P
vGlut-40XMYC
6XV5-vMAT
Q
vGlut-40XMYC
IA2-GFP
R
6XV5-vMAT
IA2-GFP
S
vGlut-40XMYC
T
6XV5-vMAT
U
IA2-GFP
V
vGlut-40XMYC
6XV5-vMAT
W
vGlut-40XMYC
IA2-GFP
X
6XV5-vMAT
IA2-GFP

1368

1369 **Figure 6S4.** Expression of the large core dense vesicle marker IA2-GFP in combination
1370 with vGlut-40XMYC and 6XV5-vMAT in the ED and AGs of the Drosophila male
1371 reproductive system. A-L) ED. A, G) vGlut-40XMYC; B, H) 6XV5-vMAT; C, I) IA2-GFP;
1372 D, J) vGlut-40XMYC, 6XV5-vMAT overlay; E, K) vGlut-40XMYC, IA2-GFP overlay; F, L)
1373 6XV5-vMAT, IA2 overlay. M-X) AG. M, S) vGlut-40XMYC; N, T) 6XV5-vMAT; O, U) IA2-
1374 GFP; P, V) vGlut-40XMYC, 6XV5-vMAT overlay; Q, W) vGlut-40XMYC, IA2-GFP
1375 overlay; R, X) 6XV5-vMAT, IA2 overlay. Scale bars: R-50μm; X-10μm.

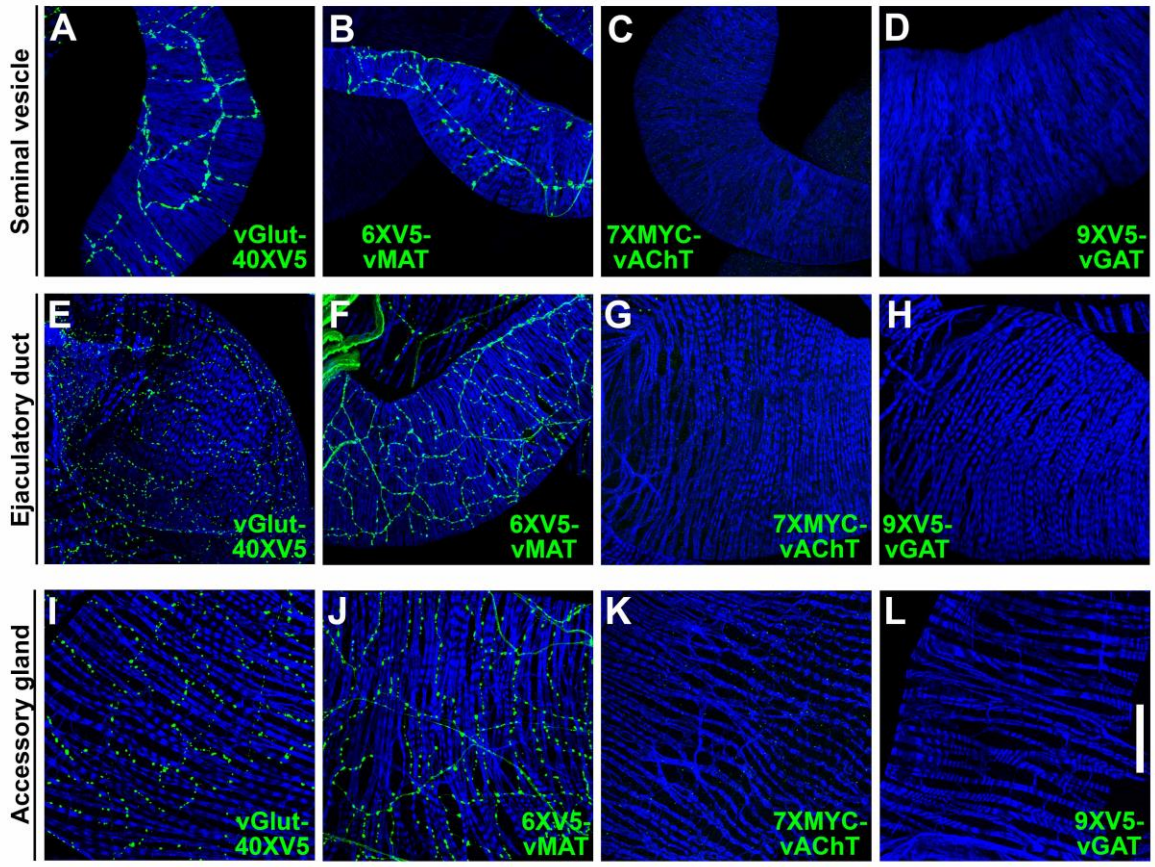

1376
1377 **Figure 6S5.** Expression of vGlut-40XMYC, 6XV5-vMAT, 7XMYC-vAChT, and 9XV5-
1378 vGAT in the SV, ED, and AG of the Drosophila male reproductive system. A-D) SV. A)
1379 vGlut-40XV5; B) 6XV5-vMAT; C) 7XMYC-vAChT; D) 9XV5-vGAT. E-H) ED. E) vGlut-
1380 40XV5; F) 6XV5-vMAT; G) 7XMYC-vAChT; H) 9XV5-vGAT. I-L) AG. I) vGlut-40XV5; J)
1381 6XV5-vMAT; K) 7XMYC-vAChT; L) 9XV5-vGAT. Scale bar: 50μm.

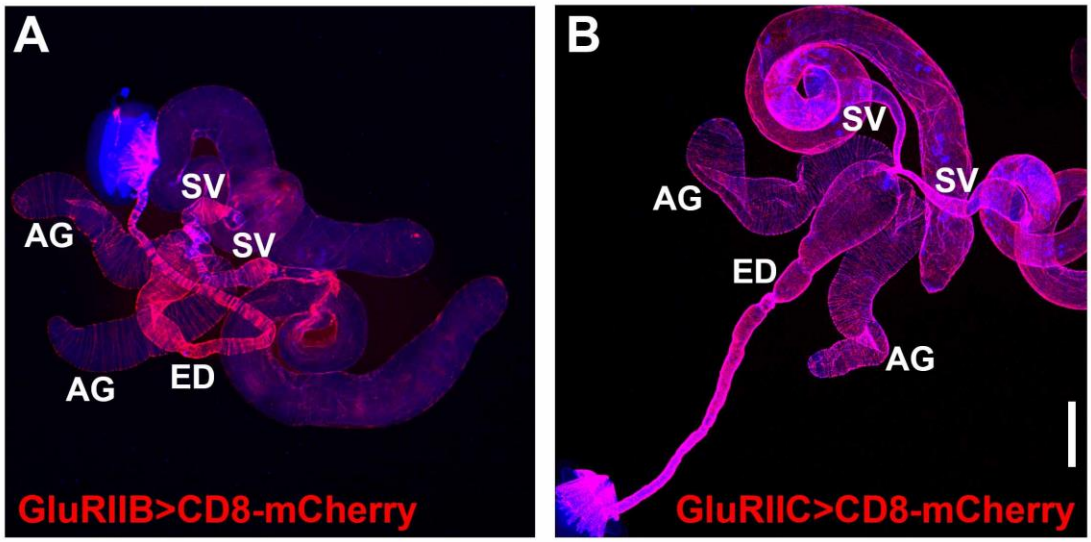

Figure 7. Glutamate receptor GAL4 expression patterns in Drosophila male reproductive system. A) GluRIIB; B) GluRIIC. Scale bar: 200μm.

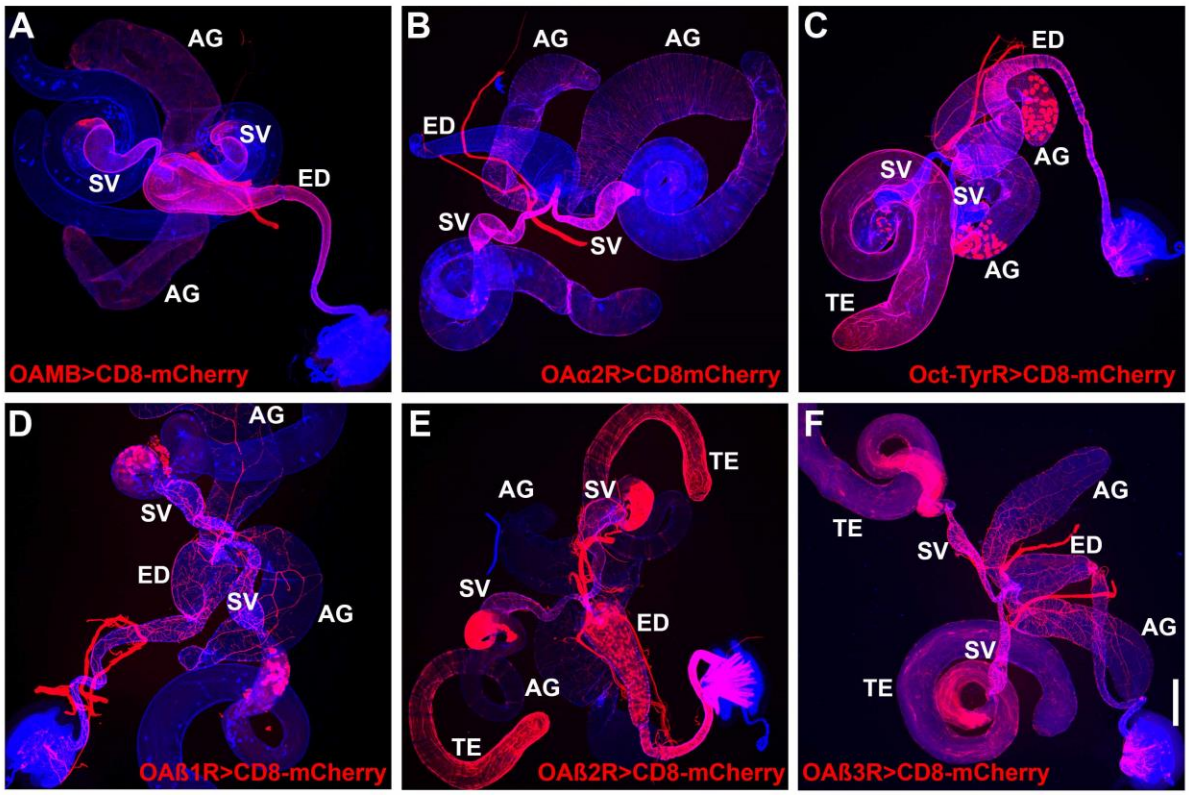

Figure 7S1. OA receptor GAL4 expression patterns in Drosophila male reproductive system. A) OAMB; B) OAα2R; C) Oct-TyrR; D) OAβ1R; E) OAβ2R; F) OAβ3R. Scale bar: 200μm.

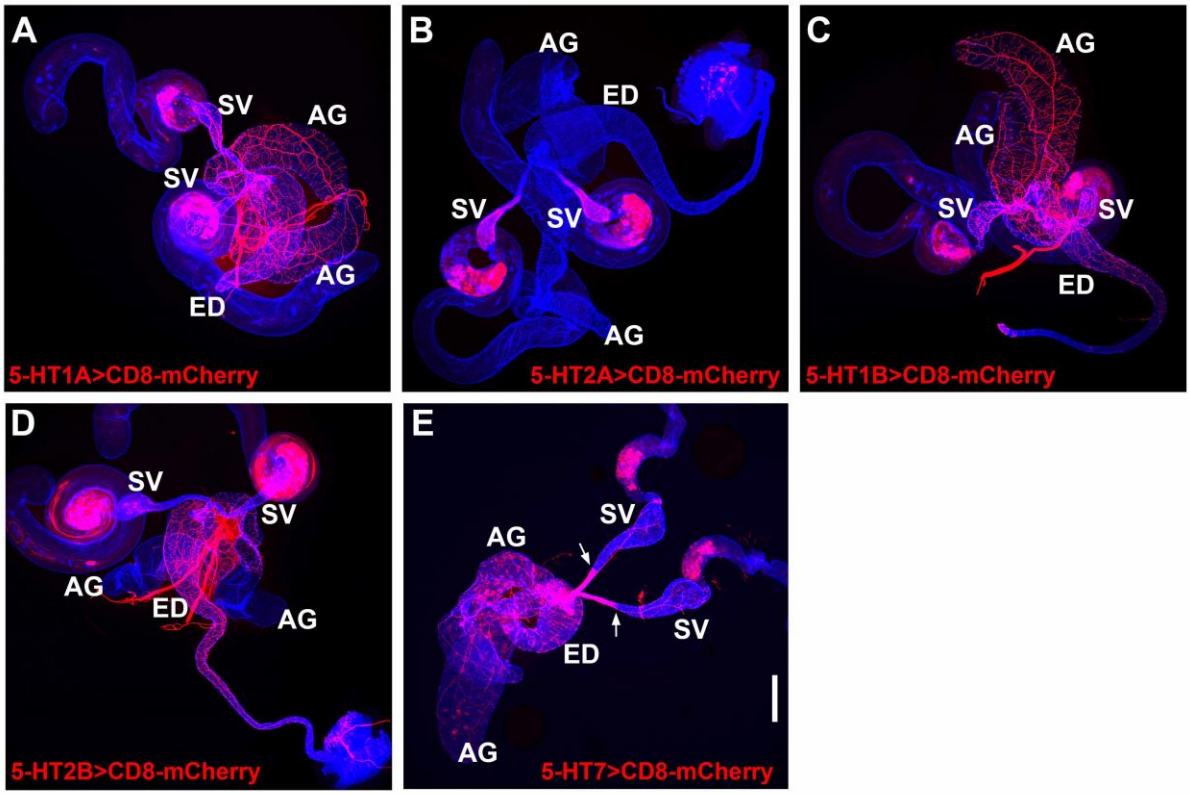

1389
1390 **Figure 7S2.** 5-HT receptor GAL4 expression patterns in Drosophila male reproductive
1391 system. A) 5-HT1A; B) 5-HT2A; C) 5-HT1B; D) 5-HT2B; E) 5-HT7. Scale bar: 200μm.

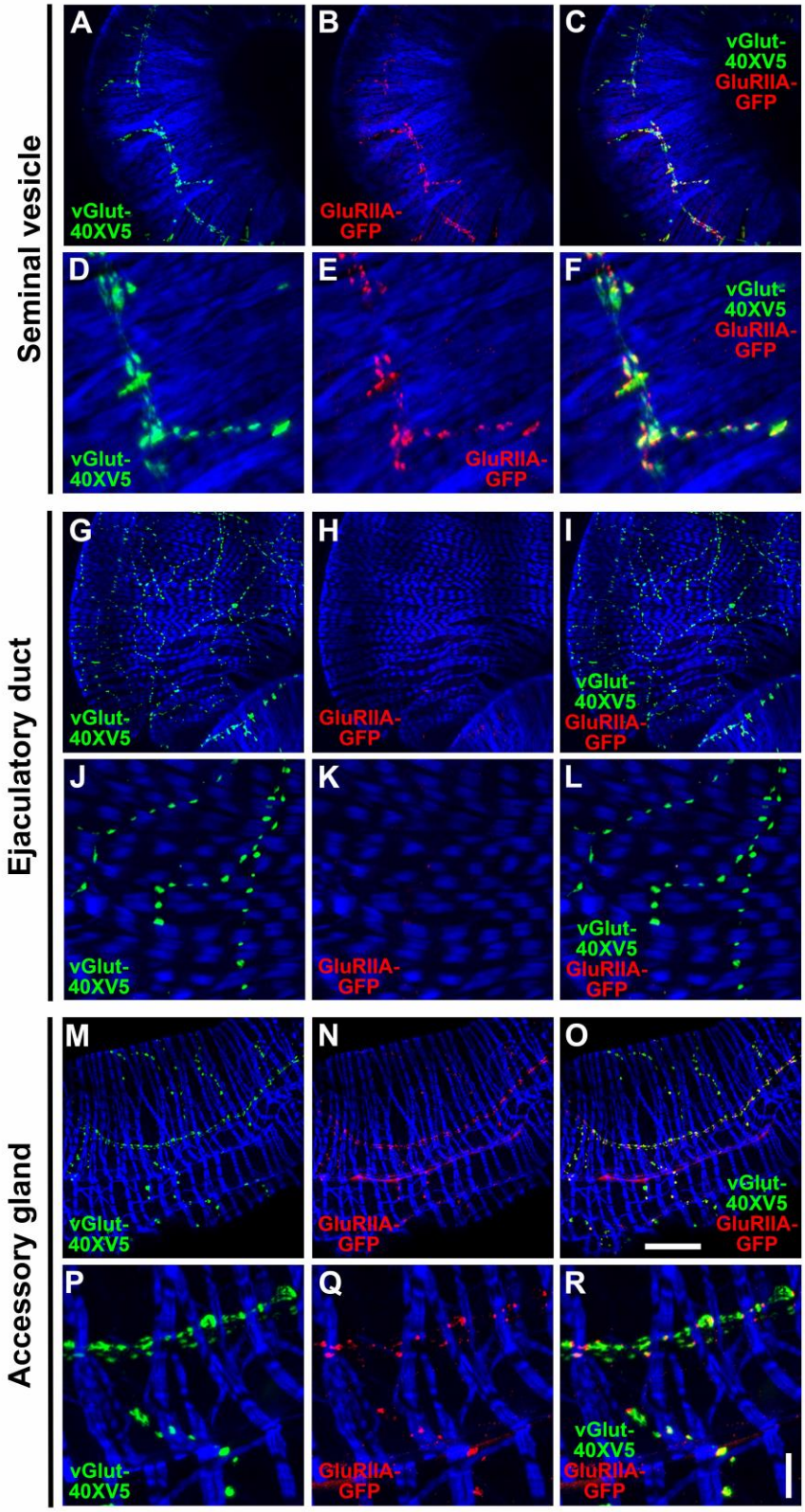
Seminal vesicle
Ejaculatory duct
Accessory gland
A
B
C
D
E
F
G
H
I
J
K
L
M
N
O
P
Q
R
vGlut-
40XV5
GluRIIA-
GFP

1392

1393 **Figure 8.** GluRIIA-GFP expression in the SV, ED, and AG of the Drosophila male
1394 reproductive system. A-F) SV. A, D) vGlut-40XV5; B,E) GluRIIA-GFP; C, F) vGlut-
1395 40XV5, GluRIIA-GFP overlay. G-L) ED. G, J) vGlut-40XV5; H, K) GluRIIA-GFP; I, L)
1396 vGlut-40XV5, GluRIIA-GFP overlay. M-R) AG. M, P) vGlut-40XV5; N, Q) GluRIIA-GFP;
1397 O, R) vGlut-40XV5, GluRIIA-GFP overlay. Scale bars: O-50μm; R-10μm.

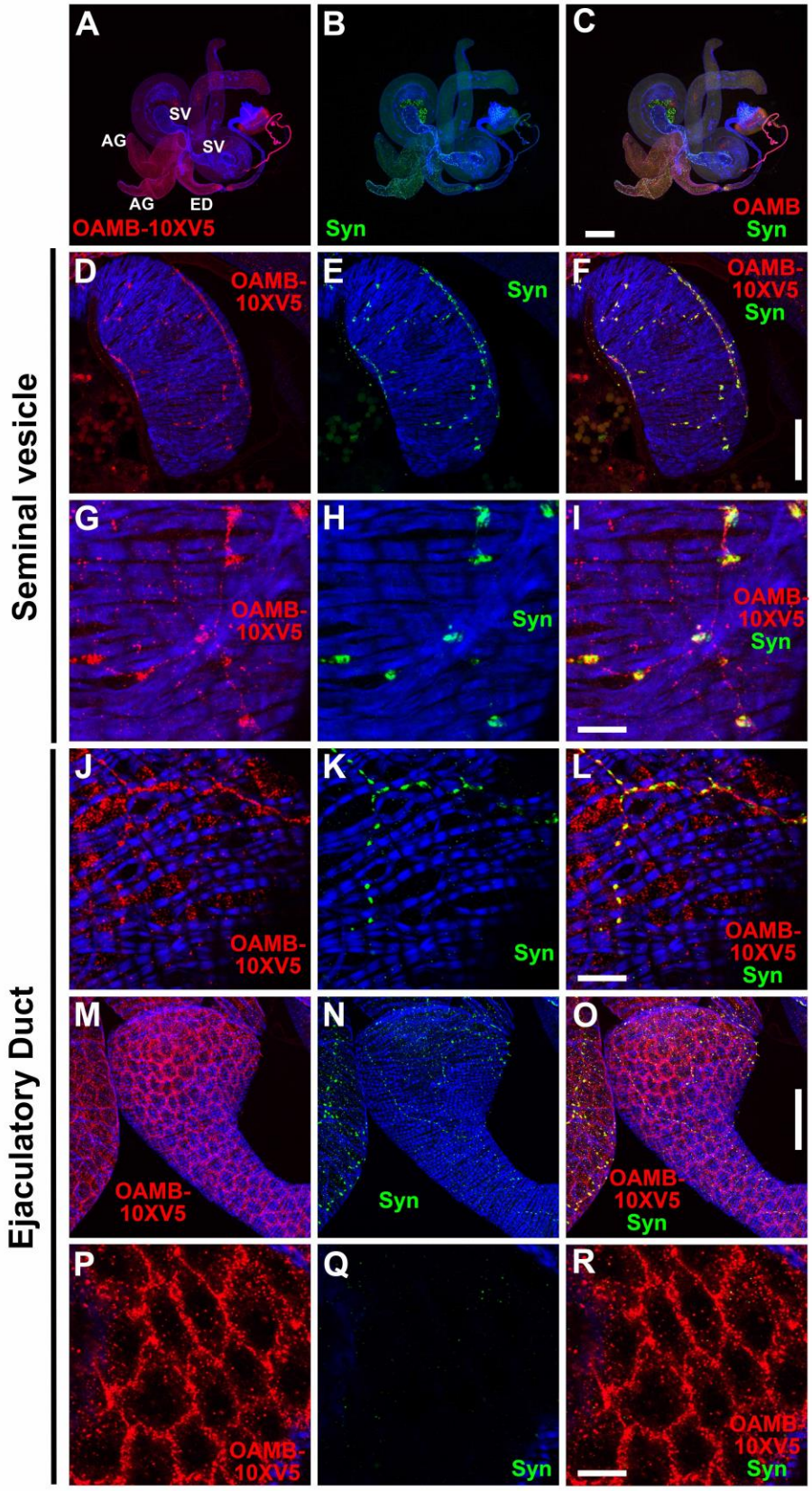
A
SV
AG
SV
AG
ED
OAMB-10XV5
B
Syn
C
OAMB
Syn
Seminal vesicle
D
OAMB-
10XV5
E
Syn
F
OAMB-
10XV5
Syn
G
OAMB-
10XV5
H
Syn
I
OAMB-
10XV5
Syn
Ejaculatory Duct
J
OAMB-
10XV5
K
Syn
L
OAMB-
10XV5
Syn
M
OAMB-
10XV5
N
Syn
O
OAMB-
10XV5
Syn
P
OAMB-
10XV5
Q
Syn
R
OAMB-
10XV5
Syn

1398

1399 **Figure 8S1.** OAMB expression in the Drosophila male reproductive system. A-C)
1400 Complete male reproductive system. A) OAMB-10XV5; B) Syn; C) OAMB-10XV5, Syn
1401 overlay. D-I) SV. D, G) OAMB-10XV5; E, H) Syn; F, I) OAMB-10XV5, Syn overlay. J-R)
1402 ED. J-L) muscle surface. J) OAMB-10XV5; K) Syn; L) OAMB-10XV5, Syn overlay. M-
1403 O) muscles and epithelial layers. M) OAMB-10XV5; N) Syn; O) OAMB-10XV5, Syn
1404 overlay. P-R) epithelial layer. P) OAMB-10XV5; Q) Syn; R) OAMB-10XV5, Syn overlay.
1405 Scale bars: C-200μm; F, O-50μm; I, L, R-10μm.

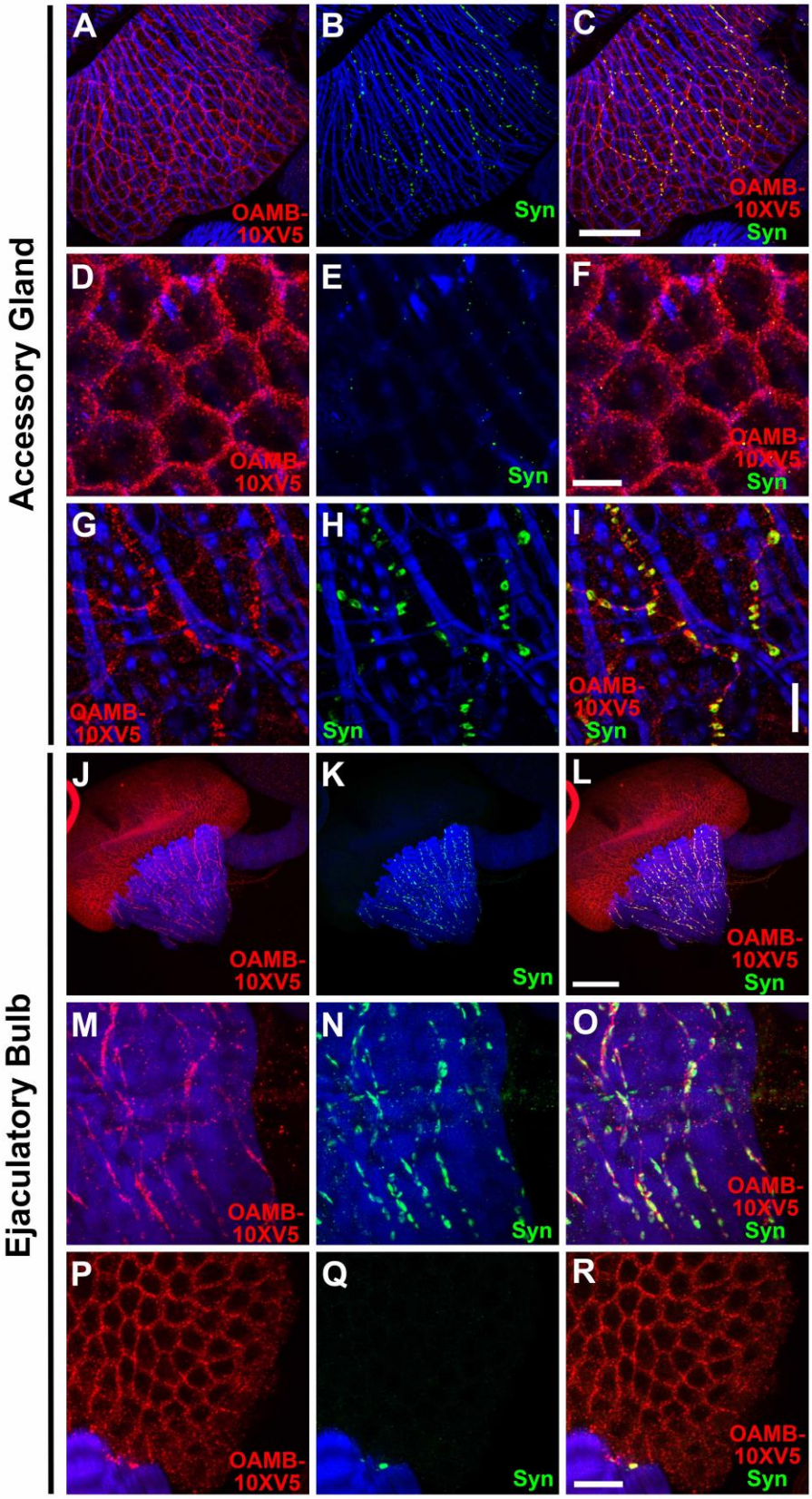
Accessory Gland
Ejaculatory Bulb
A
B
C
D
E
F
G
H
I
J
K
L
M
N
O
P
Q
R
OAMB-10XV5
Syn
OAMB-10XV5 Syn

1406

1407 **Figure 8S2.** OAMB expression in the Drosophila male reproductive system. A-C) AG.
1408 A) OAMB-10XV5; B) Syn; C) OAMB-10XV5, Syn overlay. D-F) Epithelial layer of AG.
1409 D) OAMB-10XV5; E) Syn; F) OAMB-10XV5, Syn overlay. G-I) Muscle layer of AG. G)
1410 OAMB-10XV5; H) Syn; I) OAMB-10XV5, Syn overlay. J-L) Ejaculatory bulb. J) OAMB-
1411 10XV5; K) Syn; L) OAMB-10XV5, Syn overlay. M-O) muscle layer of ejaculatory bulb.
1412 M) OAMB-10XV5; N) Syn; O) OAMB-10XV5, Syn overlay. P-Q) Epithelial layer of
1413 ejaculatory bulb. P) OAMB-10XV5; Q) Syn; R) OAMB-10XV5, Syn overlay. Scale bars:
1414 C, L-50μm; F, I, R-10μm.

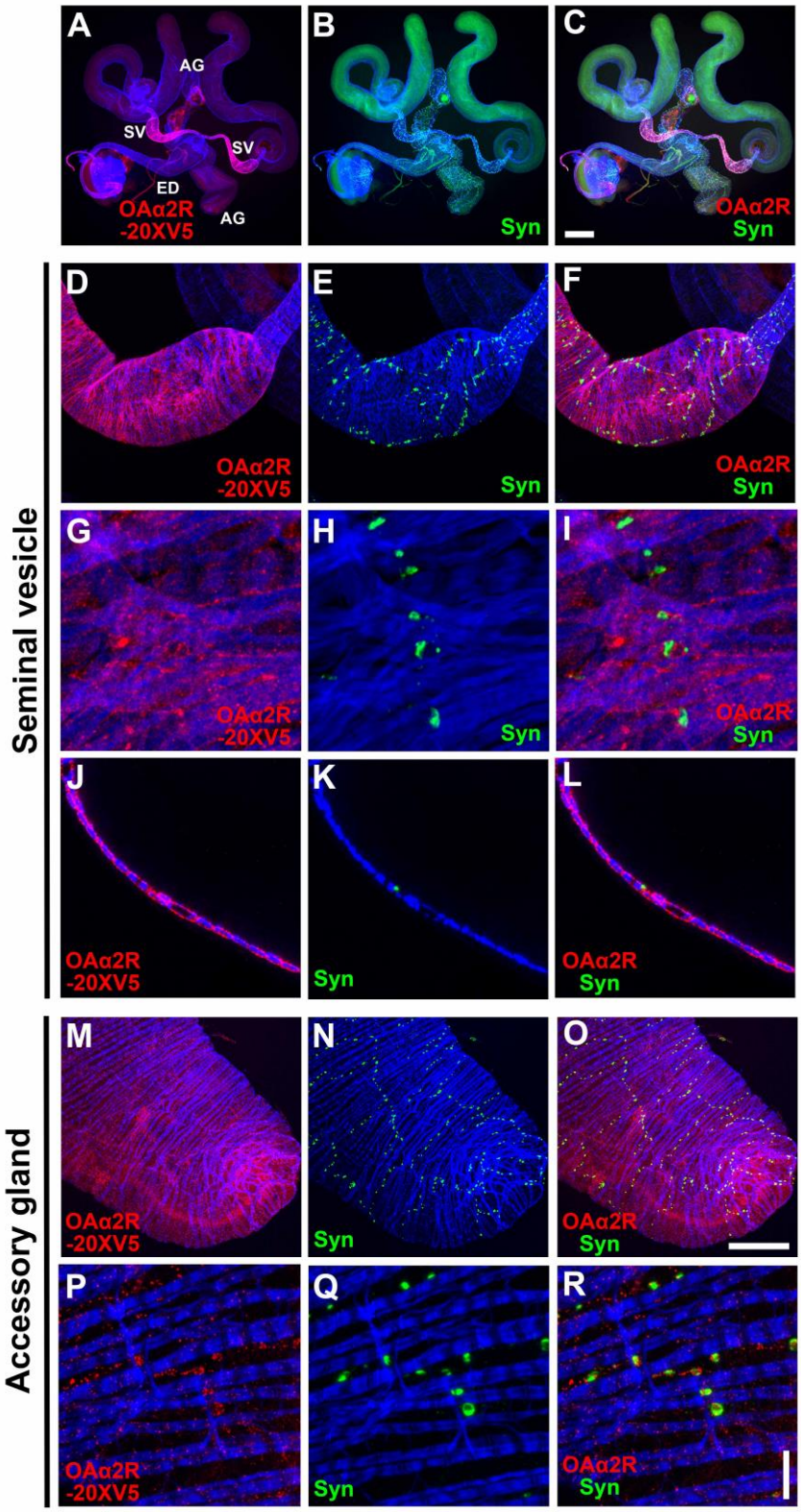
A
AG
SV
SV
ED
OAα2R
-20XV5
AG
B
Syn
C
OAα2R
Syn
Seminal vesicle
D
OAα2R
-20XV5
E
Syn
F
OAα2R
Syn
G
OAα2R
-20XV5
H
Syn
I
OAα2R
Syn
J
OAα2R
-20XV5
K
Syn
L
OAα2R
Syn
Accessory gland
M
OAα2R
-20XV5
N
Syn
O
OAα2R
Syn
P
OAα2R
-20XV5
Q
Syn
R
OAα2R
Syn

1415

1416 **Figure 8S3.** OAα2R-20XV5 expression in the Drosophila male reproductive system. A-
1417 C) Complete male reproductive system. A) OAα2R-20XV5; B) Syn; C) OAα2R-20XV5,
1418 Syn overlay. D-I) SV. D, G) OAα2R-20XV5; E, H) Syn; F, I) OAα2R-20XV5, Syn
1419 overlay. Cross-section of SV. J) OAα2R-20XV5: K) Syn; L) OAα2R-20XV5, Syn
1420 overlay. M-R) AG. M, P) OAα2R-20XV5; N, Q) Syn; O, R) OAα2R-20XV5, Syn overlay.
1421 Scale bars: C-200μm; O-50μm; R-10μm.

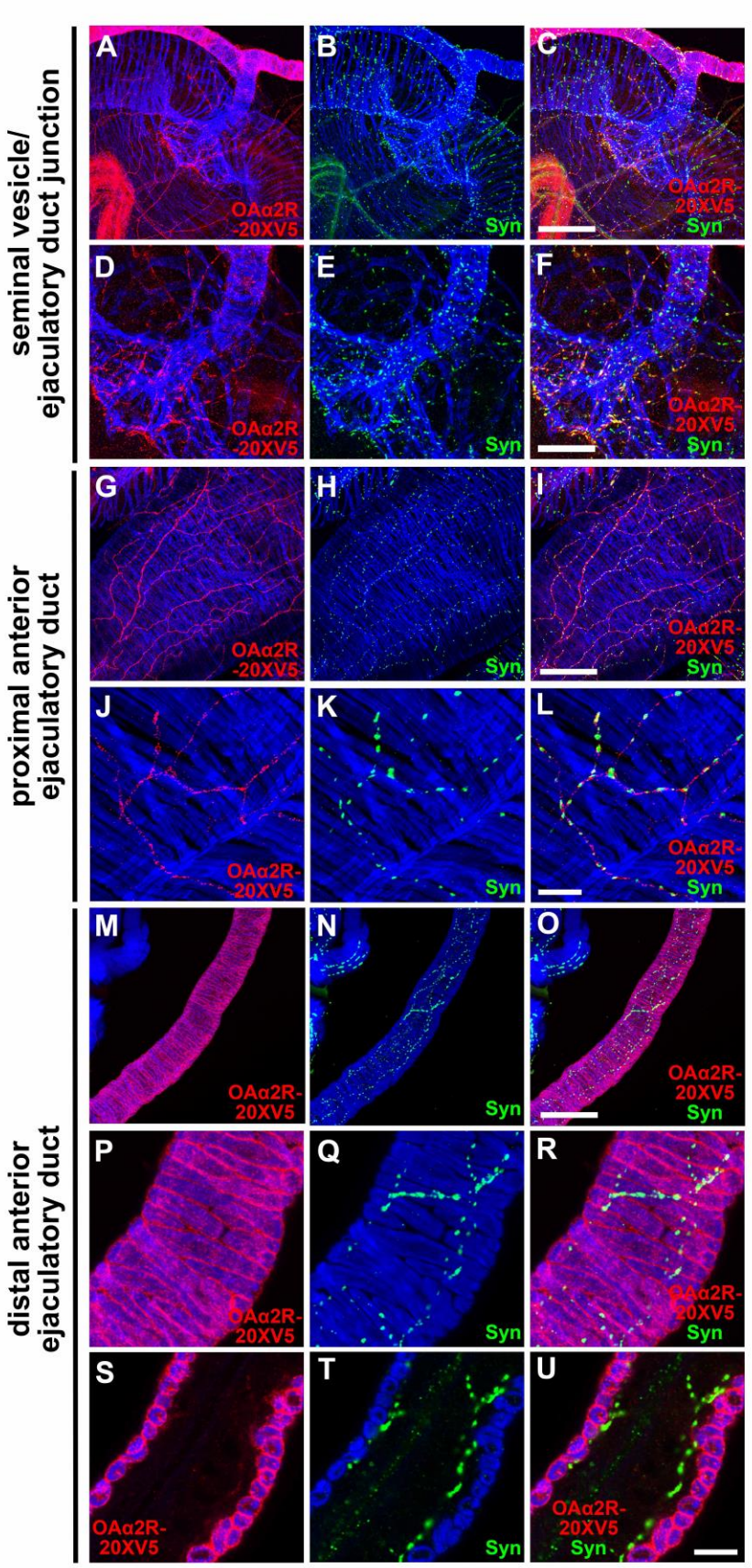
seminal vesicle/
ejaculatory duct junction
proximal anterior
ejaculatory duct
distal anterior
ejaculatory duct
A
B
C
D
E
F
G
H
I
J
K
L
M
N
O
P
Q
R
S
T
U
OAα2R
-20XV5
Syn
OAα2R-
20XV5
Syn

1422

1423 **Figure 8S4.** OAα2R-20XV5 expression in the Drosophila male reproductive system. A-
1424 C) SV/ED junction. A, D) OAα2R-20XV5; B, E) Syn; C, F) OAα2R-20XV5, Syn overlay.
1425 G-L) Proximal anterior ED. G, J) OAα2R-20XV5; H, K) Syn; I, L) OAα2R-20XV5, Syn
1426 overlay. M-U) Distal anterior ED. M, P, S) OAα2R-20XV5; N, Q, T) Syn; O, R, U)
1427 OAα2R-20XV5, Syn overlay. Scale bars: C, I, O-50μm; F-25μm; L, U-10μm.

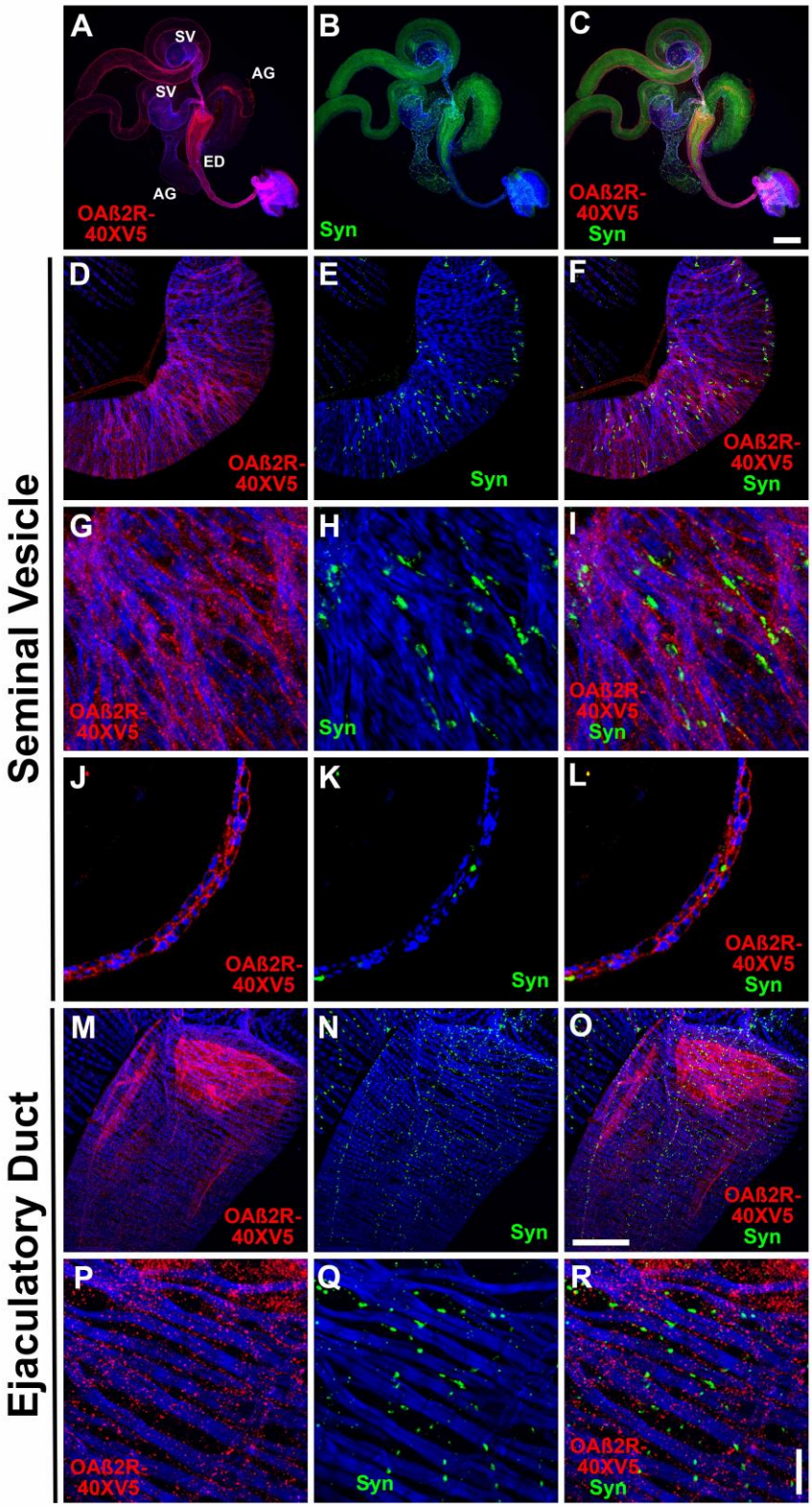
A
SV
SV
AG
ED
AG
OAß2R-
40XV5
B
Syn
C
OAß2R-
40XV5
Syn
Seminal Vesicle
D
OAß2R-
40XV5
E
Syn
F
OAß2R-
40XV5
Syn
G
OAß2R-
40XV5
H
Syn
I
OAß2R-
40XV5
Syn
J
OAß2R-
40XV5
K
Syn
L
OAß2R-
40XV5
Syn
Ejaculatory Duct
M
OAß2R-
40XV5
N
Syn
O
OAß2R-
40XV5
Syn
P
OAß2R-
40XV5
Q
Syn
R
OAß2R-
40XV5
Syn

1428

1429 **Figure 8S5.** OAβ2R-40XV5 expression in the Drosophila male reproductive system. A-
1430 C) Complete male reproductive system. A) OAβ2R-40XV5; B) Syn; C) OAβ2R-40XV5,
1431 Syn overlay. D-I) SV. D, G,) OAβ2R; E, H) Syn; F, I) OAβ2R-40XV5, Syn overlay. J-L)
1432 Cross section of SV. J) OAβ2R-40XV5; K) Syn; L) OAβ2R-40XV5, Syn overlay. M-R)
1433 ED. M, P) OAβ2R; N, Q) Syn; O, R) OAβ2R-40XV5, Syn overlay. Scale bars: C-
1434 200μm; O-50μm; R-10μm.

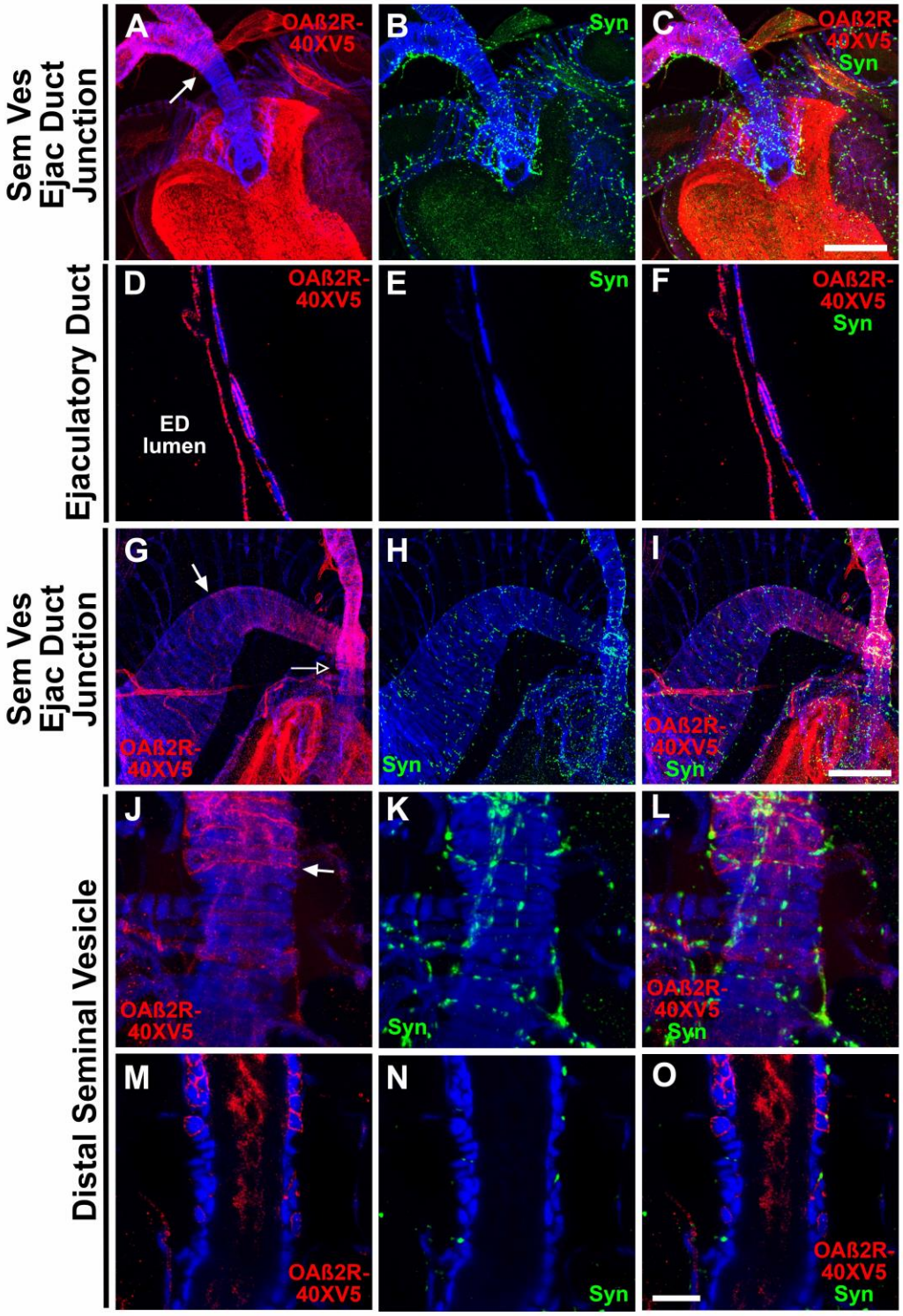
Sem Ves
Ejac Duct
Junction
A
OAß2R-
40XV5
B
Syn
C
OAß2R-
40XV5
Syn
Ejaculatory Duct
D
OAß2R-
40XV5
ED
lumen
E
Syn
F
OAß2R-
40XV5
Syn
Sem Ves
Ejac Duct
Junction
G
OAß2R-
40XV5
H
Syn
I
OAß2R-
40XV5
Syn
Distal Seminal Vesicle
J
OAß2R-
40XV5
K
Syn
L
OAß2R-
40XV5
Syn
M
OAß2R-
40XV5
N
Syn
O
OAß2R-
40XV5
Syn

1435

1436 **Figure 8S6.** OAβ2R-40XV5 expression in the Drosophila male reproductive system.
1437 A-C) Junction of SV and ED. A) OAβ2R-40XV5; B) Syn; C) OAβ2R-40XV5, Syn
1438 overlay. D-F) Cross section of ED. D) OAβ2R-40XV5; E) Syn; F) OAβ2R-40XV5, Syn
1439 overlay. G-I) Junction of SV and ED. G) OAβ2R-40XV5; H) Syn; I) OAβ2R-40XV5, Syn
1440 overlay. J-L) Distal SV. J) OAβ2R-40XV5; E) Syn; F) OAβ2R-40XV5, Syn overlay. M-
1441 O) Cross section of distal SV. M) OAβ2R-40XV5; N) Syn; O) OAβ2R-40XV5, Syn
1442 overlay. Scale bars: C, I-50μm; O-10μm.

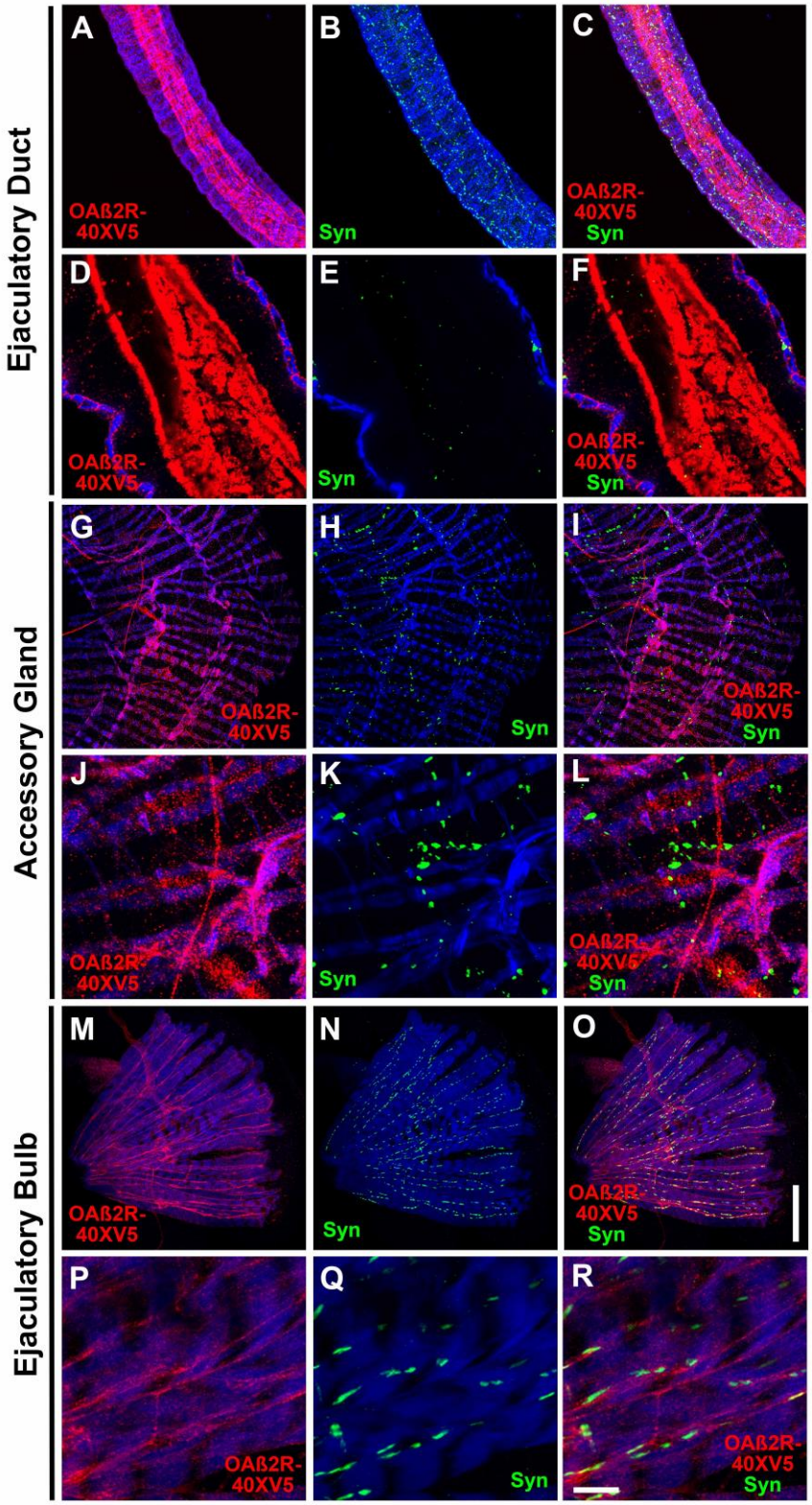
Ejaculatory Duct
Accessory Gland
Ejaculatory Bulb
A
B
C
D
E
F
G
H
I
J
K
L
M
N
O
P
Q
R
OAß2R-
40XV5
Syn

1443

1444 **Figure 8S7.** OAβ2R-40XV5 expression in the Drosophila male reproductive system. A-
1445 C) Distal anterior ED. A) OAβ2R-40XV5; B) Syn; C) OAβ2R-40XV5, Syn overlay. D-F)
1446 Cross section of distal anterior ED. D) OAβ2R-40XV5; E) Syn; F) OAβ2R-40XV5, Syn
1447 overlay. G-L) AG. G, J) OAβ2R-40XV5; H, K) Syn; I, L) OAβ2R-40XV5, Syn overlay. M-
1448 O) Ejaculatory bulb. M, O) OAβ2R-40XV5; N, Q) Syn; O, R) OAβ2R-40XV5, Syn
1449 overlay. Scale bars: O-50μm; R-10μm.

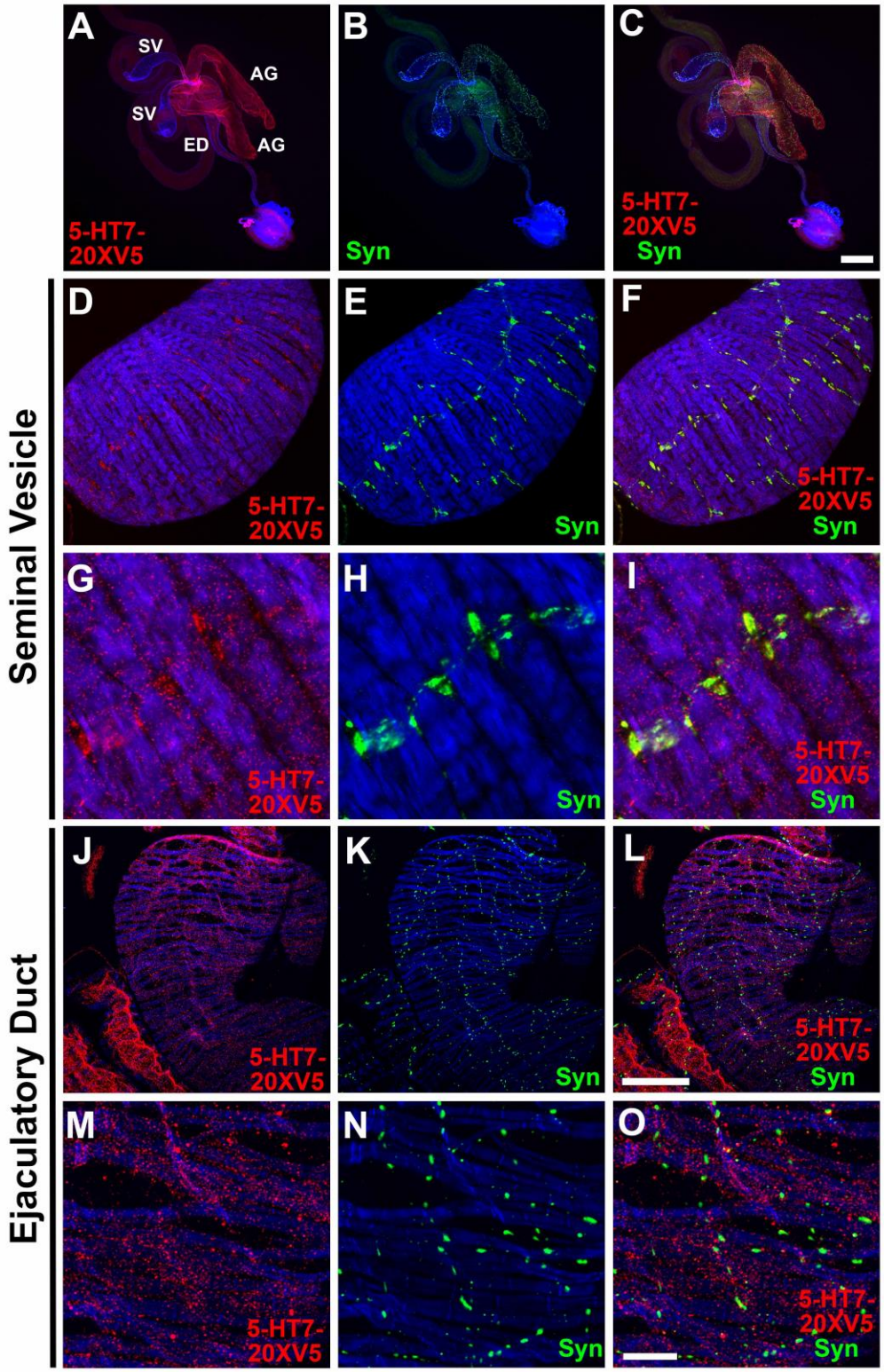
A
SV
AG
SV
ED
AG
5-HT7-
20XV5
B
Syn
C
5-HT7-
20XV5
Syn
Seminal Vesicle
D
5-HT7-
20XV5
E
Syn
F
5-HT7-
20XV5
Syn
G
5-HT7-
20XV5
H
Syn
I
5-HT7-
20XV5
Syn
Ejaculatory Duct
J
5-HT7-
20XV5
K
Syn
L
5-HT7-
20XV5
Syn
M
5-HT7-
20XV5
N
Syn
O
5-HT7-
20XV5
Syn

1450

1451 **Figure 8S8.** 5-HT7-20XV5 expression in the Drosophila male reproductive system. A-
1452 C) Complete male reproductive system. A) 5-HT7-20XV5.; B) Syn; C) 5-HT7-20XV5,
1453 Syn overlay. D-I) SV. D, G) 5-HT7-20XV5.; E, H) Syn; F, I) 5-HT7-20XV5, Syn overlay.
1454 J-O) ED. J, M) 5-HT7-20XV5.; K, N) Syn; L, O) 5-HT7-20XV5, Syn overlay. Scale bars:
1455 C-200μm; L-50μm; O-10μm.

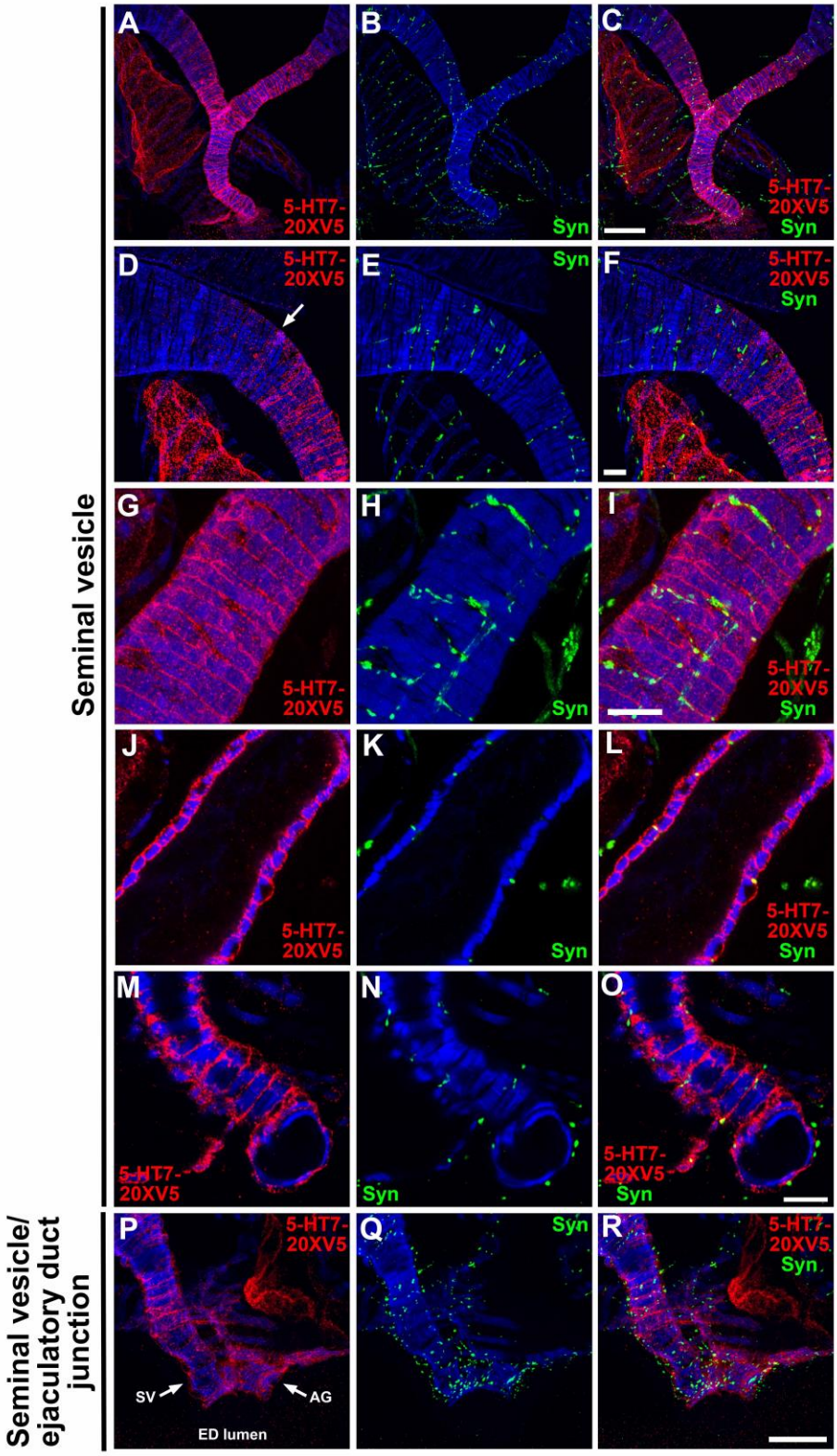
Seminal vesicle
Seminal vesicle/ ejaculatory duct junction
A
B
C
D
E
F
G
H
I
J
K
L
M
N
O
P
Q
R
5-HT7-20XV5
Syn
SV
AG
ED lumen

1456

1457 **Figure 8S9.** 5-HT7-20XV5 expression in the Drosophila male reproductive system. A-I)
1458 SV. A, D, G,) 5-HT7-20XV5.; B, E, H,) Syn; C, F, I,) 5-HT7-20XV5, Syn overlay. J-L)
1459 Cross section of SV. J) 5-HT7-20XV5.; K) Syn; L) 5-HT7-20XV5, Syn overlay. M-O) SV
1460 terminus. M) 5-HT7-20XV5.; N) Syn; O) 5-HT7-20XV5, Syn overlay. P-R) SV/ED
1461 junction. P) 5-HT7-20XV5.; Q) Syn; R) 5-HT7-20XV5, Syn overlay. Scale bars: C, G-
1462 50μm; F, O-10μm; R-25μm.

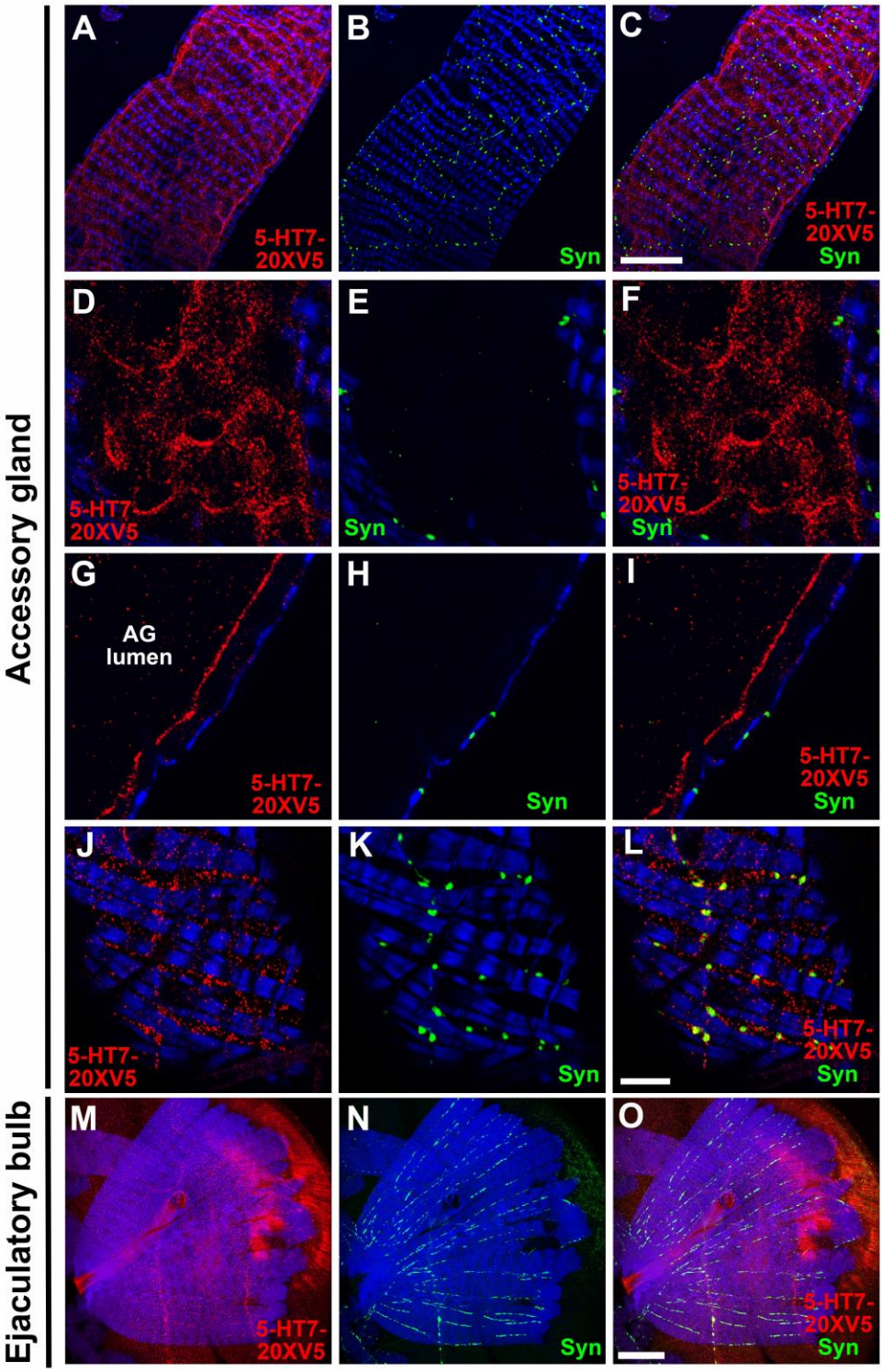
Accessory gland
Ejaculatory bulb
A
B
C
D
E
F
G
H
I
J
K
L
M
N
O
5-HT7-20XV5
Syn
AG lumen

1463

1464 **Figure 8S10.** 5-HT7-20XV5 expression in the Drosophila male reproductive system. A-
1465 C) AG. A) 5-HT7-20XV5.; B) Syn; C) 5-HT7-20XV5, Syn overlay. D-F) Epithelial layer
1466 of AG. D) 5-HT7-20XV5.; E) Syn; F) 5-HT7-20XV5, Syn overlay. G-I) Cross-section of
1467 epithelial layer of AG. G) 5-HT7-20XV5.; H) Syn; I) 5-HT7-20XV5, Syn overlay. J-L)
1468 Muscle layer of AG. J) 5-HT7-20XV5.; K) Syn; L) 5-HT7-20XV5, Syn overlay. M-O)
1469 Ejaculatory bulb. M) 5-HT7-20XV5.; N) Syn; O) 5-HT7-20XV5, Syn overlay. Scale bars:
1470 C, O-50μm; L-10μm.

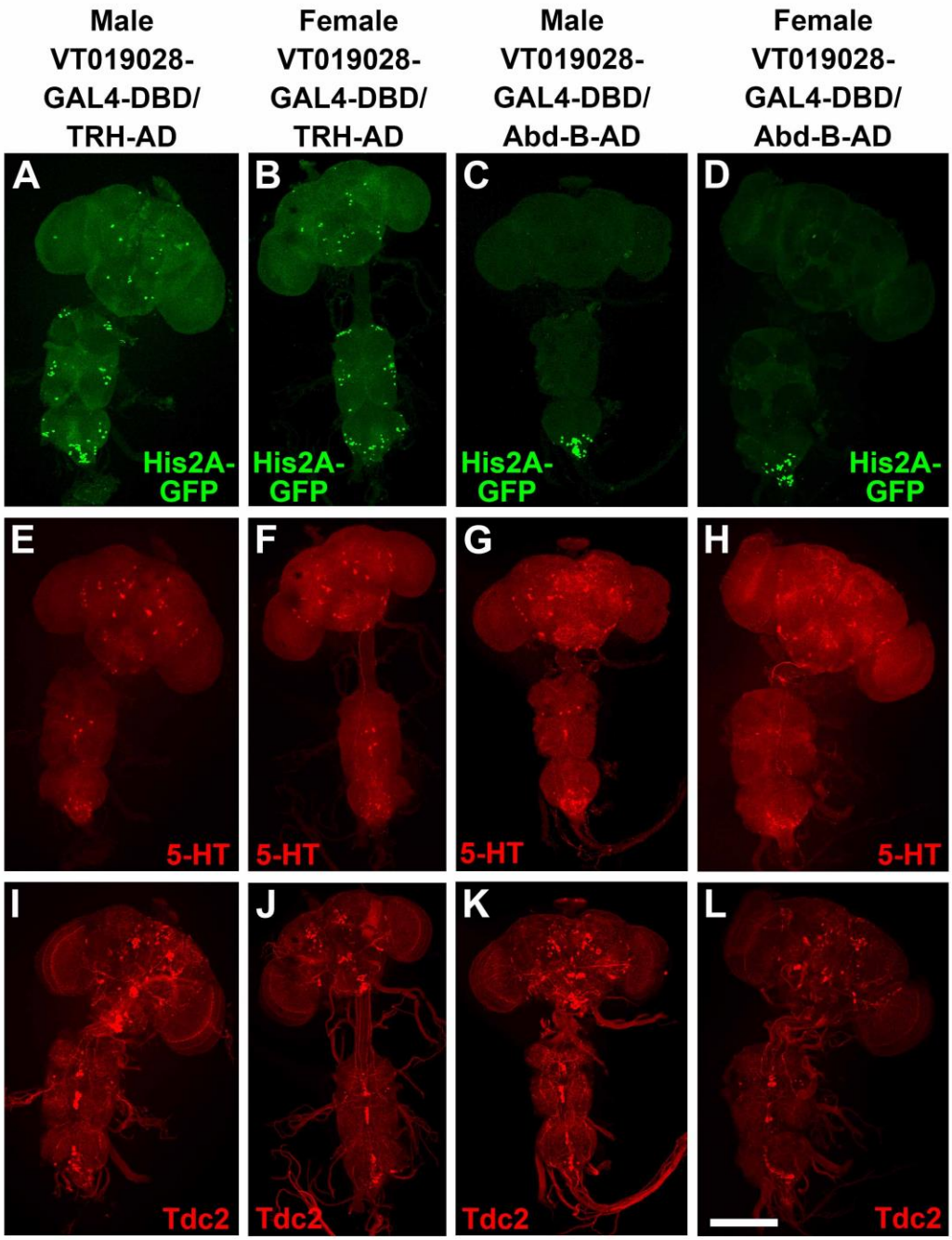

Figure 9. Low resolution images of nuclear expression of *VT019028-GAL4-DBD* in combination with *TRH-AD* and *AbdB-AD* in Drosophila male and female adult nervous system relative to 5-HT and Tdc2. A-D) nuclear expression using HIS2A-GFP marker. A) male *VT019028-GAL4-DBD*/*TRH-AD*; B) female *VT019028-GAL4-DBD*/*TRH-AD*; C) male *VT019028-GAL4-DBD*/*AbdB-AD*; B) female *VT019028-GAL4-DBD*/*AbdB-AD*. E-H) 5-HT expression. E) male *VT019028-GAL4-DBD*/TRH-AD; F) female *VT019028-*

1479 *GAL4-DBD*/*TRH-AD*; G) male *VT019028-GAL4-DBD*/*AbdB-AD*; H) female *VT019028-*
1480 *GAL4-DBD*/*AbdB-AD*. Tdc2 expression. I) male *VT019028-GAL4-DBD*/*TRH-AD*; J)
1481 female *VT019028-GAL4-DBD*/*TRH-AD*; K) male *VT019028-GAL4-DBD*/*AbdB-AD*; L)
1482 female *VT019028-GAL4-DBD*/*AbdB-AD*. Scale bar: 200μm.

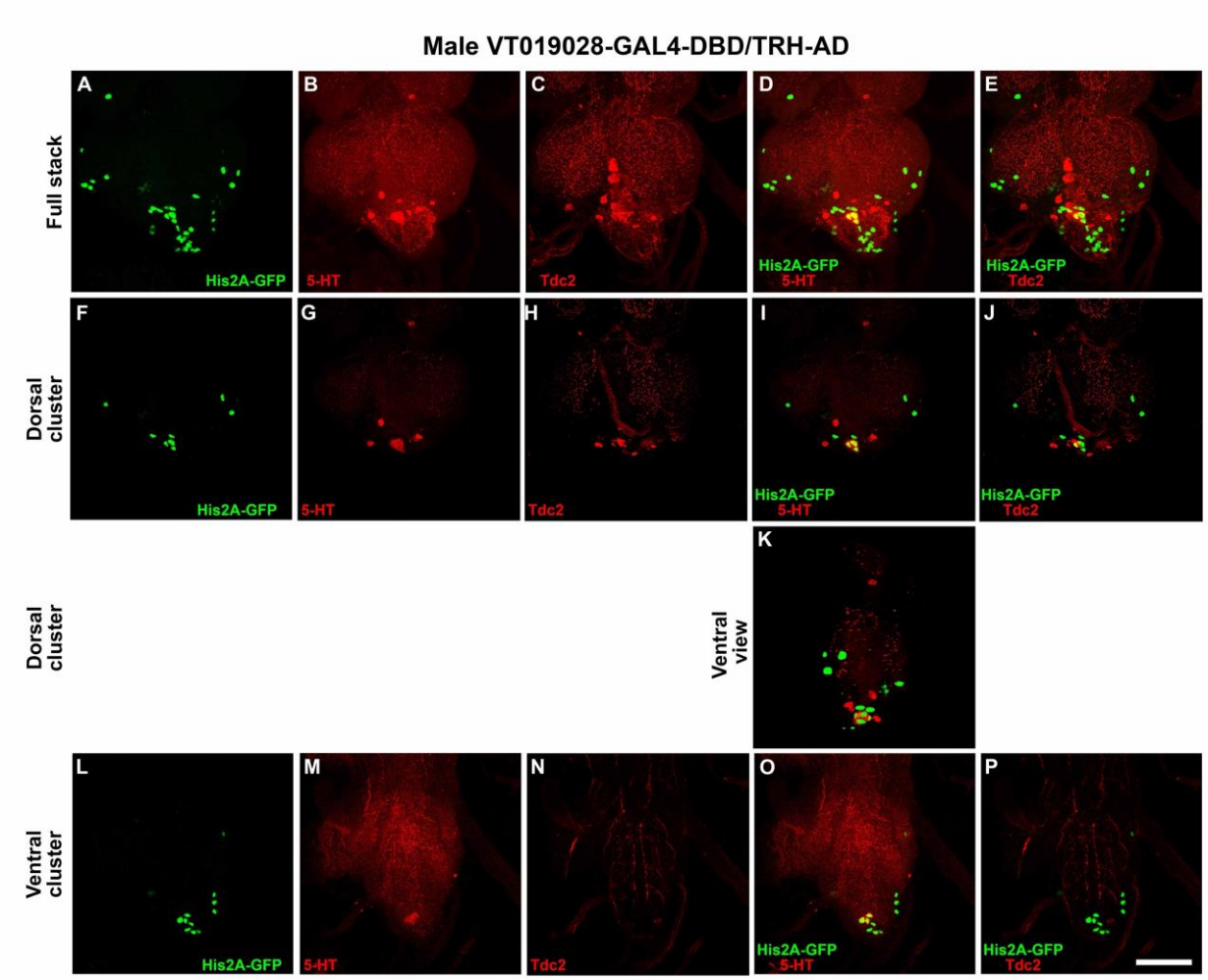

1483
1484 **Figure 9S1.** High resolution images of nuclear expression of *VT019028-GAL4-DBD* in
1485 combination with *TRH-AD* in posterior ventral nerve cord of Drosophila male adult
1486 nervous system relative to 5-HT and Tdc2. A-E) Dorsal view of complete stack of
1487 confocal images. A) His2A-GFP; B) 5-HT; C) Tdc2; D) His2A-GFP, 5-HT overlay; E)
1488 His2A-GFP, Tdc2 overlay. F) Ventral view of His2A-GFP/5-HT overlay of subset of
1489 slices containing the dorsal cluster of 5-HT neurons; G-K) Dorsal view of subset of
1490 slices containing the dorsal cluster of 5-HT neurons. G) His2A-GFP; H) 5-HT; I) Tdc2;
1491 J) His2A-GFP, 5-HT overlay; K) His2A-GFP, Tdc2 overlay. L-P) Dorsal view of subset of
1492 slices containing the ventral cluster of 5-HT neurons. L) His2A-GFP; M) 5-HT; N) Tdc2;
1493 O) His2A-GFP, 5-HT overlay; P) His2A-GFP, Tdc2 overlay. Scale bar: 50μm.

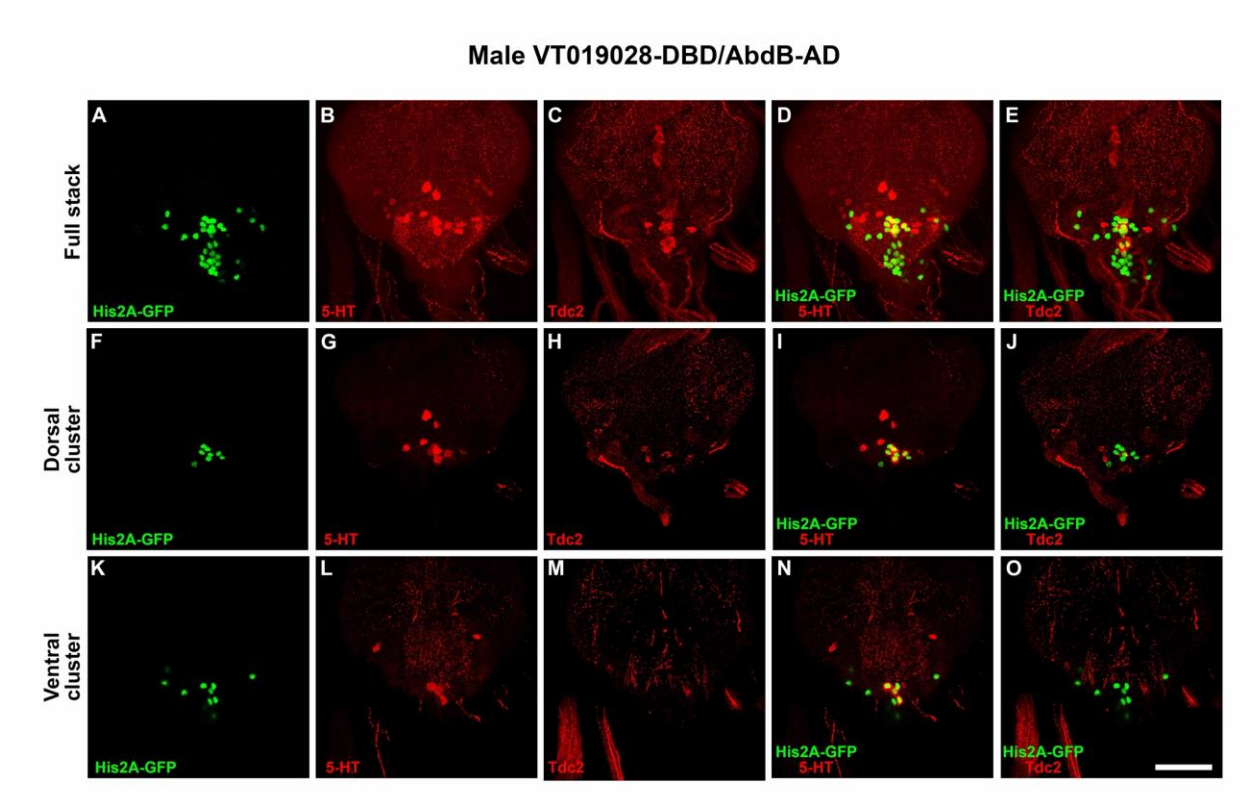

Figure 9S2. High resolution images of nuclear expression of *VT019028-GAL4-DBD* in combination with *AbdB-AD* in posterior ventral nerve cord of Drosophila male adult nervous system relative to 5-HT and Tdc2. A-E) Dorsal view of complete stack of confocal images. A) His2A-GFP; B) 5-HT; C) Tdc2; D) His2A-GFP, 5-HT overlay; E) His2A-GFP, Tdc2 overlay. F-J) Dorsal view of subset of slices containing the dorsal cluster of 5-HT neurons. F) His2A-GFP; G) 5-HT; H) Tdc2; I) His2A-GFP, 5-HT overlay; J) His2A-GFP, Tdc2 overlay. K-O) Dorsal view of subset of slices containing the ventral cluster of 5-HT neurons. K) His2A-GFP; L) 5-HT; M) Tdc2; N) His2A-GFP, 5-HT overlay; O) His2A-GFP, Tdc2 overlay. Scale bar: 50μm.

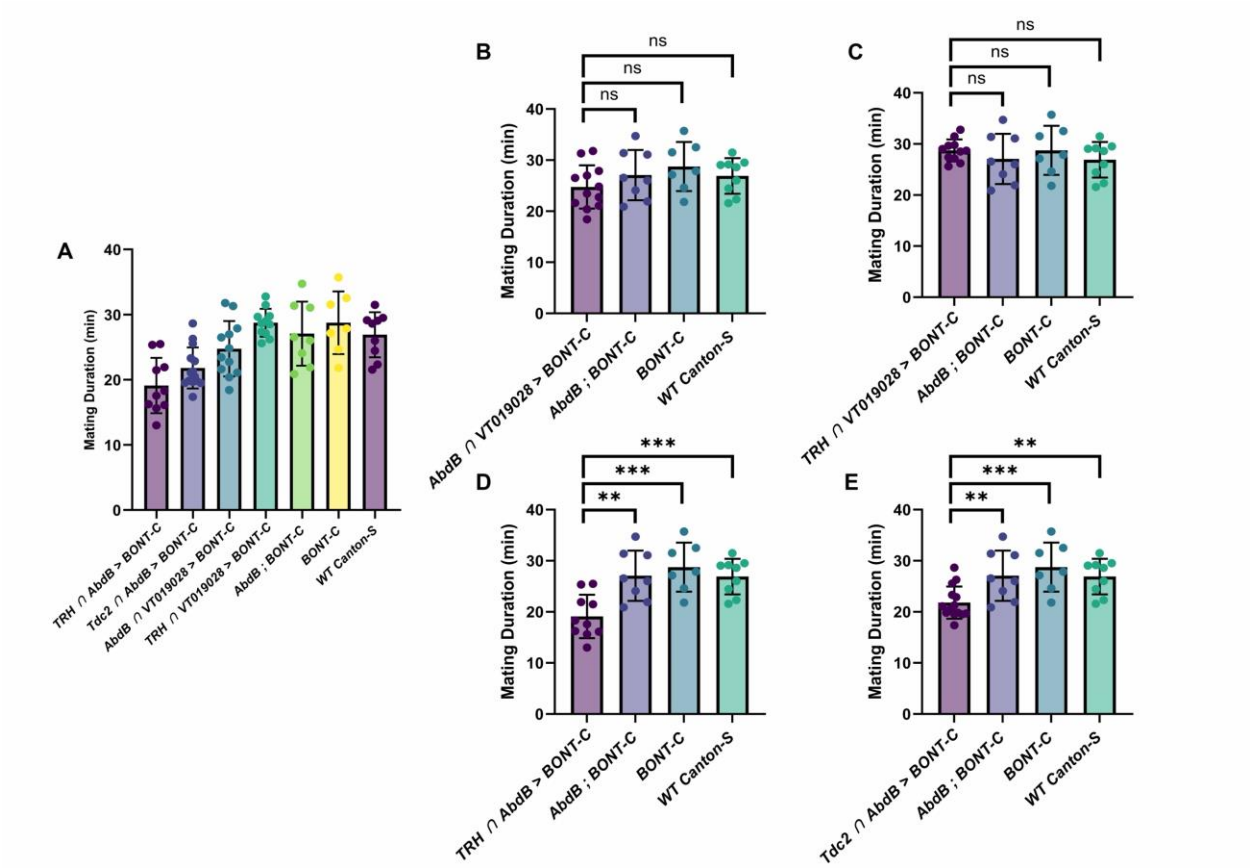

Figure 10. Comparison of mating duration between genotypes. Bar plots show the mean ± SD for each group with individual data points overlaid on each bar. Statistical comparisons were made using unpaired two-tailed t tests where appropriate. Asterisks above indicate significance levels: $p < 0.001$ (**), $p < 0.0001$ (***), ns = not significant. (A) Columns from left to right: TRH ∩ AbdB > BONT-C: n= 10, mean= 19.11, SD=4.251. Tdc2 ∩ AbdB > BONT-C: n=14, mean=21.80, SD= 3.155. AbdB ∩ VT019028 > BONT-C: n=12, mean=24.75, SD=4.247. TRH ∩ VT019028 > BONT-C: n=11, mean=28.74, SD=2.155. AbdB ; BONT-C: n=8, mean=27.07, SD=4.907. BONT-C: n=7, mean=28.75, SD=4.809. WT Canton-S: n=9, mean=26.91, SD=3.473.

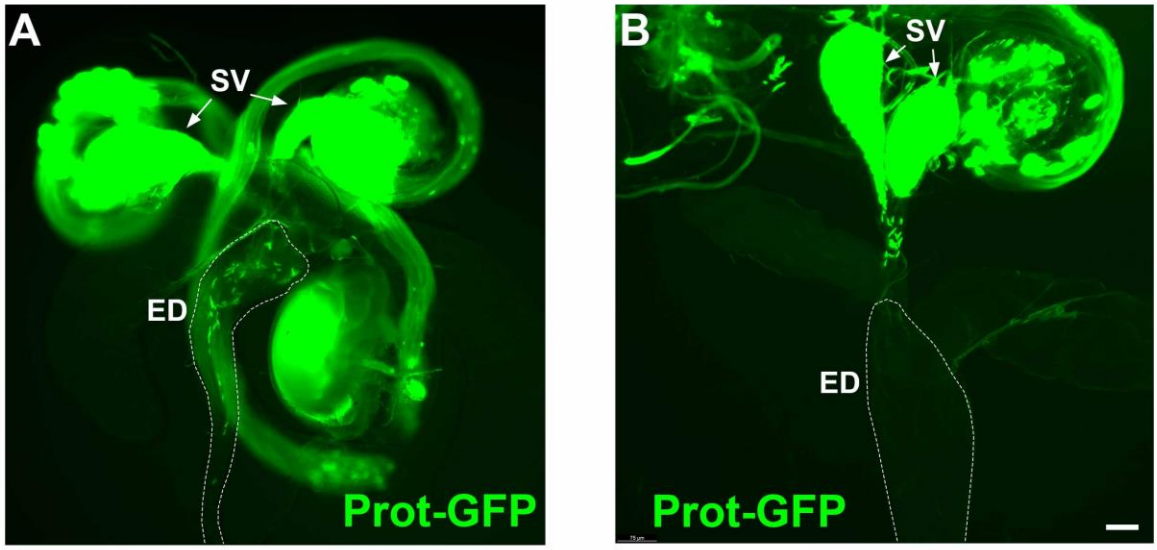

Figure 10S1. Expression of ProtB-GFP fluorescent marker of sperm nuclei in male reproductive system of control and *TRH-AD*/*VT019028-GAL4-DBD* neuron-silenced flies interrupted mid-mating. A) control. B) *TRH-AD*/*VT019028-GAL4-DBD* neurons silenced with BONT-C. Prot-GFP-Protamine GFP. SV-SV, ED-ED. Scale bar: 75μm.

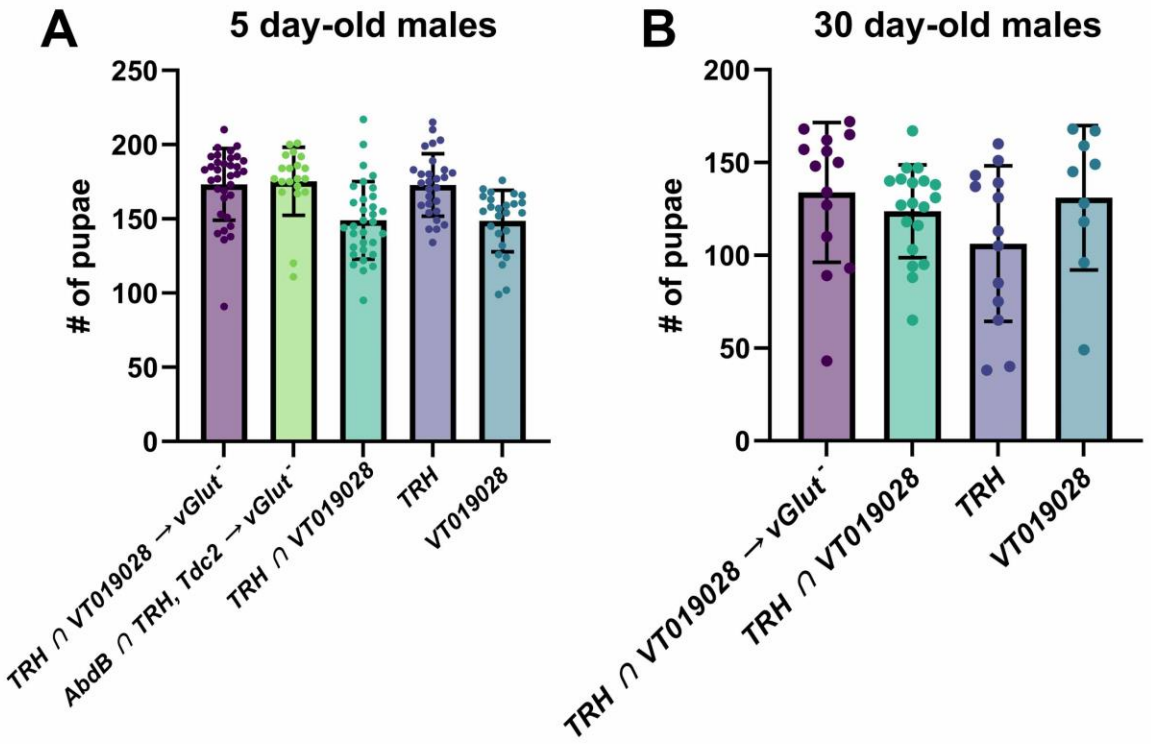

Figure 10S2. Comparison of male drosophila fecundity between genotypes. Bar plots show the mean ± SD for each group with individual data points overlaid on each bar. Figure 10S1A males were aged 5 days before copulation. Figure 10S1B males were aged 30 days before copulation. (A) Columns from left to right: TRH ∩ VT019028 → vGlut-: n=34, mean=173.2, SD=24.22. AbdB ∩ TRH, Tdc2 → vGlut-: n=20, mean=175.3, SD=22.92. TRH ∩ VT019028: n=32, mean=149.0, SD=26.10. TRH: n=28, mean=172.8, SD=21.11. VT019028: n=25, mean=148.6, SD=20.81. (B) TRH ∩ VT019028 → vGlut-: n=14, mean=133.9, SD=37.64. TRH ∩ VT019028: n=19, mean=123.7, SD, 25.02. TRH: n=13, mean=106.3, SD=41.93. VT019028: n=9, mean=131.0, SD=38.88.

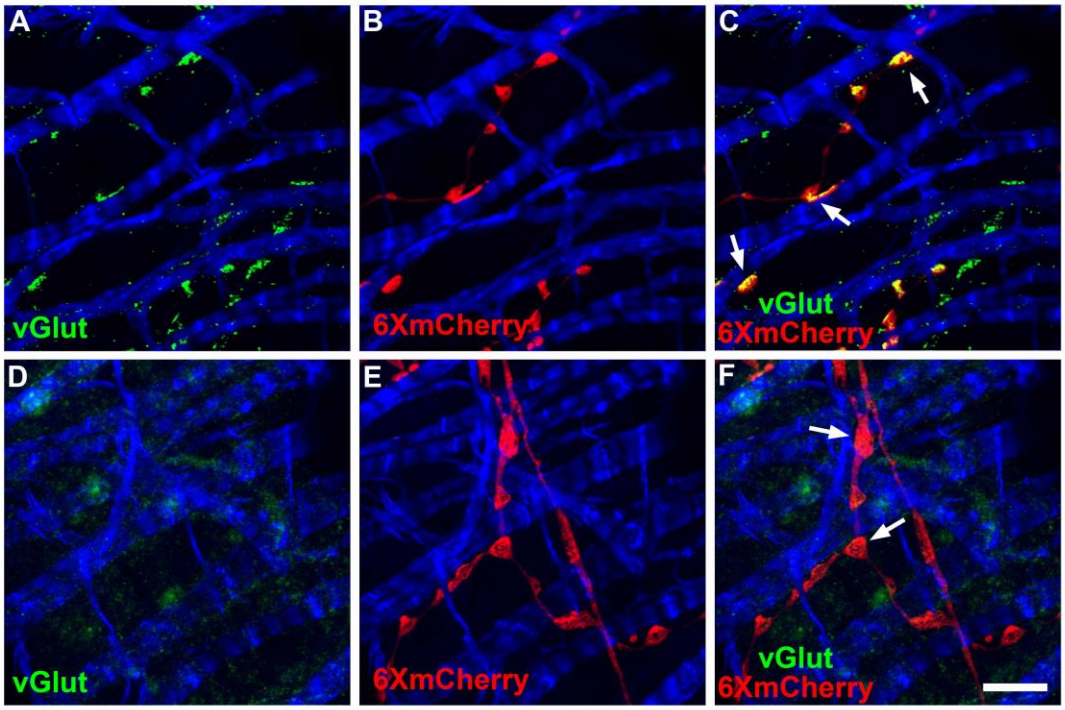

Figure 10S3. vGlut expression in AGs of control and vGlut conditional mutant. A-C) control male. A) vGlut; B) 6XmCherry; C) overlay. D-F) experimental male conditionally silenced for vGlut in *TRH-AD*/*VT019028-GAL4* neurons. Scale bar: 50μm.

Video 1. Male reproductive system of a ProtB-GFP control. Sperm with green fluorescent nuclei are visible in the ejaculatory duct of a male subjected to a mid-mating interruption.

Video 2. Male reproductive system of a ProtB-GFP experimental male in which a subset of the *TRH-AD*/*VT019028-GAL4-DBD* subset of serotonergic neurons innervating the male reproductive system have been silenced. Sperm with green fluorescent nuclei are restricted to the seminal vesicle and never enter the ejaculatory duct from a male subjected to a mid-mating interruption.

Video 3. GCAMP8m Ca++ imaging of an ejaculatory duct experiencing spontaneous peristaltic waves of muscle contractions.

Video 4. GCAMP8m Ca++ imaging of the SV/ED junction showing the initiation site of the spontaneous peristaltic waves.

Video 5. GCAMP8m Ca++ imaging of the SV/ED junction showing the subtle variation in the initiation site of spontaneous peristaltic waves as compared to Video 4.

Video 6. GCAMP8m Ca++ imaging of the SV showing spontaneous uncoordinated muscle activity.

Video 7. GCAMP8m Ca++ imaging of an AG showing spontaneous uncoordinated muscle activity.

Video 8. GCAMP8m Ca++ imaging of a testes showing spontaneous uncoordinated muscle activity.

Video 9. GCAMP8m Ca++ imaging of the AG showing strong coordinated muscle activity.

Genotype	Male Fertile	Female Fertile
yw; *TRH-GAL4DBD*/*AbdB-AD*, *UAS-BONT-C*	No	No
yw; *Tdc2-GAL4DBD*/*AbdB-AD*, *UAS-BONT-C*	Yes	No
yw; *VT019028-GAL4-DBD*/*AbdB-AD*, *UAS-BONT-C*	No	Yes
yw; *TRH-AD*; *UAS-BONT-C*/*VT019028-GAL4-DBD*	No	Yes
yw; *AbdB-AD*/*UAS-BONT-C*	Yes	Yes
yw; *UAS-BONT-C*	Yes	Yes
Canton-S wildtype	Yes	Yes

Table 1. Male and female fertility phenotypes.

Complete Genotypes

Figure 1. B) *yw*.

Figure 2. A) *yw*: *Tdc2-GAL4*/+: *UAS-CD8-mCherry*/+; B) *yw*: *TRH-GAL4*/+: *UAS-CD8-mCherry*/+; C) *yw*: *vGlut-GAL4*/+: *UAS-CD8-mCherry*/+; D) *yw*: *vGlut-GAL4-DBD*/+; *Tdc2-AD*/*UAS-CD8-mCherry*/+; E) *yw*; *vGlut-AD*/+; *Tdc2-GAL4-DBD*, *UAS-CD8-mCherry*; F) *yw*; *TRH-AD*/*vGlut-GAL4-DBD*; *UAS-CD8-mCherry*/+; G) *yw*; *vGlut-AD*/+; *TRH-GAL4-DBD*/*UAS-CD8-mCherry*; H) *yw*; *Tdc2-AD*/TRH-GAL4-DBD, *UAS-CD8-mCherry*.

Figure 3. *yw*; *B3RT-Tdc2-LexA*/*20XUAS-6XGFP*; *TRH-GAL4*/*13XLexAop-6XmCherry*.

Figure 3S1. *yw*; *B3RT-vGlut-LexA*/*20XUAS-6XGFP*; TRH-GAL4/*13XLexAop-6XmCherry*.

1588
1589 **Figure 3S2.** *yw*; *B3RT-vGlut-LexA*/*Tdc2-GAL4*; TRH-GAL4/*20XUAS-*
1590 *6XGFP*/*13XLexAop-6XmCherry*.
1591
1592 **Figure 3S3.** A-C) *yw*; *B3RT-vGlut-LexA*/*20XUAS-6XGFP*; fru-GAL4/*13XLexAop-*
1593 *6XmCherry*. D) *yw*; *Tdc2-AD*/*dsx-GAL4-DBD*, *UAS-CD8-mCherry*. E) *yw*; *TRH-AD*/+;
1594 *dsx-GAL4-DBD*, *UAS-CD8-mCherry*/+.
1595
1596 **Figure 4.** A-F) *w*, *TBH-GFP*; *vGlut-40XV5*/*vGlut-40XV5*. J-L) *yw*; *vGlut-40XV5*/*vGlut-*
1597 *40XV5*.
1598
1599 **Figure 4S1.** A-L) *w*, *TBH-GFP*; *vGlut-40XV5*/*vGlut-40XV5*. M-X) yw; *vGlut-*
1600 *40XV5*/*vGlut-40XV5*.
1601
1602 **Figure 4S2.** A-L) *w*, *TBH-GFP*; *vGlut-40XV5*/*vGlut-40XV5*. M-X) yw; *vGlut-*
1603 *40XV5*/*vGlut-40XV5*.
1604
1605 **Figure 4S3.** A-L) *w*, *TBH-GFP*; *vGlut-40XV5*/*vGlut-40XV5*. M-X) yw; *vGlut-*
1606 *40XV5*/*vGlut-40XV5*.
1607
1608 **Figure 4S4**. A-F) *w*, *TBH-GFP*; *vGlut-40XV5*/*vGlut-40XV5*.
1609
1610 **Figure 5.** A-L) *yw*; *B2RT-STOP-B2RT-40XMYC*, *RSRT-STOP-RSRT-6XV5-vMAT*/+;
1611 *TRH-GAL4*, *UAS-CD8-mCherry*, *UAS-B2*, *UAS-R*. M-O) yw; *B2RT-STOP-B2RT-*
1612 *40XMYC*, *RSRT-STOP-RSRT-6XV5-vMAT*/*Tdc2-GAL4*; *UAS-CD8-mCherry*, *UAS-B2*,
1613 *UAS-R*/+.
1614
1615 **Figure 5S1.** A-L) *yw*; *B2RT-STOP-B2RT-40XMYC*, *RSRT-STOP-RSRT-6XV5-vMAT*/+;
1616 *TRH-GAL4*, *UAS-CD8-mCherry*, *UAS-B2*, *UAS-R*. M-O) *yw*; *B2RT-STOP-B2RT-*
1617 *40XMYC*, *RSRT-STOP-RSRT-6XV5-vMAT*/*Tdc2-GAL4*; *UAS-CD8-mCherry*, *UAS-B2*,
1618 *UAS-R*/+.
1619
1620 **Figure 5S2.** A-L) *yw*; *B2RT-STOP-B2RT-40XMYC*, *RSRT-STOP-RSRT-6XV5-vMAT*/+;
1621 *TRH-GAL4*, *UAS-CD8-mCherry*, *UAS-B2*, *UAS-R*. M-O) *yw*; *B2RT-STOP-B2RT-*
1622 *40XMYC*, *RSRT-STOP-RSRT-6XV5-vMAT*/*Tdc2-GAL4*; *UAS-CD8-mCherry*, *UAS-B2*,
1623 *UAS-R*/+.
1624
1625 **Figure 5S3.** A-I) *yw*; *B2RT-STOP-B2RT-40XMYC*, *RSRT-STOP-RSRT-6XV5-vMAT*/+;
1626 *TRH-GAL4*, *UAS-CD8-mCherry*, *UAS-B2*, *UAS-R*.
1627
1628 **Figure 5S4.** A-I) *yw*; *B2RT-STOP-B2RT-40XMYC*, *RSRT-STOP-RSRT-6XV5-*
1629 *vMAT*/*Tdc2-GAL4*; *UAS-CD8-mCherry*, *UAS-B2*, *UAS-R*/+.
1630
1631 **Figure 5S5.** A-B) *yw*.
1632

1633 **Figure 6.** A-I) *yw*; *vGlut-40XMYC*, *6XV5-vMAT*/*vGlut-40XMYC*, *6XV5-vMAT*. A'-I') *yw*;
1634 *vGlut-40XMYC*, *6XV5-vMAT*/*vGlut-40XMYC*, *6XV5-vMAT*. A''-I'') *yw*; *vGlut-40XMYC*,
1635 *6XV5-vMAT*/*vGlut-40XMYC*, *6XV5-vMAT*.
1636
1637 **Figure 6S1.** A-X) *yw*; *vGlut-40XMYC*, *6XV5-vMAT*/*vGlut-40XMYC*, *6XV5-vMAT*.
1638
1639 **Figure 6S2.** A-V) *yw*; *vGlut-40XMYC*, *6XV5-vMAT*/*vGlut-40XMYC*, *6XV5-vMAT*.
1640
1641 **Figure 6S3.** A-O) *yw*; *vGlut-40XMYC*, *6XV5-vMAT*/*IA2-GFP*.
1642 **Figure 6S4.** A-O) *yw*; *vGlut-40XMYC*, *6XV5-vMAT*/*IA2-GFP*.
1643
1644 **Figure 6S5.** A, E, I) *yw*; *vGlut-40X5*/*vGlut-40XV5*. B, F, J) *yw*; *6XV5-vMAT*/*6XV5-vMAT*.
1645 C, G, K) *yw*; *7XMYC-vAChT*/*7XMYC-vAChT*. D, H, L) *yw*; *9XV5-vGAT*/*9XV5-vGAT*.
1646
1647 **Figure 7.** A) *yw*; *GluRIIB-GAL4*/+; *UAS-CD8-mCherry*. B) *yw*; *GluRIIC-GAL4*/+; *UAS-*
1648 *CD8-mCherry*.
1649
1650 **Figure 7S1.** A) *yw*; *OAMB-GAL4*/*UAS-CD8-mCherry*. B) *yw*; OAα2R-GAL4/*UAS-CD8-*
1651 *mCherry*. C) *yw*; *Oct-TyrR-GAL4*/*UAS-CD8-mCherry*. D) *yw*; OAβ1R-GAL4/*UAS-CD8-*
1652 *mCherry*. E) *yw*; *OAβ2R-GAL4*/*UAS-CD8-mCherry*. F) *yw*; OAβ3R-GAL4/*UAS-CD8-*
1653 *mCherry*.
1654
1655 **Figure 7S2.** A) *yw*; *5-HT71A-GAL4*/+; UAS-CD8-mCherry/+. B) yw; *5-HT71B-GAL4*/+;
1656 *UAS-CD8-mCherry*/+. C) *yw*; *5-HT2A-GAL4*/*UAS-CD8-mCherry*. D) yw; *5-HT2B-*
1657 *GAL4*/*UAS-CD8-mCherry*. E) *yw*; *5-HT7-GAL4*/*UAS-CD8-mCherry*.
1658
1659 **Figure 8.** A-R) *yw*; *vGlut-40XV5*/*GluRIIA-GFP*.
1660
1661 **Figure 8S1.** A-R) *yw*; *OAMB-10XV5*/*OAMB-10XV5*.
1662
1663 **Figure 8S2.** A-R) *yw*; *OAMB-10XV5*/*OAMB-10XV5*.
1664
1665 **Figure 8S3.** A-R) *yw*; *OAα2R-20XV5*/*OAα2R-20XV5*.
1666
1667 **Figure 8S4.** A-U) *yw*; *OAα2R-20XV5*/*OAα2R-20XV5*.
1668
1669 **Figure 8S5.** A-R) *yw*; *OAβ2R-40XV5*/*OAβ2R-40XV5*.
1670
1671 **Figure 8S6.** A-O) *yw*; *OAβ2R-40XV5*/*OAβ2R-40XV5*.
1672
1673 **Figure 8S7.** A-R) *yw*; *OAβ2R-40XV5*/*OAβ2R-40XV5*.
1674
1675 **Figure 8S8.** A-O) *yw*; *5-HT7-20XV5*/*5-HT7-20XV5*.
1676
1677 **Figure 8S9.** A-R) *yw*; *5-HT7-20XV5*/*5-HT7-20XV5*.
1678

1679 **Figure 8S10.** A-O) *yw*; *5-HT7-20XV5*/*5-HT7-20XV5*.
1680
1681 **Figure 9.** A, E, I) male *yw*; *UAS-H2A-GFP*/*TRH-AD*; *VT019028-GAL4-DBD*/+. B, F, J)
1682 female *yw*; *UAS-H2A-GFP*/*TRH-AD*; *VT019028-GAL4-DBD*/+. C, G, K) male yw; *UAS-*
1683 *H2A-GFP*/+; *VT019028-GAL4-DBD*/*AbdB-AD*. D, H, L) female *yw*; *UAS-H2A-GFP*/+;
1684 *VT019028-GAL4-DBD*/*AbdB-AD*.
1685
1686 **Figure 9S1.** A-P) male *yw*; *UAS-H2A-GFP*/*TRH-AD*; *VT019028-GAL4-DBD*/+.
1687
1688 **Figure 9S2.** A-O) male *yw*; *UAS-H2A-GFP*/+; *VT019028-GAL4-DBD*/*AbdB-AD*.
1689
1690 **Figure 9S3.** A) male *yw*; *UAS-H2A-GFP*/*TRH-AD*; *VT019028-GAL4-DBD*/+. B) male
1691 *yw*; *UAS-H2A-GFP*/+; *VT019028-GAL4-DBD*/*AbdB-AD*.
1692
1693 **Figure 10.** A) column 1-*yw*; *TRH-GAL4-DBD*/*AbdB-AD*, *UAS-BONT-C*/+; column 2-*yw*;
1694 *Tdc2-GAL4-DBD*/ *AbdB-AD*, *UAS-BONT-C*. column 3-*yw*; *AbdB-AD*, *UAS-BONT-*
1695 *C*/*VT019028-GAL4-DBD*. column 4-*yw*; *TRH-AD*/+; *VT019028-GAL4-DBD*, *UAS-BONT-*
1696 *C*. column 5-*yw*; *AbdB-AD*, *UAS-BONT-C*. column 6-*UAS-BONT-C*. column 7-wildtype
1697 *Canton-S*. B) column 1-*yw*; *AbdB-AD*, *UAS-BONT-C*/*VT019028-GAL4-DBD*. column 2-
1698 *yw*; *AbdB-AD*, *UAS-BONT-C*. column 3-*UAS-BONT-C*. column 1-wildtype *Canton-S*. C)
1699 column 2-*yw*; *TRH-AD*/+; *VT019028-GAL4-DBD*, *UAS-BONT-C*. column 3-yw; *AbdB-*
1700 *AD*, *UAS-BONT-C*. column 4-*UAS-BONT-C*. column 7-wildtype *Canton-S*. D) column 1-
1701 *yw*; *TRH-GAL4-DBD*/*AbdB-AD*, *UAS-BONT-C*/+; column 2-*yw*; AbdB-AD, *UAS-BONT-*
1702 *C*. column 3-*UAS-BONT-C*. column 4-wildtype *Canton-S*. E) column 1-yw; *Tdc2-GAL4-*
1703 *DBD*/ *AbdB-AD*, *UAS-BONT-C*. column 2-*yw*; *AbdB-AD*, *UAS-BONT-C*. column 3-*UAS-*
1704 *BONT-C*. column 4-wildtype *Canton-S*.
1705
1706 **Figure 10S1.** A) *yw*; *ProtB-GFP*/+; B) *yw*; *ProtB-GFP*/+; *VT019028-GAL4-DBD*, *UAS-*
1707 *BONT-C*.
1708
1709 **Figure 10S2.** A) column 1-*yw*; *B3RT-vGlut-LexA*/*TRH-AD*, vGlut^{SS1}; *VT019028-GAL4-*
1710 *DBD*/*UAS-B3*. column 2-*yw*; *B3RT-vGlut-LexA*/*vGlut*^{SS1}; *TRH-GAL4-DBD*, *Tdc2-GAL4-*
1711 *DBD*/*AbdB-AD*, *UAS-B3*. column 3-*yw*; *B3RT-vGlut-LexA*/TRH-AD; *VT019028-GAL4-*
1712 *DBD*/*UAS-B3*. column 4-*yw*; *B3RT-vGlut-LexA*/*TRH-AD*, *vGlut*^{SS1}; *UAS-B3*/+. column 5-
1713 *yw*; *B3RT-vGlut-LexA*/*vGlut*^{SS1}; *VT019028-GAL4-DBD*/*UAS-B3*. B) column 1-*yw*; *B3RT-*
1714 *vGlut-LexA*/*TRH-AD*, *vGlut*^{SS1}; *VT019028-GAL4-DBD*/*UAS-B3*. column 2- yw; *B3RT-*
1715 *vGlut-LexA/TRH-AD; VT019028-GAL4-DBD/UAS-B3. column 3- yw; B3RT-vGlut-*
1716 *LexA*/*TRH-AD*, *vGlut*^{SS1}; *UAS-B3*/+. column 4-*yw*; *B3RT-vGlut-LexA*/*vGlut*^{SS1};
1717 *VT019028-GAL4-DBD*/*UAS-B3*.
1718
1719 **Figure 10S3.** A-F) *yw*; *B3RT-vGlut-LexA*/*TRH-AD*, vGlut^{SS1}; *VT019028-GAL4-*
1720 *DBD*/*UAS-B3*, *LexAop-6XmCherry*.
1721
1722 **Video 1.** *yw*; *ProtB-GFP*/+.
1723
1724 **Video 2.** *yw*; *ProtB-GFP*/+; *VT019028-GAL4-DBD*, *UAS-BONT-C*.

Videos 3-9. *yw*: *MHC-GCAMP8m*.

References

Abbe, E., 1873 Beitrage zur Theorie des microskops und der mikroskopischen Wahrnehmung. Anatomie IX**:** 413-468.

Acebes, A., Y. Grosjean, C. Everaerts and J. F. Ferveur, 2004 Cholinergic control of synchronized seminal emissions in Drosophila. Curr Biol 14**:** 704-710.

Allen, J. M., T. E. Adrian, K. Tatemoto, J. M. Polak, J. Hughes *et al.*, 1982 Two novel related peptides, neuropeptide Y (NPY) and peptide YY (PYY) inhibit the contraction of the electrically stimulated mouse vas deferens. Neuropeptides 3**:** 71-77.

Alwaal, A., B. N. Breyer and T. F. Lue, 2015 Normal male sexual function: emphasis on orgasm and ejaculation. Fertil Steril 104**:** 1051-1060.

Bairati, A., 1968 [The structure and ultrastructure of the male genital apparatus of the Drosophila melanogaster Meig. 2. The genital duct and accessory glands]. Italian Journal of Zoology 2**:** 105-182.

Baker, C. A., X. J. Guan, M. Choi and M. Murthy, 2024 The role of fruitless in specifying courtship behaviors across divergent Drosophila species. Sci Adv 10**:** eadk1273.

Bakshinska, D., W. Y. Liu, R. Schultz, R. S. Stowers, A. Hoagland *et al.*, 2025 Synapse-specific catecholaminergic modulation of neuronal glutamate release. Proc Natl Acad Sci U S A 122**:** e2420496121.

Banerjee, S., S. Vernon, W. Jiao, B. J. Choi, E. Ruchti *et al.*, 2021 Miniature neurotransmission is required to maintain Drosophila synaptic structures during ageing. Nat Commun 12**:** 4399.

Beckers, C. J., A. Mrestani, F. Komma and S. Dannhauser, 2024 Versatile Endogenous Editing of GluRIIA in Drosophila melanogaster. Cells 13.

Beguelini, M. R., C. C. I. Puga, F. F. Martins, A. H. S. Betoli, S. R. Taboga *et al.*, 2013 Morphological Variation of Primary Reproductive Structures in Males of Five Families of Neotropical Bats. Anatomical Record-Advances in Integrative Anatomy and Evolutionary Biology 296**:** 156-167.

Billeter, J. C., and S. F. Goodwin, 2004 Characterization of Drosophila fruitless-gal4 transgenes reveals expression in male-specific fruitless neurons and innervation of male reproductive structures. J Comp Neurol 475**:** 270-287.

Billeter, J. C., E. J. Rideout, A. J. Dornan and S. F. Goodwin, 2006a Control of male sexual behavior in Drosophila by the sex determination pathway. Curr Biol 16**:** R766-776.

Billeter, J. C., A. Villella, J. B. Allendorfer, A. J. Dornan, M. Richardson *et al.*, 2006b Isoform-specific control of male neuronal differentiation and behavior in Drosophila by the fruitless gene. Curr Biol 16**:** 1063-1076.

Bretman, A., C. Fricke and T. Chapman, 2009 Plastic responses of male Drosophila melanogaster to the level of sperm competition increase male reproductive fitness. Proc Biol Sci 276**:** 1705-1711.

Brown, G. L., and J. S. Gillespie, 1957 The output of sympathetic transmitter from the spleen of the cat. J Physiol 138**:** 81-102.

Buck, S. A., S. A. Rubin, T. Kunkhyen, C. D. Treiber, X. Xue *et al.*, 2023 Sexually dimorphic mechanisms of VGLUT-mediated protection from dopaminergic neurodegeneration. bioRxiv.

Burnstock, G., 2009 Purinergic cotransmission. Exp Physiol 94**:** 20-24.

Burnstock, G., 2014 Purinergic signalling in the reproductive system in health and disease. Purinergic Signal 10**:** 157-187.

Carro-Juarez, M., S. L. Cruz and G. Rodriguez-Manzo, 2003 Evidence for the involvement of a spinal pattern generator in the control of the genital motor pattern of ejaculation. Brain Res 975**:** 222-228.

Carter, D., M. Champney, B. Hwang and R. M. Eglen, 1995 Characterization of a postjunctional 5-HT receptor mediating relaxation of guinea-pig isolated ileum. Eur J Pharmacol 280**:** 243-250.

Castellanos, M. C., J. C. Tang and D. W. Allan, 2013 Female-biased dimorphism underlies a female-specific role for post-embryonic Ilp7 neurons in Drosophila fertility. Development 140**:** 3915-3926.

Certel, S. J., B. D. McCabe and R. S. Stowers, 2022 A conditional GABAergic synaptic vesicle marker for Drosophila. J Neurosci Methods 372**:** 109540.

Chan, A. K., and P. Y. von der Weid, 2003 5-HT decreases contractile and electrical activities in lymphatic vessels of the guinea-pig mesentery: role of 5-HT 7-receptors. Br J Pharmacol 139**:** 243-254.

Chang Chien, C. C., L. W. Hsin and M. J. Su, 2015 Activation of serotonin 5-HT(7) receptor induces coronary flow increase in isolated rat heart. Eur J Pharmacol 748**:** 68-75.

Chehensse, C., P. Facchinetti, S. Bahrami, P. Andrey, J. M. Soler *et al.*, 2017 Human spinal ejaculation generator. Ann Neurol 81**:** 35-45.

Cizmar, D., L. Roller, M. Pillerova, K. Slama and D. Zitnan, 2019 Multiple neuropeptides produced by sex-specific neurons control activity of the male accessory glands and gonoducts in the silkworm Bombyx mori. Sci Rep 9**:** 2253.

Cole, S. H., G. E. Carney, C. A. McClung, S. S. Willard, B. J. Taylor *et al.*, 2005 Two functional but noncomplementing Drosophila tyrosine decarboxylase genes: distinct roles for neural tyramine and octopamine in female fertility. J Biol Chem 280**:** 14948-14955.

Crickmore, M. A., and L. B. Vosshall, 2013 Opposing dopaminergic and GABAergic neurons control the duration and persistence of copulation in Drosophila. Cell 155**:** 881-893.

Damstra, H. G. J., B. Mohar, M. Eddison, A. Akhmanova, L. C. Kapitein *et al.*, 2023 Ten-fold Robust Expansion Microscopy. Bio Protoc 13**:** e4698.

DeLecce, T., G. S. Vance, V. Zeigler-Hill, L. L. M. Welling and T. K. Shackelford, 2025 Ejaculate Adjustment in Response to Sperm Competition Risk in Humans. Arch Sex Behav 54**:** 277-287.

Demerec, M., 1950 *Biology of Drosophila*. Wiley, New York,.

Deng, B., Q. Li, X. Liu, Y. Cao, B. Li *et al.*, 2019 Chemoconnectomics: Mapping Chemical Transmission in Drosophila. Neuron 101**:** 876-893 e874.

Deshpande, S. A., Z. Freyberg, H. O. Lawal and D. E. Krantz, 2020 Vesicular neurotransmitter transporters in Drosophila melanogaster. Biochim Biophys Acta Biomembr 1862**:** 183308.

Deshpande, S. A., E. W. Rohrbach, J. D. Asuncion, J. Harrigan, A. Eamani *et al.*, 2022 Regulation of Drosophila oviduct muscle contractility by octopamine. iScience 25**:** 104697.

DiAntonio, A., 2006 Glutamate receptors at the Drosophila neuromuscular junction. Int Rev Neurobiol 75**:** 165-179.

DiAntonio, A., S. A. Petersen, M. Heckmann and C. S. Goodman, 1999 Glutamate receptor expression regulates quantal size and quantal content at the Drosophila neuromuscular junction. J Neurosci 19**:** 3023-3032.

Diao, F., H. Ironfield, H. Luan, F. Diao, W. C. Shropshire *et al.*, 2015 Plug-and-play genetic access to drosophila cell types using exchangeable exon cassettes. Cell Rep 10**:** 1410-1421.

Diao, F., D. Vasudevan, E. S. Heckscher and B. H. White, 2024 Hox gene-specific cellular targeting using split intein Trojan exons. Proc Natl Acad Sci U S A 121**:** e2317083121.

Dionne, H., K. L. Hibbard, A. Cavallaro, J. C. Kao and G. M. Rubin, 2018 Genetic Reagents for Making Split-GAL4 Lines in Drosophila. Genetics 209**:** 31-35.

Drobnis, E. Z., and A. K. Nangia, 2017 Cardiovascular/Pulmonary Medications and Male Reproduction. Adv Exp Med Biol 1034**:** 103-130.

Dwivedi, S., M. Bautista, S. Shrestha, H. Elhasasna, T. Chaphekar *et al.*, 2021 Sympathetic signaling facilitates progression of neuroendocrine prostate cancer. Cell Death Discov 7**:** 364.

Eberhard, W. G., 1985 *Sexual selection and animal genitalia*. Harvard University Press, Cambridge, Mass.

Fisher, Y. E., H. H. Yang, J. Isaacman-Beck, M. Xie, D. M. Gohl *et al.*, 2017 FlpStop, a tool for conditional gene control in Drosophila. Elife 6.

Fromme, L., D. R. Yogui, M. H. Alves, A. L. J. Desbiez, M. Langeheine *et al.*, 2021 Morphology of the genital organs of male and female giant anteaters ( ). Peerj 9.

Gage, M. J. G., and R. R. Baker, 1991 Ejaculate Size Varies with Sociosexual Situation in an Insect. Ecological Entomology 16**:** 331-337.

Gao, S., S. Y. Takemura, C. Y. Ting, S. Huang, Z. Lu *et al.*, 2008 The neural substrate of spectral preference in Drosophila. Neuron 60**:** 328-342.

Garbaczewska, M., J. C. Billeter and J. D. Levine, 2013 Drosophila melanogaster males increase the number of sperm in their ejaculate when perceiving rival males. J Insect Physiol 59**:** 306-310.

Gilbert, D. G., 1981 Ejaculate Esterast 6 and Initial Sperm Use by Female Drosophila melanogaster. Journal of Insect Physiology 27**:** 641-650.

Gomes, L. F., J. P. Badke, U. Zama, H. Dolder and J. Lino-Neto, 2012 Morphology of the male reproductive system and spermatozoa in Centris Fabricius, 1804 (Hymenoptera: Apidae, Centridini). Micron 43**:** 695-704.

Goulding, M., S. Bourane, L. Garcia-Campmany, A. Dalet and S. Koch, 2014 Inhibition downunder: an update from the spinal cord. Curr Opin Neurobiol 26**:** 161-166.

Gowda, S. B. M., P. D. Paranjpe, O. V. Reddy, D. Thiagarajan, S. Palliyil *et al.*, 2018 GABAergic inhibition of leg motoneurons is required for normal walking behavior in freely moving Drosophila. Proc Natl Acad Sci U S A 115**:** E2115-E2124.

Guerrero, S. M., M. L. Calderón, G. R. de Pérez and M. P. R. Pinilla, 2004 Morphology of the male reproductive duct system of (Crocodylia, Alligatoridae). Annals of Anatomy-Anatomischer Anzeiger 186**:** 235-245.

Han, Y., C. Chien, P. Goel, K. He, C. Pinales *et al.*, 2022 Botulinum neurotoxin accurately separates tonic vs. phasic transmission and reveals heterosynaptic plasticity rules in Drosophila. Elife 11.

He, K., and D. Dickman, 2025 Building and modifying diverse synaptic properties: Insights from Drosophila. Curr Opin Neurobiol 92**:** 102995.

Hiramoto, A., J. Jonaitis, S. Niki, H. Kohsaka, R. D. Fetter *et al.*, 2021 Regulation of coordinated muscular relaxation in Drosophila larvae by a pattern-regulating intersegmental circuit. Nat Commun 12**:** 2943.

Honda, K., A. Miyata-Osawa and T. Takenaka, 1985 alpha 1-Adrenoceptor subtype mediating contraction of the smooth muscle in the lower urinary tract and prostate of rabbits. Naunyn Schmiedebergs Arch Pharmacol 330**:** 16-21.

Hopkins, B. R., I. Sepil, M. L. Thezenas, J. F. Craig, T. Miller *et al.*, 2019 Divergent allocation of sperm and the seminal proteome along a competition gradient in Drosophila melanogaster. Proc Natl Acad Sci U S A 116**:** 17925-17933.

Inoue, M., T. Kitazawa, J. Cao and T. Taneike, 2003 5-HT7 receptor-mediated relaxation of the oviduct in nonpregnant proestrus pigs. Eur J Pharmacol 461**:** 207-218.

Jois, S., Y. B. Chan, M. P. Fernandez and A. K. Leung, 2018 Characterization of the Sexually Dimorphic fruitless Neurons That Regulate Copulation Duration. Front Physiol 9**:** 780.

Kaufman, B. P. a. D., M., 1942 Utilization of sperm by Female Drosophila Melanogaster. The American Naturalist 76**:** 445-469.

Klagges, B. R., G. Heimbeck, T. A. Godenschwege, A. Hofbauer, G. O. Pflugfelder *et al.*, 1996 Invertebrate synapsins: a single gene codes for several isoforms in Drosophila. J Neurosci 16**:** 3154-3165.

Kreiner, T., W. Sossin and R. H. Scheller, 1986 Localization of Aplysia neurosecretory peptides to multiple populations of dense core vesicles. J Cell Biol 102**:** 769-782.

Lange, A. B., A. Kisana, J. Leyria and I. Orchard, 2023 The Male Reproductive System of the Kissing Bug, Rhodnius prolixus Stal, 1859 (Hemiptera: Reduviidae: Triatominae): Arrangements of the Muscles and the Myoactivity of the Selected Neuropeptides. Insects 14.

Lee, G., and J. C. Hall, 2001 Abnormalities of male-specific FRU protein and serotonin expression in the CNS of fruitless mutants in Drosophila. J Neurosci 21**:** 513-526.

Lee, P. T., J. Zirin, O. Kanca, W. W. Lin, K. L. Schulze *et al.*, 2018 A gene-specific T2A-GAL4 library for Drosophila. Elife 7.

Leung, E., L. K. Walsh, M. T. Pulido-Rios and R. M. Eglen, 1996 Characterization of putative 5-ht7 receptors mediating direct relaxation in Cynomolgus monkey isolated jugular vein. Br J Pharmacol 117**:** 926-930.

Li-Kroeger, D., O. Kanca, P. T. Lee, S. Cowan, M. T. Lee *et al.*, 2018 An expanded toolkit for gene tagging based on MiMIC and scarless CRISPR tagging in Drosophila. Elife 7.

Liao, A., F. Cavigliasso, L. Savary and T. J. Kawecki, 2024 Effects of an entomopathogenic fungus on the reproductive potential of Drosophila males. Ecol Evol 14**:** e11242.

Macartney, E. L., V. Zeender, A. Meena, A. N. De Nardo, R. Bonduriansky *et al.*, 2021 Sperm depletion in relation to developmental nutrition and genotype in Drosophila melanogaster. Evolution 75**:** 2830-2841.

Maciel, E. D. S., R. Zieri and S. M. de Almeida-Santos, 2024 Male genital system of Ameiva ameiva (Squamata: Teiidae). Anat Rec (Hoboken) 307**:** 3596-3605.

Magnon, C., S. J. Hall, J. Lin, X. Xue, L. Gerber *et al.*, 2013 Autonomic nerve development contributes to prostate cancer progression. Science 341**:** 1236361.

Majane, A. C., J. M. Cridland and D. J. Begun, 2022 Single-nucleus transcriptomes reveal evolutionary and functional properties of cell types in the Drosophila accessory gland. Genetics 220.

Manier, M. K., J. M. Belote, K. S. Berben, D. Novikov, W. T. Stuart *et al.*, 2010 Resolving mechanisms of competitive fertilization success in Drosophila melanogaster. Science 328**:** 354-357.

Marciniak, P., A. Urbanski, M. Kudlewska, M. Szymczak and G. Rosinski, 2017 Peptide hormones regulate the physiological functions of reproductive organs in Tenebrio molitor males. Peptides 98**:** 35-42.

Matsumoto-Miyai, K., M. Yoshizumi and M. Kawatani, 2015 Regulatory Effects of 5-Hydroxytryptamine Receptors on Voiding Function. Adv Ther 32 Suppl 1**:** 3-15.

McCullough, E. L., E. Whittington, A. Singh, S. Pitnick, M. F. Wolfner *et al.*, 2022 The life history of Drosophila sperm involves molecular continuity between male and female reproductive tracts. Proc Natl Acad Sci U S A 119**:** e2119899119.

McKinney, H. M., L. M. Sherer, J. L. Williams, S. J. Certel and R. S. Stowers, 2020 Characterization of Drosophila octopamine receptor neuronal expression using MiMIC-converted Gal4 lines. J Comp Neurol 528**:** 2174-2194.

Michel, M. C., and W. Vrydag, 2006 Alpha1-, alpha2- and beta-adrenoceptors in the urinary bladder, urethra and prostate. Br J Pharmacol 147 Suppl 2**:** S88-119.

Miyazaki, T., H. Kobayashi and T. Tosaka, 1998 Presynaptic inhibition by noradrenaline of the EPSC evoked in neonatal rat sympathetic preganglionic neurons. Brain Res 790**:** 170-177.

Moatt, J. P., C. Dytham and M. D. Thom, 2014 Sperm production responds to perceived sperm competition risk in male Drosophila melanogaster. Physiol Behav 131**:** 111-114.

Monastirioti, M., C. E. Linn, Jr. and K. White, 1996 Characterization of Drosophila tyramine beta-hydroxylase gene and isolation of mutant flies lacking octopamine. J Neurosci 16**:** 3900-3911.

Norville, K., S. T. Sweeney and C. J. Elliott, 2010 Postmating change in physiology of male Drosophila mediated by serotonin (5-HT). J Neurogenet 24**:** 27-32.

O'Connor, S. C., K. L. Brain and M. R. Bennett, 1999 Individual sympathetic varicosities possess different sensitivities to alpha 2 and P2 receptor agonists and antagonists in mouse vas deferens. Br J Pharmacol 128**:** 1739-1753.

Oliveira, M. S., J. E. Serrao, G. Dias, L. C. B. Martins and V. A. Araújo, 2021 Anatomy and histology of the male reproductive tractof Machtima crucigera (Fabricius, 1775) (Heteroptera: Coreidae). Zoologischer Anzeiger 293**:** 156-162.

Parnas, D., A. P. Haghighi, R. D. Fetter, S. W. Kim and C. S. Goodman, 2001 Regulation of postsynaptic structure and protein localization by the Rho-type guanine nucleotide exchange factor dPix. Neuron 32**:** 415-424.

Pauls, D., C. Blechschmidt, F. Frantzmann, B. El Jundi and M. Selcho, 2018 A comprehensive anatomical map of the peripheral octopaminergic/tyraminergic system of Drosophila melanogaster. Sci Rep 8**:** 15314.

Pavlou, H. J., A. C. Lin, M. C. Neville, T. Nojima, F. Diao *et al.*, 2016 Neural circuitry coordinating male copulation. Elife 5.

Pelletier, G., and R. Leclerc, 1979 Localization of Leu-enkephalin in dense core vesicles of axon terminals. Neurosci Lett 12**:** 159-163.

Petersen, L. K., and R. S. Stowers, 2011 A Gateway MultiSite recombination cloning toolkit. PLoS One 6**:** e24531.

Pizzari, T., C. K. Cornwallis, H. Lovlie, S. Jakobsson and T. R. Birkhead, 2003 Sophisticated sperm allocation in male fowl. Nature 426**:** 70-74.

Port, F., H. M. Chen, T. Lee and S. L. Bullock, 2014 Optimized CRISPR/Cas tools for efficient germline and somatic genome engineering in Drosophila. Proc Natl Acad Sci U S A 111**:** E2967-2976.

Pound, N., and M. J. G. Gage, 2004 Prudent sperm allocation in Norway rats, :: a mammalian model of adaptive ejaculate adjustment. Animal Behaviour 68**:** 819-823.

Prins, N. H., M. R. Briejer, P. J. Van Bergen, L. M. Akkermans and J. A. Schuurkes, 1999 Evidence for 5-HT7 receptors mediating relaxation of human colonic circular smooth muscle. Br J Pharmacol 128**:** 849-852.

Qi, Y. X., G. Xu, G. X. Gu, F. Mao, G. Y. Ye *et al.*, 2017 A new Drosophila octopamine receptor responds to serotonin. Insect Biochem Mol Biol 90**:** 61-70.

Recio, P., M. V. Barahona, L. M. Orensanz, S. Bustamante, A. C. Martinez *et al.*, 2009 5-hydroxytryptamine induced relaxation in the pig urinary bladder neck. Br J Pharmacol 157**:** 271-280.

Rohrbach, E. W., J. D. Asuncion, P. Meera, M. Kralovec, S. A. Deshpande *et al.*, 2024a Heterogeneity in the projections and excitability of tyraminergic/octopaminergic neurons that innervate the Drosophila reproductive tract. Front Mol Neurosci 17**:** 1374896.

Rohrbach, E. W., E. M. Knapp, S. A. Deshpande and D. E. Krantz, 2024b Expression and potential regulatory functions of Drosophila octopamine receptors in the female reproductive tract. G3 (Bethesda) 14.

Scheibner, J., A. U. Trendelenburg, L. Hein and K. Starke, 2001 Stimulation frequency-noradrenaline release relationships examined in alpha2A-, alpha2B- and alpha2C-adrenoceptor-deficient mice. Naunyn Schmiedebergs Arch Pharmacol 364**:** 321-328.

Schindelin, J., I. Arganda-Carreras, E. Frise, V. Kaynig, M. Longair *et al.*, 2012 Fiji: an open-source platform for biological-image analysis. Nat Methods 9**:** 676-682.

Segawa, T., H. Murakami, H. Ogawa and H. Yajima, 1978 Effect of enkephalin and substance P on sympathetic nerve transmission in mouse vas deferens. Jpn J Pharmacol 28**:** 13-19.

Sepil, I., B. R. Hopkins, R. Dean, M. L. Thezenas, P. D. Charles *et al.*, 2019 Quantitative Proteomics Identification of Seminal Fluid Proteins in Male Drosophila melanogaster. Mol Cell Proteomics 18**:** S46-S58.

Shearin, H. K., A. R. Dvarishkis, C. D. Kozeluh and R. S. Stowers, 2013 Expansion of the gateway multisite recombination cloning toolkit. PLoS One 8**:** e77724.

Shearin, H. K., I. S. Macdonald, L. P. Spector and R. S. Stowers, 2014 Hexameric GFP and mCherry reporters for the Drosophila GAL4, Q, and LexA transcription systems. Genetics 196**:** 951-960.

Shen, H., R. A. M. Marino, R. A. McDevitt, G. H. Bi, K. Chen *et al.*, 2018 Genetic deletion of vesicular glutamate transporter in dopamine neurons increases vulnerability to MPTP-induced neurotoxicity in mice. Proc Natl Acad Sci U S A 115**:** E11532-E11541.

Sherer, L. M., E. Catudio Garrett, H. R. Morgan, E. D. Brewer, L. A. Sirrs *et al.*, 2020 Octopamine neuron dependent aggression requires dVGLUT from dual-transmitting neurons. PLoS Genet 16**:** e1008609.

Shirangi, T. R., A. M. Wong, J. W. Truman and D. L. Stern, 2016 Doublesex Regulates the Connectivity of a Neural Circuit Controlling Drosophila Male Courtship Song. Dev Cell 37**:** 533-544.

Siwicki, K. K., and E. A. Kravitz, 2009 Fruitless, doublesex and the genetics of social behavior in Drosophila melanogaster. Curr Opin Neurobiol 19**:** 200-206.

Somogyi, G. T., and W. C. de Groat, 1990 Modulation of the release of [3H]norepinephrine from the base and body of the rat urinary bladder by endogenous adrenergic and cholinergic mechanisms. J Pharmacol Exp Ther 255**:** 204-210.

Soni, K. K., H. S. Jeong and S. Jang, 2022 Neurons for Ejaculation and Factors Affecting Ejaculation. Biology (Basel) 11.

Starke, K., 1972 Alpha sympathomimetic inhibition of adrenergic and cholinergic transmission in the rabbit heart. Naunyn Schmiedebergs Arch Pharmacol 274**:** 18-45.

Stowers, R. S., 2025 Multimerized Epitope Tags for High Sensitivity Protein Detection. G3 (Bethesda).

Susic-Jung, L., C. Hornbruch-Freitag, J. Kuckwa, K. H. Rexer, U. Lammel *et al.*, 2012 Multinucleated smooth muscles and mononucleated as well as multinucleated striated muscles develop during establishment of the male reproductive organs of Drosophila melanogaster. Dev Biol 370**:** 86-97.

Tainio, H., 1995 Peptidergic innervation of the human prostate, seminal vesicle and vas deferens. Acta Histochem 97**:** 113-119.

Tayler, T. D., D. A. Pacheco, A. C. Hergarden, M. Murthy and D. J. Anderson, 2012 A neuropeptide circuit that coordinates sperm transfer and copulation duration in Drosophila. Proc Natl Acad Sci U S A 109**:** 20697-20702.

Tison, K. V., H. M. McKinney and R. S. Stowers, 2020 Demonstration of a Simple Epitope Tag Multimerization Strategy for Enhancing the Sensitivity of Protein Detection Using Drosophila vAChT. G3 (Bethesda) 10**:** 495-504.

Tomas, A. L., M. A. G. Bento, L. D. Mutti, F. J. Zara and L. S. L. Greco, 2019 New insights in the male anatomy, spermatophore formation, and sperm structure in Atyidae: The red cherry shrimp. Invertebrate Biology 138**:** 17-28.

Trendelenburg, A. U., A. Meyer, W. Klebroff, S. Guimaraes and K. Starke, 2003 Crosstalk between presynaptic angiotensin receptors, bradykinin receptors and

alpha 2-autoreceptors in sympathetic neurons: a study in alpha 2-adrenoceptor-deficient mice. Br J Pharmacol 138**:** 1389-1402.

Trendelenburg, A. U., K. Starke and N. Limberger, 1994 Presynaptic alpha 2A-adrenoceptors inhibit the release of endogenous dopamine in rabbit caudate nucleus slices. Naunyn Schmiedebergs Arch Pharmacol 350**:** 473-481.

Truitt, W. A., and L. M. Coolen, 2002 Identification of a potential ejaculation generator in the spinal cord. Science 297**:** 1566-1569.

Verhulst, E. C., and L. van de Zande, 2015 Double nexus--Doublesex is the connecting element in sex determination. Brief Funct Genomics 14**:** 396-406.

Villella, A., and J. C. Hall, 2008 Neurogenetics of courtship and mating in Drosophila. Adv Genet 62**:** 67-184.

Wedell, N., and P. A. Cook, 1999 Butterflies tailor their ejaculate in response to sperm competition risk and intensity. Proceedings of the Royal Society B-Biological Sciences 266**:** 1033-1039.

Wigby, S., N. C. Brown, S. E. Allen, S. Misra, J. L. Sitnik *et al.*, 2020 The Drosophila seminal proteome and its role in postcopulatory sexual selection. Philos Trans R Soc Lond B Biol Sci 375**:** 20200072.

Williams, J. L., H. K. Shearin and R. S. Stowers, 2019 Conditional Synaptic Vesicle Markers for Drosophila. G3 (Bethesda) 9**:** 737-748.

Wolfner, M. F., 1997 Tokens of love: functions and regulation of Drosophila male accessory gland products. Insect Biochem Mol Biol 27**:** 179-192.

Wong, R., and A. B. Lange, 2014 Octopamine modulates a central pattern generator associated with egg-laying in the locust, Locusta migratoria. J Insect Physiol 63**:** 1-8.

Wuest, M., B. Eichhorn, M. O. Grimm, M. P. Wirth, U. Ravens *et al.*, 2009 Catecholamines relax detrusor through beta 2-adrenoceptors in mouse and beta 3-adrenoceptors in man. J Pharmacol Exp Ther 328**:** 213-222.

Yamamoto, D., 2007 The neural and genetic substrates of sexual behavior in Drosophila. Adv Genet 59**:** 39-66.

Yartsev, V. V., and S. S. Evseeva, 2021 The Male Urogenital System of a Salamander

(Amphibia, Caudata). Current Herpetology 40**:** 10-21.

Yu, J., Y. Zhang, K. Clements, N. Chen and L. C. Griffith, 2025 Genetically-encoded markers for confocal visualization of single dense core vesicles. Commun Biol 8**:** 383.

Zhang, Y., M. Rozsa, Y. Liang, D. Bushey, Z. Wei *et al.*, 2023 Fast and sensitive GCaMP calcium indicators for imaging neural populations. Nature 615**:** 884-891.